

COMMIX-PPC: A Three-Dimensional Transient Multicomponent Computer Program for Analyzing Performance of Power Plant Condensers

Volume I: Equations and Numerics

Manuscript Completed: August 1991

Date Published: February 1993

Prepared by

T. H. Chien, H. M. Domanus, and W. T. Sha
Materials and Components Technology Division

ARGONNE NATIONAL LABORATORY
9700 South Cass Avenue
Argonne, IL 60439

Prepared for

Taiwan Power Company
Taipei, Taiwan
Republic of China

MASTER

DISTRIBUTION OF THIS DOCUMENT IS UNLIMITED

As approved by the U.S. Nuclear Regulatory Commission and the U.S. Department of Energy, the COMMIX-PPC computer code was developed by modifying the in-house version of the COMMIX-2A computer code. The development of COMMIX-PPC is a team effort and the participants are listed below according to their activities.

Documentation:	T. H. Chien and W. T. Sha
COMMIX-2A Version:	T. H. Chien, H. M. Domanus, and W. T. Sha
Code Programming and Development:	T. H. Chien, H. M. Domanus, and W. T. Sha
Overall Project Direction and Management:	W. T. Sha

COMMIX-PPC: A Three-Dimensional Transient Multicomponent Computer Program for Analyzing Performance of Power Plant Condensers

Volume I: Equations and Numerics

Abstract

The COMMIX-PPC computer program is an extended and improved version of earlier COMMIX codes and is specifically designed for evaluating the thermal performance of power plant condensers. The COMMIX codes are general-purpose computer programs for the analysis of fluid flow and heat transfer in complex industrial systems. In COMMIX-PPC, two major features have been added to previously published COMMIX codes. One feature is the incorporation of one-dimensional equations of conservation of mass, momentum, and energy on the tube side and the proper accounting for the thermal interaction between shell and tube side through the porous-medium approach. The other added feature is the extension of the three-dimensional conservation equations for shell-side flow to treat the flow of a multicomponent medium.

COMMIX-PPC is designed to perform steady-state and transient, three-dimensional analysis of fluid flow with heat transfer in a power plant condenser. However, the code is designed in a generalized fashion so that, with some modification, it can be used to analyze processes in any heat exchanger or other single-phase engineering applications.

The following unique features are retained from other COMMIX codes:

- **Porous-Medium Formulation.** COMMIX-PPC uses a new porous-medium formulation with the parameters of volume porosity, directional surface porosity, distributed resistance, and distributed heat source or sink. With this formulation, the COMMIX code has the capability to model an anisotropic flow domain with stationary structures, and it can be used to treat irregular geometries. The porous-medium formulation with the additional parameter of directional surface porosity represents a unified approach to thermal-hydraulic analysis. Because of this feature, it is now possible to perform a multidimensional thermal-hydraulic simulation of either a single component, such as a rod bundle, reactor plenum, or piping system, or a multicomponent system that is a combination of two or more engineering components.
- **New finite-volume formulation for equations of conservation of mass, momentum, and energy.** The momentum formulation employs the concept of a volume-averaged velocity as used in COMMIX-1C. It makes the numerical calculation more robust than in previous COMMIX versions. It also makes the location of pressure change coincide with that of density change for one-dimensional flows. In addition, the new discretized momentum equations also satisfy the one-dimensional Bernoulli equation.
- **Three Matrix Solvers.** In COMMIX-PPC, three matrix solvers, the successive overrelaxation method, the direct matrix inversion method, and the precondi-

tioned conjugate gradient method for symmetric matrix, are available to solve the pressure equation and scalar transport equations. Depending on the size of the computational domain, the user can choose the solver that is best suited for a given problem. These three matrix solvers greatly increase the flexibility and efficiency of numerical computation for COMMIX-1C compared to previous codes.

- **Geometrical Package.** A special geometrical package has been developed and implemented to permit modeling of any complex geometry in the most storage-efficient way.

Volume I (Equations and Numerics) of this report describes in detail the basic equations, formulation, solution procedures, and models for auxiliary phenomena. Volume II (User's Guide and Manual) contains the input instruction, flow charts, sample problems, and descriptions of available options and boundary conditions.

COMMIX-PPC is a product of the continuing evolution of the family of COMMIX codes. The technical contents of the latest version of COMMIX-1C, when appropriate and relevant, will be duplicated here.

CONTENTS

Executive Summary.....	1
1 Introduction.....	3
1.1 Major Features of COMMIX-PPC.....	4
1.1.1 Porous-Medium Formulation.....	4
1.1.2 Fully Implicit Algorithm.....	5
1.1.3 Three Matrix Solvers.....	5
1.1.4 One-Dimensional Formulation for Tube-Side Flow.....	5
1.1.5 Geometry Package.....	5
1.1.6 Multicomponent System.....	6
1.2 Other Features of COMMIX-PPC.....	6
1.3 Organization of the Report.....	7
2 Governing Conservation Equations and Auxiliary Equations for Shell Side.....	8
2.1 Conservation Equations.....	8
2.2 Auxiliary Equations.....	9
2.2.1 Saturation Temperature.....	9
2.2.2 Mass Source.....	9
2.2.3 Physical Properties.....	10
3 General Form of the Conservation Equations	12
4 Control Volume.....	13
4.1 Construction of a Computational Cell.....	13
4.2 Control Volume for Nonflow Variables	16
4.3 Control Volume for Flow Variables.....	16
5 Finite-Volume Formulation	19
5.1 Convection Term.....	19
5.1.1 Main Control Volume	19
5.1.2 Momentum Control Volume.....	20
5.2 Diffusion Term	27
5.2.1 Main Control Volume	27
5.2.2 Momentum Control Volume.....	29
5.3 Unsteady Term	29
5.3.1 Main Control Volume	29
5.3.2 Momentum Control Volume.....	29
5.4 Source Term.....	32
5.5 General Finite-Volume Equation for the Main Control Volume.....	32
5.6 General Finite-Volume Equation for the z-Momentum Control Volume.....	33
6 Pressure Equation	38
7 Turbulence Modeling.....	40
7.1 Constant Turbulent Viscosity Model	40
7.2 k- ϵ Two-Equation Turbulence Model.....	42
7.2.1 Transport Equation for k.....	42

7.2.2	Transport Equation for ϵ	43
7.2.3	Sequence of Steps in the $k-\epsilon$ Two-Equation Turbulence Model	44
7.3	Boundary Conditions for Turbulence Transport Equations.....	45
7.3.1	Symmetry Boundary.....	45
7.3.2	Inlet and Outlet Boundaries.....	45
7.4	Wall-Function Treatment	46
7.4.1	A Wall-Function Model.....	47
7.4.2	Evaluating k and ϵ for Cells Adjacent to Walls.....	49
7.5	Solution Procedure for Calculating Turbulent Flows	51
7.6	Discussion..	51
8	One-Dimensional Formulation for Condenser Tube-Side Flow	53
8.1	Governing Conservation Equations	53
8.2	Finite-Volume Formulation.....	54
8.2.1	Control Volume.....	54
8.2.2	Finite Volume Equations for Continuity, Momentum, and Energy Conservation.....	54
8.2.2.1	Continuity Equation.....	54
8.2.2.2	Momentum Equation.....	55
8.2.2.3	Energy Equation.....	57
8.2.3	Pressure Equation	59
9	Auxiliary Relations and Supplementary Physical Models	59
9.1	Rigorous Fluid-Property Routines.....	59
9.2	Simplified Fluid-Property Option	60
9.3	Heat Transfer Correlations.....	60
9.3.1	Heat Transfer Correlation for Condensation of a Steam/Air Mixture in a Power Condenser.....	60
9.3.2	Heat Transfer Coefficient due to Presence of Noncondensable Air	61
9.3.3	Heat Transfer Coefficient of Film Condensation for a Tube Bank ..	62
9.3.3.1	Inundation Effect	63
9.3.3.2	Condensate Subcooling Effect	65
9.3.3.3	Vapor Shear Effect	65
9.3.4	Thermal Resistance of the Tube Wall.....	65
9.3.5	Thermal Resistance of the Fouling Layer.....	66
9.3.6	Heat Transfer Coefficient for the Flow of Cooling Water Inside a Tube	66
9.4	Structure/Fluid Momentum Interaction.....	66
9.5	Shell Side and Tube Side Thermal Coupling.....	68
9.5.1	Introduction.....	68
9.5.2	Geometrical Description.....	68
9.5.3	Governing Equation	69
9.5.4	Finite-Difference Formulations.....	69
9.5.4.1	Internal Cells.....	69
9.5.4.2	Outer Surface Cell.....	71
9.5.4.3	Inner Cell.....	72

9.5.5	Heat Transfer to Adjacent Fluid.....	74
9.5.6	Steam Condensation Rate.....	74
10	Initial and Boundary Conditions	75
10.1	Initial Conditions.....	75
10.2	Boundary Conditions	75
10.2.1	Fluid Velocity Boundary Conditions.....	75
10.2.2	Temperature Boundary Conditions.....	78
10.2.3	Pressure Boundary Conditions.....	82
10.3	Additional Options.....	83
11	Solution Procedures.....	84
11.1	Introduction	84
11.2	Fully Implicit Solution Sequence.....	84
11.3	Matrix Solvers	86
11.3.1	Successive Overrelaxation Iterative Scheme.....	86
11.3.2	Direct Matrix Inversion Method.....	86
11.3.3	Preconditioned Conjugate Gradient Method.....	87
11.3.4	Discussion	88
11.4	Iteration Criteria	88
12	Summary and Discussion	91
12.1	Major Features of COMMIX-PPC.....	91
12.1.1	Porous-Medium Formulation.....	91
12.1.2	Geometry Modeling	92
12.1.3	Matrix Solvers	92
12.1.4	Multicomponent Capability.....	93
12.1.5	Shell-Tube-Side Thermal Coupling.....	93
12.2	Code Application and Validation	94
12.3	Future Developments.....	94
	Acknowledgments	95
	References.....	95
	Appendix: Structure/Fluid Thermal Interaction.....	99

FIGURES

1	Construction of Cell Volumes.....	15
2	Cell Volume around Point 0 in i,j,k Notation.....	17
3	Staggered Grid.....	17
4	Momentum Control Volumes	18
5	Convective Fluxes for the Main Control Volume.....	20
6	Convective Fluxes and Average Velocities for the z-Momentum Control Volume.....	21
7	Diffusion Fluxes for the Main Control Volume.....	28
8	Diffusion Fluxes for the z-Momentum Control Volume.....	30
9	Control Volume for Field Variables.....	31
10	Two-Layer Wall-Function Model ($y_p > y_s$).....	48
11	Control Volume for Nonflow Variable	55
12	Control Volume for Flow Velocities.....	55
13	Control Volume for the Continuity Equation.....	55
14	Control Volume for the Momentum Equation.....	56
15	Control Volume for the Energy Equation.....	58
16	Component Parts of Thermal Resistances for Condensation of a Steam/Air Mixture.....	62
17	Condensate Film on Horizontal Tubes	64
18	Condensate Film on Staggered Tubes.....	64
19	Condenser Tube in a Flow Domain.....	69
20	Cross Section of Thermal-Structure Element	70
21	Energy Balance of Partition Cell ℓ	70
22	Energy Balance of Cell 1.....	72
23	Energy Balance of Cell L.....	73
24	Near-Boundary Cells.....	77
25	Model Suitable for Uniform Velocity at Outlet Option	79
26	Constant-Temperature Boundary.....	80

27	Nonconvective Constant-Temperature Boundary	80
28	Recommended Surface Arrangements for Pressure Boundary Condition.....	83
29	COMMIX-PPC Flow Chart	85
30	Grid Arrangement in a Two-Dimensional Piping System, Illustrating Storage Requirements in COMMIX-PPC	93
A.1	Flow Domain, Showing Cylindrical Structure.....	101
A.2	Element of Thermal Structure, Showing Outer and Inner Surfaces.....	101
A.3	Four Quarter-Cylindrical Structures, Each Interacting with One Fluid Cell.....	102
A.4	Typical Structure Element, Showing Material Regions and Gaps.....	102
A.5	Cross Section of a Thermal-Structure Element.....	103
A.6	Energy Balance of a Partition Cell ℓ	103
A.7	Energy Balance of Cell 1 Adjacent to Coolant.....	105
A.8	Cell Surrounded by Different Materials with Air Gap between Them	105
A.9	Cell with Adiabatic Boundary.....	107

TABLES

1	Source Terms in the Cartesian Coordinate System	14
2	Source Terms in the Cylindrical Coordinate System	14
3	Transformations for Cartesian and Cylindrical Coordinate Systems	15
4	Convention Used in COMMIX-PPC to Define Neighboring-Cell Control Volumes.....	16
5	Convention Used in COMMIX-PPC to Define Neighboring Control Volumes for z-Direction Momentum Equations.....	18
6	Convective Fluxes for the Main Control Volume.....	21
7	Convective Fluxes for the z-Momentum Control Volume.....	26
8	Diffusion Strengths for the Main Control Volume	28
9	Diffusion Strengths for the z-Momentum Control Volume.....	30
10	Fully Implicit Finite-Volume Equation for the Main Control Volume and Its Coefficients.....	34
11	Coefficients of the Fully Implicit Finite-Volume Equation for the z-Momentum Control Volume.....	37
12	Coefficients of the Pressure Equation.....	41
13	Fully Implicit Solution Sequence for Turbulent Flows.....	52
14	Summary of Constants Employed in the k- ϵ Two-Equation Turbulence Model	53
15	Fluid Velocity Boundary Options.....	76
16	Suitable Temperature Boundary Options.....	79
17	Fully Implicit Solution Sequence.....	87
18	Properties of the Three Matrix Solvers in COMMIX-PPC	89
19	Convergence Criteria for the Iterative Scheme and the Iterative Matrix Solvers Used in COMMIX-PPC	90

Executive Summary

The COMMIX (*Component Mixing*) code is a general-purpose computer program for the analysis of fluid flow in real-world engineering systems. Because the needs of users have changed since its inception in 1976, the code has undergone several stages of development, and several versions/extensions are now available. The present COMMIX-PPC is yet another extension, designed specifically for analyzing the performance of power plant condensers. To meet the objective of this application, the following two major additions have been incorporated into the code.

- The three-dimensional conservation equations for shell-side flow have been extended to treat the flow of a multicomponent medium. This is necessary because the shell side generally contains a mixture of steam and air. The capability to treat the flow of a multicomponent medium is also essential for assessing the effect of noncondensibles on condenser performance. On the other hand, the computation is simplified by assuming that the steam is at the saturated state and its bulk temperature is determined solely by its partial pressure in the mixture.
- Tube-side fluid flow and heat transfer have been developed and incorporated into the code. The use of one-dimensional conservation equations of mass, momentum, and energy for tube-side flow greatly reduces the required computer time without sacrificing accuracy. It also facilitates handling of thermal coupling between the condensation of vapor on the shell side and the forced convection of a single-phase liquid on the tube side.

In addition to the foregoing two major additions, several minor modifications and additions have been made, mainly dictated by the consideration of condensation of steam in the presence of noncondensibles. However, it is emphasized that many of the salient features of COMMIX are retained in COMMIX-PPC.

A major unique feature of COMMIX is its porous-medium formulation, which was rigorously derived through local volume averaging. The formulation makes use of the concept of volume porosity, directional surface porosity (a dimensionless vector quantity associated with a surface element), distributed resistance, and distributed heat source or sink. Volume porosity is the ratio of the volume occupied by fluid in a control volume to the total control volume. Surface porosity is similarly defined as the ratio of the area available for fluid flow through a control surface to the total control surface area. Both arise naturally in the averaging process. In the conventional porous-medium formulation, only the volume porosity, distributed resistance, and distributed heat source are used. The concept of directional surface porosity is relatively new. It facilitates the modeling of anisotropic structural resistance to flow. Irregular geometries can also be adapted in the present porous-medium formulation.

The predictive capability of the numerical analysis of fluid flow and heat transfer in complicated engineering systems, e.g., nuclear reactor cores or the shell side of a steam condenser, depends strongly on how well the distributed resistances are modeled. The resistances would vary with their orientation relative to the general flow direction and are often not known *a priori*. The directional surface porosity is a geometrical quantity and can be accurately and unambiguously calculated. Its introduction lessens the dependency of the

velocity field on the modeling of the flow resistance and hence, improves the accuracy of the numerical prediction. This is a major advantage of the present porous-medium formulation.

The finite-volume formulation used in COMMIX for the mass, momentum, and energy conservation equations has recently been extended to include variable-density flows. The modified formulation employs the concept of a volume-average mass-weighted velocity. As a consequence, the numerical procedure is more robust than the previous COMMIX versions. It also forces the location of pressure change to coincide with that of density change in one-dimensional flows. In addition, the discretized momentum equation also satisfies the one-dimensional Bernoulli equation.

The COMMIX code provides detailed implied velocity and temperature fields for the system under consideration. The conservation equations of mass, momentum, and energy, and the transport equations of the turbulence parameters are solved as a boundary-value problem in space and an initial-value problem in time. The discretized equations are obtained by integrating the conservation equations over a control volume. The code is flexible and has a wide range of applicability. It is capable of solving thermal-hydraulic problems involving either a single engineering component, such as a rod bundle, reactor plenum, piping system, or heat exchanger, or an engineering system that consists of a combination of these components.

COMMIX uses a fully implicit solution scheme called SIMPLEST-ANL. It is a modification of the well-known numerical procedure SIMPLER, has a modular structure, and permits the use of either Cartesian or cylindrical coordinate systems. COMMIX-PPC contains physical-property packages for water vapor and liquid water. In addition to these two packages, an option is available for users to input simplified property correlations that are valid in the desired range of applications.

There are three matrix solvers in COMMIX-PPC: the successive overrelaxation method (SOR), the direct matrix inversion method (DMIM), and the preconditioned conjugate gradient method (PCG). SOR and DMIM are suitable for both symmetric and nonsymmetric matrices and are selected for solving the pressure equation and scalar transport equations. PCG is only applicable to a symmetric matrix and thus may be used for the pressure equation. Depending on the size of the matrix, the user may choose the particular solver that is best suited for the problem in question. With the availability of the three matrix solvers, the efficiency of the numerical computation capability of COMMIX-PPC is greatly increased.

Another unique feature of the COMMIX code is its geometry package. The basic concept is to use computational cells (either in Cartesian or cylindrical coordinates) as building blocks that are stacked to approximate the shape of the physical systems under consideration. Then, volume porosity and directional surface porosity are used to account for differences between the geometry used in the computation and the actual configuration. This feature permits the COMMIX code to model irregular and complex geometries with relative ease. Furthermore, the computer storage requirement of the COMMIX code is optimized; only the computational cells used in the calculations are counted.

Volume I, Equations and Numerics, of this report describes in detail the basic conservation equations, finite-volume formulation, turbulence modeling, one-dimensional

treatment of tube-side flow, and solution procedures. Auxiliary models for the following phenomena are also described:

- Momentum interaction between fluid and stationary solid structures.
- Thermal interaction between shell- and tube-side fluid and stationary solid structures.

In Volume II, User's Guide and Manual, we provide flow charts, descriptions of subroutines, geometry modeling, initialization procedures, input descriptions, etc. A sample problem is included to familiarize readers with the input/output structures of the code. Also included is a sensitivity study about the effects of inlet air mass fraction and exit mass flow rate at the air extraction pipe on steam condensation rate.

In both volumes, wherever applicable, technical content of COMMIX-1C is duplicated.

1 Introduction

In the power industry, one way to save energy and reduce operating cost of a power plant is to improve condenser performance. This requires detailed information on the heat- and mass-transfer rates and pressure drop at the local level. Because the heat- and mass-transfer processes associated with steam flow in a condenser is complex and the local rates are difficult to measure experimentally, one resorts to numerical models to obtain such information.

In the past three decades, several condenser models¹⁻⁸ have been developed to study fluid flow and heat transfer in power plant condensers or power condensers. All are two-dimensional models. Because the steam flow in power condensers is essentially three-dimensional, these models cannot provide detailed information on pressure, temperature, velocity, and concentration distribution. Hence, they are not useful for studying optimization of tube arrangement, baffle plate shape and spacing, and configuration of other components to improve condenser performance.

A three-dimensional computer code, COMMIX-PPC (power plant condenser), is being developed at Argonne National Laboratory to analyze the performance of power plant condensers. This three-dimensional code is an offshoot of the in-house version of the COMMIX-2A computer code, which is intended for two-phase applications in a reactor component or a multicomponent reactor system. It was developed under U.S. Nuclear Regulatory Commission sponsorship and, due to funding limitations, has yet to be completed. COMMIX-2A is a product of the development, over many years, of a series of COMMIX codes.⁹⁻¹²

COMMIX-PPC is designed to analyze three-dimensional, transient or steady state, laminar or turbulent, multicomponent flow in power plant condensers. The tube nest, or bundle, is treated as a porous medium. On the shell side, the present model considers a mixture of only steam and air. Unless the rate and locations of air leakage are known, air is assumed to be uniformly mixed in inlet steam. As the air and steam mixture flows past the tube bundle, condensed water is assumed to be removed instantaneously. The steam is taken to be saturated. Cooling water on the tube side is modeled as a one-dimensional

single-phase flow; hence, large storage capacity for tube-side variables is not needed. Also, because the steam is taken to be saturated, its temperature can be calculated directly from the equation of state once the pressure is known. Thus, the mixture energy on the shell side is not needed. To economize on storage and reduce the size of the matrix for solving the dependent variables, we decided to handle tube-side and shell-side flows sequentially. COMMIX-PPC solves the three-dimensional, time-dependent, conservation equations of mixture mass, mixture momentum, and a component mass, either air or steam, for shell-side flow, and the one-dimensional conservation equations of mass, momentum, and energy for the tube-side flow. The shell-side and tube-side flow are coupled through the heat transfer process. The solution is obtained by an iterative procedure.

Although COMMIX-PPC is designed for power condenser calculations, it can also be used as a general-purpose computer code for analyzing single-phase flow in complex engineering systems with minimal or no modifications.

1.1 Major Features of COMMIX-PPC

1.1.1 Porous-Medium Formulation

As do all codes in the COMMIX series, COMMIX-PPC employs conservation equations of mass, momentum, and a component mass using a new porous-medium formulation based on local volume averaging.¹³⁻¹⁹ The formulation utilizes four parameters, i.e., volume porosity, directional surface porosity, distributed flow resistance, and distributed heat source (sink), to model fluid-dynamic and thermal effects of internal solid structures. In the conventional porous-medium formulation, only three parameters (volume porosity, distributed resistance, and distributed heat source) are used. The addition of a fourth parameter, directional surface porosity,¹³⁻²¹ is a relatively new concept.

Volume porosity is defined as the ratio of the volume occupied by fluid in a control volume to the total control volume. The directional surface porosity is similarly defined as the ratio of the area available for fluid flow through a control surface to the total control surface area. The adjective "directional" was incorporated to emphasize the fact that surface porosity is an anisotropic quantity.

Introducing the fourth parameter, directional surface porosity, has distinct advantages. First, the need for introducing distributed resistance and directional surface porosity arises naturally in volume averaging of the governing conservation equations.¹⁷ Second, in the thermal-hydraulic analysis of complex systems, be it a reactor core or power condenser, the flow resistance due to internal structures, e.g., tube bundle and irregular geometry such as baffles or other flow obstacles, is generally not reliably known; however, it can be modeled separately as a distributed resistance in the control volume and a directional surface porosity of the control surface. The latter is a purely geometrical parameter and can be unambiguously calculated. Thus, in the new porous-medium formulation, the numerical results depend only on how well the distributed resistance is modeled. This is a definite improvement over the conventional porous-medium formulation, in which the effects of the distributed resistance in the control volume and the flow restriction at the control surface are intermingled and thus are more difficult to assess. The concept of incorporating directional surface porosity greatly facilitates the modeling of velocity and

temperature fields in anisotropic media and, in general, improves resolution and accuracy. Another useful feature of the new porous-medium formulation is that irregular geometry can be more conveniently treated.

If we set the directional surface porosity equal to one, the new formulation reduces to the conventional porous-medium formulation. Therefore, we can consider the conventional porous-medium formulation as a subset of the new porous-medium formulation. Furthermore, if we set the volume porosity equal to one and the distributed flow resistance and heat source equal to zero, the porous-medium formulation reduces to a continuum formulation. Thus, the new porous-medium formulation can be considered a generalization of the approach to thermal-hydraulic analysis.

1.1.2 Fully Implicit Algorithm

A fully implicit algorithm named SIMPLEST-ANL¹⁰ is used. This algorithm is a modification of the Patankar-Spalding numerical procedure²² known as SIMPLE/SIMPLER. It is particularly suitable for analyzing steady-state systems, although it can also be used for slow and moderate transients.

1.1.3 Three Matrix Solvers

All discretized equations in COMMIX-PPC can be expressed in the following form:

$$a_0^* \phi_0 - \sum_{i=1}^6 a_i^* \phi_i - b_0^* = 0,$$

where ϕ is a dependent variable and a and b are coefficients. The subscript 0 stands for the centerpoint, and the subscript i stands for the indices of the six neighboring points. This general form of the discretized equation lends itself to various solution schemes. In COMMIX-PPC, three matrix solvers [successive over-relaxation (SOR), direct matrix inversion method (DMIM), and preconditioned conjugate gradient (PCG)] are available and the user can choose any one of them to solve the discretized equations.

1.1.4 One-Dimensional Formulation for Tube-Side Flow

In COMMIX-PPC, the shell-side and tube-side flow are calculated sequentially. The shell-side flow uses a three-dimensional formulation, whereas the tube-side flow is solved by a one-dimensional formulation. A great deal of computer storage for tube-side flow variables is saved. Both shell-side and tube-side flows are coupled thermally and their final solutions are obtained by an iterative procedure.

1.1.5 Geometry Package

The geometry package developed and implemented in several previous versions of COMMIX is retained in COMMIX-PPC. This package is capable of approximating any irregular geometry. It uses basic computational cells as building blocks to model the geometry under consideration. Volume porosities and directional surface porosities are

then used to account for differences between the approximated computation and the actual configuration.

To save computer storage, a computational cell is defined by one number rather than by its conventional (i, j, k) location, where i, j, and k are the computational cell indices in the three principal axes (e.g., x, y, and z in the Cartesian coordinate system). With this approach, the storage requirement depends only on the total number of computational cells and not on the value of the product IMAX x JMAX x KMAX, where IMAX, JMAX, and KMAX denote the maximum values of computational cell indices in the three corresponding principal axes.

A normal three-dimensional computational cell has six surfaces. To facilitate proper modeling of a cell of complex and irregular geometry (most geometries in engineering systems are complex and irregular), the code provides the flexibility of allowing a user to specify an additional seventh surface, called irregular surface, to cut a computational cell for simulating the physical geometry.

1.1.6 Multicomponent System

For analysis of condenser performance, it is necessary to predict steam and air distribution inside a condenser. Thus, the code also must have a multicomponent capability.

1.2 Other Features of COMMIX-PPC

COMMIX-PPC comprises

- Two models to give it a wide range of applications in turbulent flows:
 - Constant turbulent diffusivity model.
 - Two-equation k- ϵ turbulence model.
- Discretized conservation equations that are formulated by integrating the differential conservation equations and transport equations for turbulence parameters over a control volume surrounding a grid point. Thus, the derivation process and resulting equations have direct physical meaning, and the solution satisfies conservation principles.
- An option that allows use of either Cartesian or cylindrical coordinates.
- A modular structure that permits rapid implementation of the latest available drag models, heat transfer models, etc.
- A built-in property data bank for water and water vapor, with an option that permits the use of simplified property correlations for any fluids and solid structures.
- A generalized resistance model to permit specification of resistance due to internal structures (baffles, tube plates, tube bundles, etc.) in the respective coordination directions.

- A generalized thermal-structure formulation to model thermal interaction between structures (duct wall, tube bundles, baffles, etc.) and surrounding fluid.
- The possibility of heat source/sink and boundary conditions being functions of time.
- A structure that permits solution of one-, two-, or three-dimensional calculations.

1.3 Organization of the Report

This volume describes the formulations of the governing conservation equations for three-dimensional, steady-state and transient multicomponent fluid flow with heat transfer. The description starts with differential equations and focuses attention on numerical methods incorporated into the COMMIX-PPC program. Section 2 presents the governing conservation equations appropriate for condenser modeling. Section 3 is devoted to the general form of governing conservation equations for a quasicontinuum domain, with the purpose of providing the basis for unified development of the numerical method and the construction of the computer program. The quasicontinuum domain is defined as one that contains finite, dispersed, stationary, heat-generating (or absorbing) solid structures. The fluid dynamic and thermal effects of solid structures in the domain are accounted for by introducing volume porosity, directional surface porosity, distributed flow resistance, and distributed heat sources. Section 4 describes the staggered-grid arrangement and the conventions used in COMMIX-PPC to define the location of a control volume. Section 5 assembles the finite-volume equations. The general finite-volume equation of the main control volume is presented in Sec. 5.5. Because a staggered-grid system is used, the control volumes for momentum equations are different and require special consideration. The special features of the momentum finite-volume equations are presented in Sec. 5.6. The pressure appearing in the momentum equation must be such that the velocity distribution obtained satisfies the continuity equation. The derivation of the pressure equation (obtained by combining the momentum and continuity equations) is presented in Sec. 6.

Section 7 is devoted to turbulence modeling. Currently, two options are available to account for turbulence effects:

- *Constant Turbulent Diffusivity Model.* This model is the simplest. The turbulent viscosity and turbulent thermal conductivity are simply assumed constant and assigned a value. No transport equation of turbulence parameters is solved.
- *The k- ϵ Two-Equation Turbulence Model.* The transport equations of turbulence kinetic energy k and dissipation rate ϵ of turbulence kinetic energy are solved to evaluate turbulence quantities. This model is more general than the Prandtl mixing-length hypothesis and the one-equation turbulence model and is computationally more economical than the complex multiequation models of turbulence that are still in the developmental stage.

Section 8 describes the one-dimensional formulation of the conservation equations for tube-side flow. Section 9 describes the supplementary models incorporated in COMMIX-PPC. These include heat transfer correlations for single-phase flow inside tubes and for film condensation outside a tube bank in the presence of entrained air, as well as generalized force and thermal-structure models. The force model computes distributed resistance to account for the friction between fluid and submerged solids. The thermal-structure model is designed to compute the distributed heat source (fluid and submerged solids) and the thermal inertia of submerged solids. This section describes only the shell- and tube-side thermal coupling. A more generalized thermal-structure model is presented in the Appendix.

Several boundary-condition options for momentum, continuity, temperature, and continuity mass equations are described in Sec. 10. In COMMIX-PPC, the fully implicit solution scheme SIMPLEST-ANL, an extension of the numerical procedures in SIMPLE/SIMPLER, is used. A scheme is described in Sec. 11. The three matrix solvers (SOR, DMIM, and PCG) available in COMMIX-PPC for solving the discretized scalar transport equations and the pressure equation are also described in Sec. 11.

Volume II of this report is prepared specifically for COMMIX-PPC users. It describes the steady-state and transient calculation and the various procedures in the preparation of load modules, input data, reading and writing of restart files, etc. A sample problem, along with its description, input, and output, is presented to provide an introduction to the capabilities of COMMIX-PPC. The code input description is also included in Volume II.

2 Governing Conservation Equations and Auxiliary Equations for Shell Side

2.1 Conservation Equations

The three-dimensional time-dependent conservation equations of mass and momentum for gas mixtures, based on the porous-medium formulation through local volume averaging¹⁷ are

Mixture continuity equation

$$\gamma_v \frac{\partial}{\partial t}(\rho) + \nabla \cdot (\gamma_A \rho \bar{v}) = \gamma_v \dot{m}''' \quad (2.1)$$

Component continuity equation

$$\gamma_v \frac{\partial}{\partial t}(\rho x_k) + \nabla \cdot (\gamma_A x_k \rho \bar{v}) = \gamma_v \dot{m}_k''' + \nabla \cdot (\gamma_A \rho D_{k,eff} \nabla x_k) \quad (2.2)$$

Mixture momentum equation

$$\gamma_v \frac{\partial}{\partial t}(\rho \bar{v}) + \nabla \cdot (\gamma_A \rho \bar{v} \bar{v}) = -\gamma_v \nabla P - \nabla \cdot (\gamma_A \mu_{eff} \nabla \cdot \bar{v}) + \gamma_v \rho \bar{g} + \gamma_v R + \gamma_v \dot{m}''' \bar{v} \quad (2.3)$$

where

k = component gas,
 ρ = mixture density, kg/m³,
 γ_A = surface porosity,
 γ_v = volume porosity,
 x_k = mass fraction for k , $\sum x_k = 1$,
 \dot{m}_k = mass source for k , kg/m³/s,
 \dot{m} = $\sum \dot{m}_k$,
 \bar{v} = velocity vector, m/s,
 P = mixture pressure, Pa,
 \bar{g} = gravitational constant, m/s²,
 μ_{eff} = $\mu_m + \mu_{turb}$ = effective viscosity of mixture, kg/m/s,
 μ_m = molecular viscosity of gas mixture, kg/m/s,
 μ_t = turbulence viscosity of gas mixture, kg/m/s,
 $D_{k,eff}$ = $D_{k,m} + D_{k,t}$ = effective diffusivity for k in the gas mixture, m²/s,
 $D_{k,m}$ = molecular diffusivity for k in the gas mixture, m²/s,
 $D_{k,t}$ = turbulent diffusivity for k in the gas mixture, m²/s,
 \bar{R} = distributed resistance per unit volume, N/m³.

2.2 Auxiliary Equations (appropriate for condensing steam under saturated condition)

2.2.1 Saturation Temperature (T_s)

$$T_s = T(P_s) \quad (2.4)$$

$$P_s = \frac{x_s}{x_s + x_a \frac{M_s}{M_a}} P \quad (2.5)$$

where

P_s = partial pressure of steam,
 P = total pressure of steam and air mixture.
 M_s = molecular weight of steam,
 M_a = molecular weight of air
 x_a = mass fraction of air
 x_s = mass fraction of steam

2.2.2 Mass Source (\dot{m}_s)

The steam condensation rate per unit volume, \dot{m}_s , can be defined by

$$\dot{m}_s = \frac{\dot{q}''}{h_{fg}}, \quad (2.6)$$

where h_{fg} is the latent heat of steam, and \dot{q}'' is the heat transfer rate from steam to cooling water per unit volume.

The value of \dot{q}'' can be calculated from

$$\dot{q}'' = UA^*(T_s - T_w), \quad (2.7)$$

where U is the overall heat transfer coefficient, A^* is the heat transfer area per unit volume, T_s is the saturation temperature, determined completely by the local partial pressure of the steam, and T_w is the temperature of the local tube-side cooling water.

2.2.3 Physical Properties

Mixture density (ρ)

The density of the gas mixture ρ is obtained from

$$\rho = \frac{1}{\sum_k \frac{x_k}{\rho_k}}, \quad (2.8)$$

where x_k is the mass fraction of k , and ρ_k is the density of component k .

Mixture enthalpy (h)

The enthalpy of the gas mixture h is calculated from

$$h = \sum_k x_k h_k. \quad (2.9)$$

where h_k is the enthalpy of k .

Mixture specific heat (C_p)

The specific heat of the gas mixture C_p can be obtained from

$$C_p = \sum_k x_k C_{pk}. \quad (2.10)$$

where C_{pk} is the specific heat of k .

Mixture molecular viscosity (μ_m)

The viscosity of a gas mixture μ_m is calculated by the method of Slattery and Bird et al.²³ It is given by the approximate equation

$$\mu_m = \frac{\sum_{i=1}^N n_i \mu_i}{\sum_{j=1}^N n_j \Phi_{ij}} \quad \text{for } i = 1, 2, \dots, N, j = 1, 2, \dots, N \quad (2.11)$$

where

$$\Phi_{ij} = \frac{\left[1 + \left(\frac{\mu_i}{\mu_j} \right)^{1/2} \left(\frac{M_j}{M_i} \right)^{1/4} \right]^2}{2\sqrt{2} \left[1 + M_i/M_j \right]^{1/2}}. \quad (2.12)$$

$$n_i = \frac{\frac{x_i}{M_i}}{\sum_{j=1}^N \frac{x_j}{M_j}}. \quad (2.13)$$

μ_i and μ_j = viscosity of the component gases,
 n_i and n_j = mole fraction of the component gases,
 M_i and M_j = molecular weight of the component gases,
 n = total number of components in the gas mixture.

Turbulent viscosity (μ_t)

In COMMIX-PPC, two options are available for calculating the turbulent viscosity μ_t . They are

- Constant turbulent diffusivity model, and
- Two-equation, $k-\epsilon$ turbulence model.

Details of the $k-\epsilon$ turbulence model are given in Sec. 7.

Mixture molecular conductivity (k_m)

Similar to the mixture viscosity calculation, the molecular conductivity of the gas mixture k_m is calculated from

$$k_m = \frac{\sum_{i=1}^N n_i k_i}{\sum_{j=1}^N n_j \Phi_{ij}}. \quad (2.14)$$

where k_i is the molecular conductivity of the component gas i , and Φ_{ij} and n_i are given by Eqs. 2.12 and 2.13, respectively, with μ_i replaced by k_i .

Molecular diffusivity of steam or air in an air mixture ($D_{k,m}$)

For a steam and air mixture, the diffusivity between steam and air $D_{k,m}$ is calculated from the equation developed by Slattery and Bird,²³ i.e.,

$$\frac{PD_{S,A}}{(P_{C,A}P_{C,S})^{1/3}(T_{C,A}T_{C,S})^{5/12}\left(\frac{1}{M_A} + \frac{1}{M_S}\right)^{1/2}} = 3.64 \times 10^{-4} \left(\frac{T}{\sqrt{T_{CA}T_{CS}}}\right)^{2.334} \quad (2.15)$$

where the subscripts S and A refer to steam and air respectively, P is pressure, T is temperature, P_C is the critical pressure, T_C is the critical temperature, and M is the molecular weight. The units for D, P, T, and M are (cm²/sec), (atm), (K), and (g/g-mole), respectively. Note that Eq. 2.15 is applicable for binary gas mixtures only.

Inserting the following values for air and steam systems,

$$\begin{aligned} M_A &= 28.97 \text{ g/g-mole} & M_S &= 18.02 \text{ g/g-mole,} \\ P_{C,A} &= 36.4 \text{ atm} & R_{C,S} &= 218 \text{ atm,} \\ T_{C,A} &= 132 \text{ K} & T_{C,S} &= 647.3 \text{ K,} \end{aligned}$$

Eq. 2.15 becomes

$$D_{k,m} = 4.3421 \times 10^{-11} \frac{T^{2.334}}{P} (\text{m}^2 / \text{sec}). \quad (2.16)$$

Turbulent diffusivity ($D_{k,t}$)

The turbulent diffusivity of steam or air in a steam/air mixture $D_{k,t}$ is defined as

$$D_{k,t} = \frac{\mu_t}{\rho S_{ch}}, \quad (2.17)$$

where μ_t is the mixture turbulent viscosity, ρ is the mixture density, and S_{ch} is the Schmidt number. In this report, the Schmidt number is taken to be unity. Thus,

$$D_{k,t} = \mu_t / \rho. \quad (2.18)$$

3 General Form of the Conservation Equations

The conservation equations of mass and momentum for a mixture, and the component continuity equation possess a common form. If we denote the general dependent variable by ϕ , the equations in the Cartesian coordinate system can be expressed as¹⁵

$$\underbrace{\frac{\partial}{\partial t}(\gamma_v \rho \phi)}_{\text{Unsteady}} + \underbrace{\frac{\Delta(\gamma_x \rho u \phi)}{\Delta x} + \frac{\Delta(\gamma_y \rho v \phi)}{\Delta y} + \frac{\Delta(\gamma_z \rho w \phi)}{\Delta z}}_{\text{Convection}}$$

$$= \underbrace{\frac{\Delta \left(\gamma_x \Gamma_\phi \frac{\partial \phi}{\partial x} \right)}{\Delta x} + \frac{\Delta \left(\gamma_y \Gamma_\phi \frac{\partial \phi}{\partial y} \right)}{\Delta y} + \frac{\Delta \left(\gamma_z \Gamma_\phi \frac{\partial \phi}{\partial z} \right)}{\Delta z}}_{\text{Diffusion}} + \underbrace{\gamma_v S_\phi}_{\text{Source}}. \quad (3.1)$$

Here, u , v , and w are the velocities in the x , y , and z directions, respectively; γ_v is the volume porosity (fraction of the volume occupied by the fluid), γ_x , γ_y , and γ_z are the directional surface porosities (fraction of the surface area that is unobstructed to fluid flow) in the x , y , and z directions, respectively, and Γ is the diffusion coefficient. The convective and diffusive terms $\Delta(\phi)/\Delta x_i$ in Eq. 3.1 are defined as

$$\frac{\Delta(\phi)}{\Delta x_i} = \frac{\phi(x_i + \Delta x_i/2) - \phi(x_i - \Delta x_i/2)}{\Delta x_i}, \quad (3.2)$$

in which x_i stands for the x , y , or z coordinate. The diffusion coefficient Γ_ϕ and the source term S_ϕ are specific to each ϕ . The conservation equations in the cylindrical coordinate system have the same general form (Eq. 3.1) when the centrifugal and Coriolis force terms are included in the source term S_ϕ . (The source terms for equations in the Cartesian and cylindrical systems are listed in Tables 1 and 2, respectively.) Therefore, all formulations in the Cartesian system can be readily transferred to cylindrical coordinates by using the relationships shown in Table 3.

For turbulent flow, the entities in Eq. 3.1 are their time averages, and the diffusion coefficient Γ is, as the effective diffusion coefficient, the sum of two contributions, molecular and turbulent. Thus,

$$\Gamma_\phi = \Gamma_{\phi, \text{molecular}} + \Phi_{\phi, \text{turbulent}}. \quad (3.3)$$

The transport equations for the turbulence parameters, kinetic energy k and dissipation rate ϵ that are needed for the computation of the turbulent coefficient, also have the same general form as Eq. 3.1. However, for the convenience of presentation, they will be discussed in Sec. 7.

4 Control Volume

4.1 Construction of a Computational Cell

The computational cells around a grid point can be defined in several ways. In COMMIX-PPC, the computational cell is defined by the locations of cell volume faces, and a grid point is placed in the geometrical center of each cell volume. Cell sizes can be nonuniform. This type of construction is shown in Fig. 1. The convention used in COMMIX-PPC for defining neighboring cells and cell faces is given in Table 4.

Table 1. Source terms in the Cartesian coordinate system^a

Equation	Variable (ϕ)	Direction	Diffusion Coefficient (Γ_ϕ)	Source Term (S_ϕ)
Continuity	1	Scalar	0	\dot{m}'''
Momentum				
(i)	u	x	μ_{eff}	$\rho g_x + V_x - R_x - \left(\frac{\partial p}{\partial x}\right) + \dot{m}'''u$
(ii)	v	y	μ_{eff}	$\rho g_y + V_y - R_y - \left(\frac{\partial p}{\partial y}\right) + \dot{m}'''v$
(iii)	w	z	μ_{eff}	$\rho g_z + V_z - R_z - \left(\frac{\partial p}{\partial z}\right) + \dot{m}'''w$
Component mass	x_k	Scalar	$\rho D_{k,\text{eff}}$	\dot{m}_k'''

^a V_x, V_y, V_z Balance of the viscous diffusion terms R_x, R_y, R_z Distributed resistances due to solid structures in a momentum control volumeTable 2. Source terms in the cylindrical coordinate system^a

Equation	Variable (ϕ)	Direction	Diffusion Coefficient (Γ_ϕ)	Source Term (S_ϕ)
Continuity	1	Scalar	0	\dot{m}'''
Momentum				
(i)	v_r	r direction	μ	$\rho \frac{v_r^2}{r} + \rho g_r + V_r - R_r - \frac{1}{r} \frac{\partial}{\partial r}(rp) + \dot{m}'''v_r$
(ii)	v_θ	θ direction	μ	$-\frac{\rho v_r v_\theta}{r} + \rho g_\theta + V_\theta - R_\theta - \frac{1}{r} \frac{\partial}{\partial \theta}(P) + \dot{m}'''v_\theta$
(iii)	v_z	z direction	μ	$\rho g_z + V_z - R_z - \frac{\partial}{\partial z}(p) + \dot{m}'''v_z$
Component mass	x_k	Scalar	$\rho D_{k,\text{eff}}$	\dot{m}_k'''

^aCentrifugal force term designated by *

Coriolis force term designated by **

 V_r, V_θ, V_z = balance of the viscous diffusion terms R_x, R_θ, R_z = distributed resistances due to solid structures in a momentum control volume

Cartesian Coordinates	Cylindrical Coordinates
x	r
y	θ
z	z
Δx	Δr
Δy	$r\Delta\theta$
Δz	Δz
u	v_r
v	v_θ
w	v_z

Table 3. Transformations for Cartesian and cylindrical coordinate systems

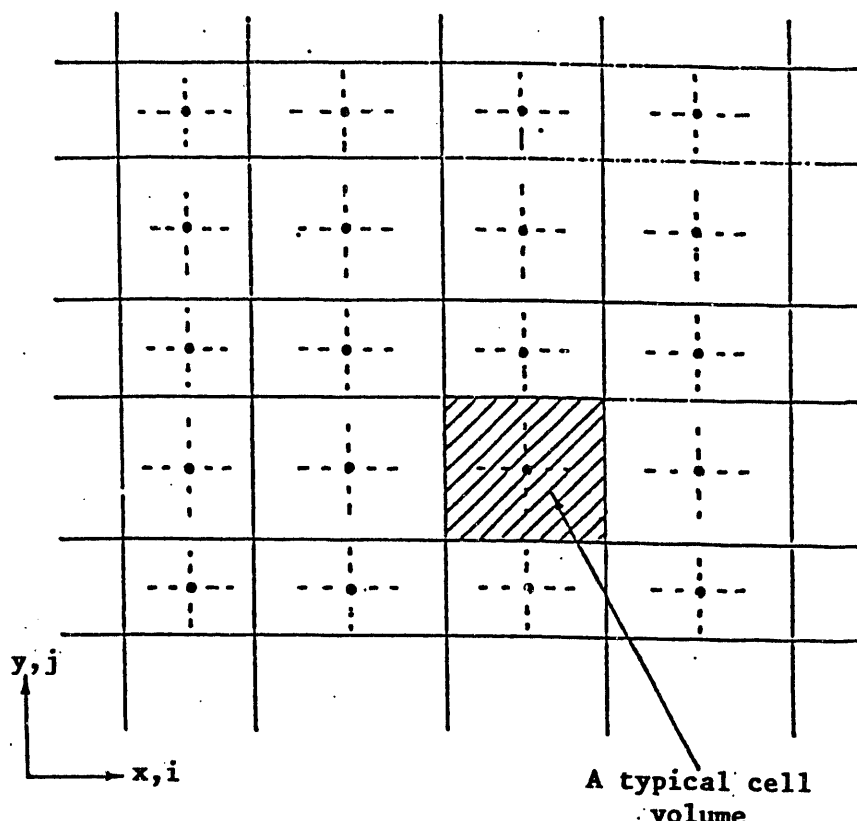


Fig. 1. Construction of cell volumes

Table 4. Convention used in COMMIX-PPC to define neighboring-cell control volumes

Subscript	Cell Centers			Cell-Face Center		
	x	y	z	x	y	z
0	i,	j,	k	-	-	-
1	i-1,	j,	k	i-1/2,	j,	k
2	i+1,	j,	k	i+1/2,	j,	k
3	i,	j-1,	k	i,	j-1/2,	k
4	i,	j+1,	k	i,	j+1/2	k
5	i,	j,	k-1	i,	j,	k-1/2
6	i,	j,	k+1	i,	j,	k+1/2

4.2 Control Volume for Nonflow Variables

A staggered-grid system is used in COMMIX. In this system, all dependent nonflow variables (pressure, temperature, density, enthalpy, mass fraction, turbulence kinetic energy, physical properties, etc.) are calculated for the cell center and all flow variables (velocity components) are calculated for the surfaces of the cell.

Consider the control volume for a nonflow variable as shown in Fig. 2. It is constructed around a grid point 0, which has grid points 1 ($i-1$), and 2 ($i+1$) as its west and east neighbors; grid points 3 ($j-1$) and 4 ($j+1$) as its front and rear neighbors; and grid points 5 ($k-1$) and 6 ($k+1$) as its south and north neighbors. To obtain the finite-volume equation, we integrate, step by step, each term of the conservation equation over the control volume.

4.3 Control Volume for Flow Variables

Although most dependent variables are calculated for a grid point, the velocity components u , v , and w are exceptions. They are calculated not for the grid point, but for displaced or "staggered" locations. The displaced locations of the velocity components are such that they are placed on the faces of a control volume. Thus, the k -component velocity w is calculated at the faces normal to the k direction.

Figure 3 shows the locations of u and w by short arrows on a two-dimensional grid; the three-dimensional counterpart can be easily visualized. Relative to a grid point, the u location is displaced only in the i direction, the w location only in the k direction, and so forth. The location for w thus lies in the k direction link, joining two adjacent grid points. It is the pressure difference between these grid points that will be used to drive the velocity w located between them. This is the main feature of the staggered grid.

A direct consequence of the staggered grid is that the control volumes to be used for the conservation of momentum must also be staggered. The control volumes shown in Figs. 1 and 2 will hereafter be referred to as the main control volumes. The control

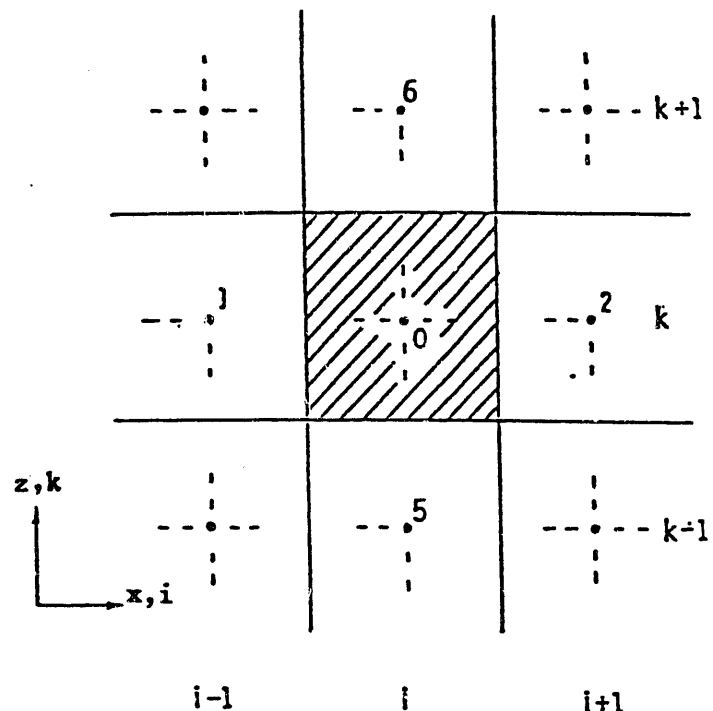


Fig. 2. Cell volume around point 0 in i,j,k notation

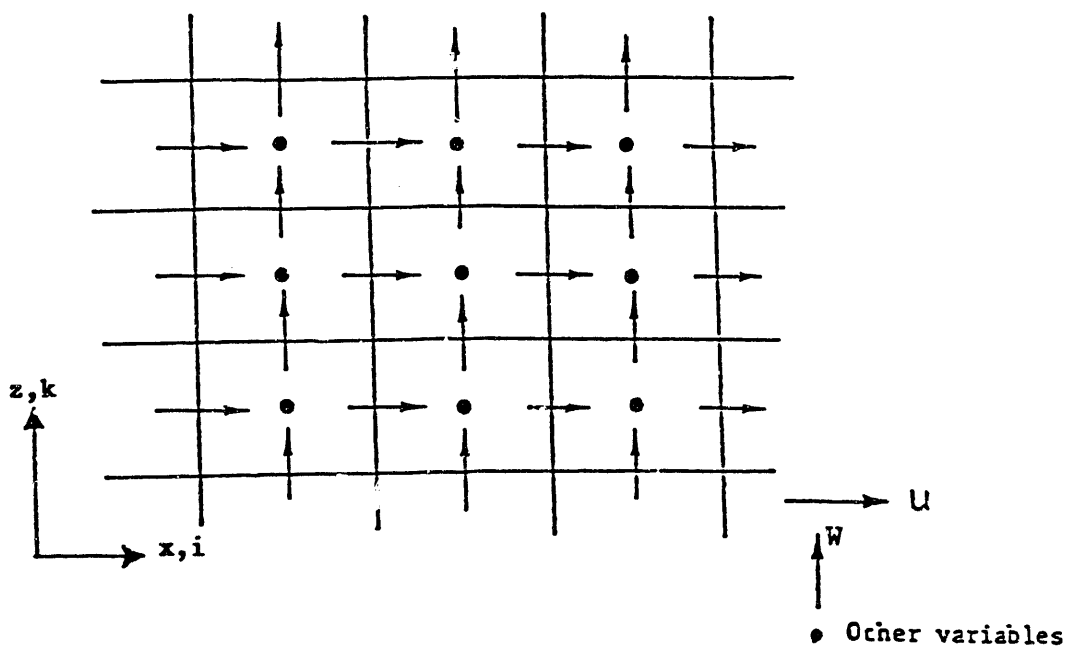


Fig. 3. Staggered grid

volumes for momentum will be staggered in the direction of the momentum so that the faces normal to that direction pass through the grid points (see Fig. 4). Thus, the pressures at these grid points can be directly used to calculate the pressure force on the momentum control volume. Table 5 lists the convention used for the subscripts, and Fig. 4 shows the momentum control volumes for the x and z directions.

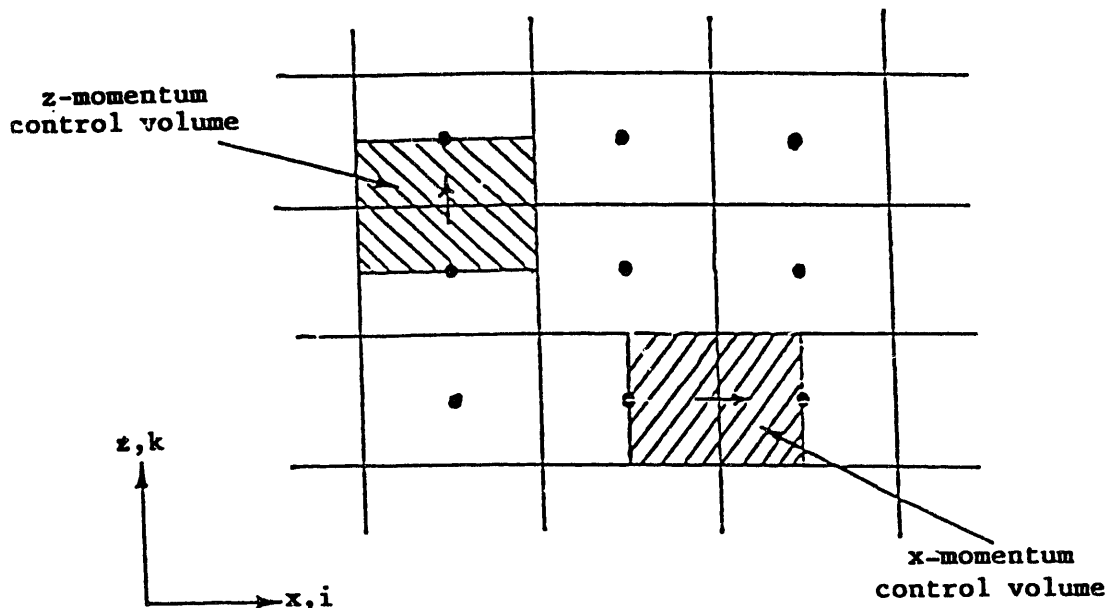


Fig. 4. Momentum control volumes

Table 5. Convention used in COMMIX-PPC to define neighboring control volumes for z-direction momentum equations

Subscript	Momentum Control Volume Centers			Momentum Control Volume Face Centers		
	x	y	z	x	y	z
0	i,	j,	k+1/2	-	-	-
1	i-1,	j,	k+1/2	i-1/2,	j,	k+1/2
2	i+1,	j,	k+1/2	i+1/2,	j,	k+1/2
3	i,	j-1,	k+1/2	i,	j-1/2,	k+1/2
4	i,	j+1,	k+1/2	i,	j+1/2	k+1/2
5	i,	j,	k-1/2	i,	j,	k
6	i,	j,	k+3/2	i,	j,	k+1

5 Finite-Volume Formulation

Although the finite-volume formulation is applicable to a grid in either the Cartesian or cylindrical coordinate systems, only a Cartesian coordinate grid system is used here to demonstrate the formulation of the finite-volume equations. Likewise, we have considered only the z-momentum equation to illustrate the formulation of the momentum equation. Extension of the derivation to the x and y momentum equations is straightforward. It should be noted that the main control volume is applicable for the component continuity equations, and the mixture continuity equation and the momentum control volume are applicable to the mixture momentum equation.

The finite-volume equations are derived by integrating the governing equation (Eq. 3.1) over a control volume. Each term in the equations is integrated separately.

5.1 Convection Term

5.1.1 Main Control Volume

The integration of the convection terms over the control volume gives

$$\int \left[\frac{\Delta(\gamma_x \rho u \phi)}{\Delta x} + \frac{\Delta(\gamma_y \rho v \phi)}{\Delta y} + \frac{\Delta(\gamma_z \rho w \phi)}{\Delta z} \right] dx dy dz \\ = F_2 \langle \phi \rangle_2^0 - F_1 \langle \phi \rangle_0^1 + F_4 \langle \phi \rangle_4^0 - F_3 \langle \phi \rangle_0^3 + F_6 \langle \phi \rangle_6^0 - F_5 \langle \phi \rangle_0^5. \quad (5.1)$$

Here, F (= density \times velocity \times flow area) denotes the mass flow across the surface of the control volume, and subscripts 1–6 stand for the west, east, front, rear, south, and north surfaces, respectively (see Fig. 5). For example, the equation

$$F_2 = F_{i+1/2} = \langle \rho \rangle_2^0 (\gamma_x u \Delta y \Delta z)_2 = \langle \rho \rangle_2^0 (u A_x)_2 = \langle \rho \rangle_{i+1}^1 (u A_x)_{i+1/2} \quad (5.2)$$

is the mass flux at the east surface, as shown in Fig. 5. In Eq. 5.1, $\langle \phi \rangle_2^0$ is the value of ϕ associated with surface "2," which is convected by mass flow F_2 . Because only the values of ϕ associated with cell volumes are available for the main control volume, a relationship must be assumed between volume values and values for the associated surfaces. The upwind difference scheme provides one such relationship. It is

$$\langle \phi \rangle_2^0 = \langle \phi \rangle_{i+1}^1 = \phi_0 = \phi_1 \quad (\text{if } F_2 \text{ is +ve}) \quad (5.3a)$$

$$= \phi_2 = \phi_{i+1} \quad (\text{if } F_2 \text{ is -ve}). \quad (5.3b)$$

A location-value superscript is used for positive velocity, and a location-value subscript is used for negative velocity. Each term on the right side of Eq. 5.1 can be written in a different format. For example,

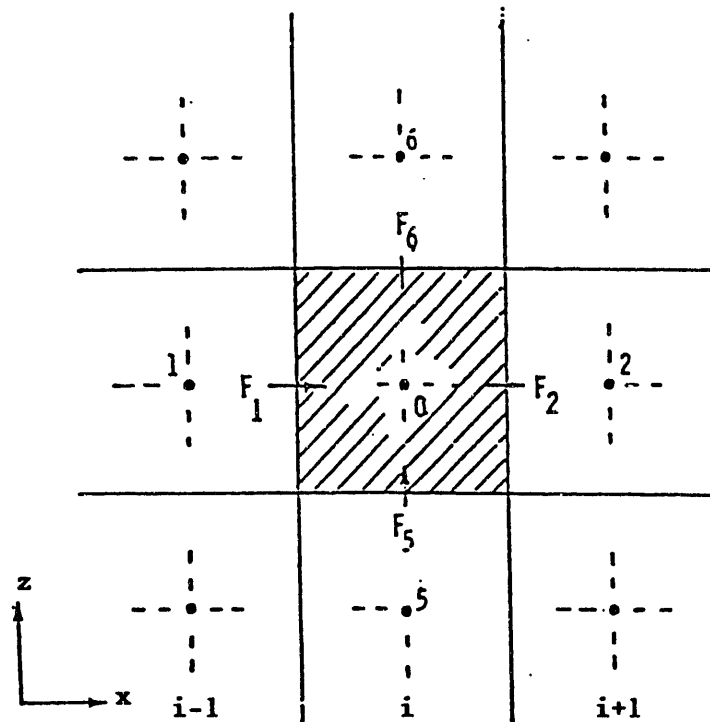


Fig. 5. Convective fluxes for the main control volume

$$F_2 \langle \phi \rangle_2^0 = |0, F_2| \phi_0 - |0, -F_2| \phi_2 . \quad (5.4)$$

The operator $|A|$ is defined as equal to the greater of two arguments, i.e.,

$$\begin{aligned} |A, B| &= A & \text{if } A > B \\ &= B & \text{if } B > A. \end{aligned} \quad (5.5)$$

Using the foregoing convention and after some simplification, we can rewrite Eq. 5.1 as

$$\begin{aligned} &\int \left[\frac{\Delta(\gamma, \rho u \phi)}{\Delta x} + \frac{\Delta(\gamma, \rho v \phi)}{\Delta y} + \frac{\Delta(\gamma, \rho w \phi)}{\Delta z} \right] dx dy dz \\ &= [|0, F_2| + |0, F_4| + |0, F_6| + |0, -F_1| + |0, -F_3| + |0, -F_5|] \phi_0 \\ &\quad - [|0, -F_2| \phi_2 + |0, -F_4| \phi_4 + |0, -F_6| \phi_6 + |0, F_1| \phi_1 + |0, F_3| \phi_3 + |0, F_5| \phi_5]. \end{aligned} \quad (5.6)$$

All six convective fluxes for the main control volume are listed in Table 6.

5.1.2 Momentum Control Volume

Figure 6 shows the staggered mesh for the z-momentum control volume. The various mass flows shown in the figure are as follows:

Table 6. Convective fluxes for the main control volume

$$\begin{aligned}
 F_1 &= (A_x u)_{i-1/2} \langle \rho \rangle_0^1 \\
 F_2 &= (A_x u)_{i+1/2} \langle \rho \rangle_2^0 \\
 F_3 &= (A_y v)_{j-1/2} \langle \rho \rangle_0^3 \\
 F_4 &= (A_y v)_{j+1/2} \langle \rho \rangle_4^0 \\
 F_5 &= (A_z w)_{k-1/2} \langle \rho \rangle_0^5 \\
 F_6 &= (A_z w)_{k+1/2} \langle \rho \rangle_6^0
 \end{aligned}$$

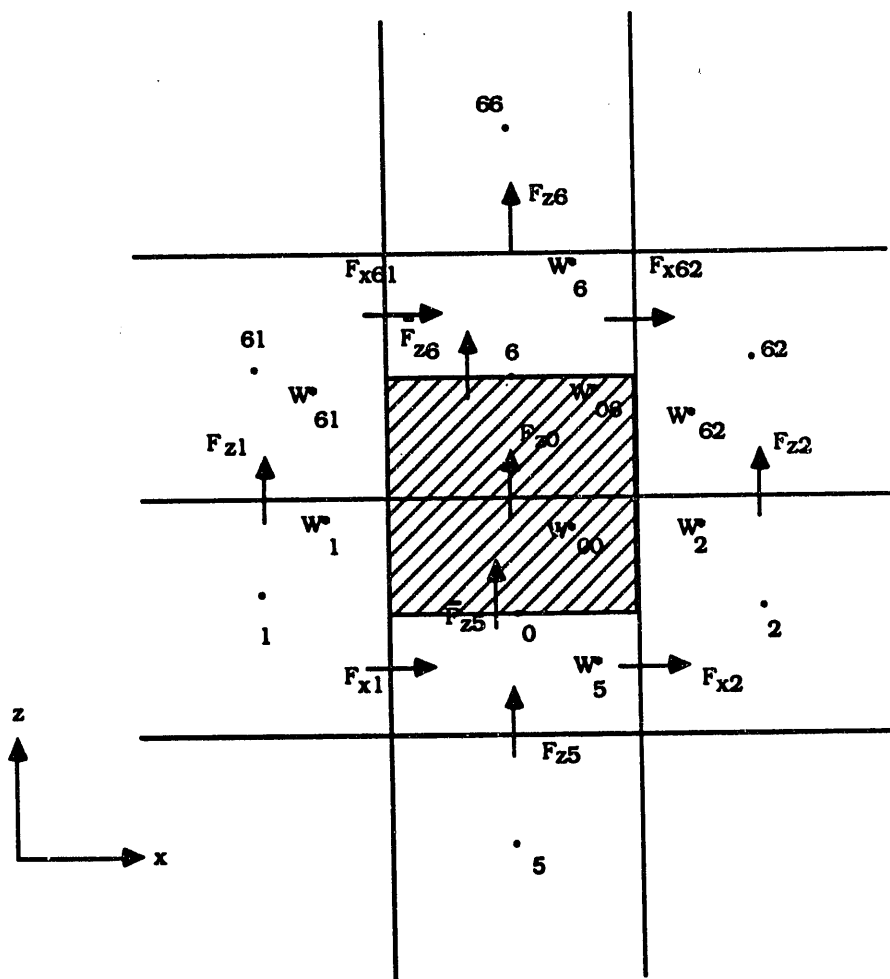


Fig. 6. Convective fluxes and average velocities for the z-momentum control volume

$$F_{z0} = \langle \rho \rangle_6^0 A_{z0} w_0. \quad (5.7a)$$

$$F_{z1} = \langle \rho \rangle_{61}^1 A_{z1} w_1. \quad (5.7b)$$

$$F_{z2} = \langle \rho \rangle_{62}^2 A_{z2} w_2. \quad (5.7c)$$

$$F_{z5} = \langle \rho \rangle_0^5 A_{z5} w_5. \quad (5.7d)$$

$$F_{z6} = \langle \rho \rangle_{66}^6 A_{z6} w_6. \quad (5.7e)$$

$$F_{x1} = \langle \rho \rangle_0^1 A_{x1} u_1. \quad (5.7f)$$

$$F_{x2} = \langle \rho \rangle_2^0 A_{x2} u_2. \quad (5.7g)$$

$$F_{x61} = \langle \rho \rangle_6^{61} A_{x61} u_{61}. \quad (5.7h)$$

$$F_{x62} = \langle \rho \rangle_{62}^6 A_{x62} u_{62}. \quad (5.7i)$$

where the velocities w and u are defined at the cell faces as shown in Fig. 3. The mass flow rates on the south and north faces of the staggered mesh (\bar{F}_{z5} and \bar{F}_{z6}) are not directly available. In COMMIX-PPC, it is assumed that

$$\bar{F}_{z5} = (F_{z0} + F_{z5})/2 \quad (5.7j)$$

and

$$\bar{F}_{z6} = (F_{z0} + F_{z6})/2. \quad (5.7k)$$

In previous COMMIX versions (COMMIX-1A¹⁰ and COMMIX-1B¹¹), velocity w is assumed to be transported by convective fluxes. In COMMIX-PPC, however, we consider that the transport quantity is a momentum per unit mass associated with a certain volume instead of the facial velocity w . Referring to Fig. 6, the z momentum (M_z) associated with the lower half of the staggered mesh is

$$(M_z)_{V_0/2} = \int_{V_0/2} \gamma_v \rho w dx dy dz. \quad (5.8a)$$

If a volume-averaged velocity w_{00}^* is defined as

$$\rho_0 \frac{V_0}{2} w_{00}^* = (M_z)_{V_0/2}. \quad (5.8b)$$

then

$$w_{00}^* = \frac{2(M_z)_{V_0/2}}{V_0 \rho_0} = \frac{2 \int_{V_0/2} \gamma_v \rho w dx dy dz}{\rho_0 V_0} \quad (5.8c)$$

or

$$W_{00}^* = \frac{2 \int_{\Delta z_0/2} \left[\int_{A_0} (\gamma_v \rho_w) dx dy \right] dz}{\rho_0 V_0} . \quad (5.8d)$$

The integral inside the bracket of Eq. 5.8d is the mass flow rate through any cross-sectional area A_z inside the volume $V_0/2$. In COMMIX-PPC, this mass flow rate is assumed to be equal to F_{z0} ; therefore, Eq. 5.8d becomes

$$W_{00}^* = \frac{\Delta z_0 F_{z0}}{\rho_0 V_0} . \quad (5.8e)$$

W_{00}^* represents the momentum per unit mass of the fluid in the volume $V_0/2$ and is the quantity to be transported. W_{00}^* has the dimension of velocity and can also be considered a volume-averaged velocity defined by Eq. 5.8c.

Similarly, a volume-averaged velocity for the upper half of the staggered mesh in Fig. 6 can be defined as follows:

$$\frac{V_6}{2} \rho_6 W_{06}^* = (M_z)_{V_6/2} = \int_{V_6/2} \gamma_v \rho w dx dy dz \quad (5.8f)$$

and

$$W_{06}^* = \frac{\Delta z_6 F_{z0}}{\rho_6 V_6} . \quad (5.8g)$$

The volume-averaged velocities (W^*) associated with their respective volumes are also shown in Fig. 6 and are defined by the following equations:

$$W_{00}^* = \frac{F_{z0} \Delta z_0}{\rho_0 V_0} = \frac{\langle \rho \rangle_6^0 A_{z0} \Delta z_0}{\rho_0 V_0} \cdot W_0 . \quad (5.9a)$$

$$W_{06}^* = \frac{F_{z0} \Delta z_6}{\rho_6 V_6} = \frac{\langle \rho \rangle_6^0 A_{z0} \Delta z_6}{\rho_6 V_6} \cdot W_0 . \quad (5.9b)$$

$$W_1^* = \frac{F_{z1} \Delta z_0}{\rho_1 V_1} = \frac{\langle \rho \rangle_{61}^1 A_{z1} \Delta z_0}{\rho_1 V_1} \cdot W_1 . \quad (5.9c)$$

$$W_2^* = \frac{F_{z2} \Delta z_0}{\rho_2 V_2} = \frac{\langle \rho \rangle_{62}^2 A_{z2} \Delta z_0}{\rho_2 V_2} \cdot W_2 . \quad (5.9d)$$

$$W_5^* = \frac{F_{z5} \Delta z_0}{\rho_0 V_0} = \frac{\langle \rho \rangle_0^5 A_{z5} \Delta z_0}{\rho_0 V_0} \cdot W_5 . \quad (5.9e)$$

$$W_6^* = \frac{F_{z6} \Delta z_6}{\rho_6 V_6} = \frac{\langle \rho \rangle_{66}^6 A_{z6} \Delta z_6}{\rho_6 V_6} \cdot W_6 . \quad (5.9f)$$

$$W_{61}^* = \frac{F_{z1} \Delta z_6}{\rho_{61} V_{61}} = \frac{\langle \rho \rangle_{61}^1 A_{z1} \Delta z_6}{\rho_{61} V_{61}} \cdot W_1 . \quad (5.9g)$$

$$W_{62}^* = \frac{F_{z2} \Delta z_6}{\rho_{62} V_{62}} = \frac{\langle \rho \rangle_{62}^2 A_{z2} \Delta z_6}{\rho_{62} V_{62}} \cdot W_2. \quad (5.9h)$$

where $V = \gamma_w \Delta x \Delta y \Delta z$ is the volume of the fluid at that location. Equations 5.9 (a-h) can be regarded as the closure relations that link the volume-averaged velocities to the facial velocities. The derivation described here is somewhat more complicated than those in previous COMMIX versions. However, the calculations with the present formulation are found to be more robust in COMMIX-1C than those in previous COMMIX versions in certain applications. In addition, as we shall demonstrate later, the present closure relations lead to a formulation that ensures that the pressure drop at a given location conforms with the density gradient in one-dimensional, steady-state flows. As shown by Padilla and Rowe,²⁴ use of the so-called donor flow formulation has the important advantage of making a numerical scheme robust when significant density gradients occur. Furthermore, as we shall also demonstrate later, the closure relations described here satisfy the one-dimensional steady-state Bernoulli equation.

The finite-volume expressions for the convective terms in the z momentum equation (Fig. 6) are presented below. The w-momentum transport due to flow in the z-direction (ρ_{ww}) is

$$\begin{aligned} & \int \frac{\Delta(\gamma_z \rho_{ww})}{\Delta z} dx dy dz \\ &= |0, \bar{F}_{z6}| W_{06}^* - |0, -\bar{F}_{z6}| W_6^* - |0, \bar{F}_{z5}| W_5^* + |0, -\bar{F}_{z5}| W_{05}^*. \end{aligned} \quad (5.10)$$

$$\begin{aligned} & \int \frac{\Delta(\gamma_x \rho_{wu})}{\Delta x} dx dy dz \\ &= \frac{1}{2} |0, F_{x2}| W_{00}^* - \frac{1}{2} |0, -F_{x2}| W_2^* + \frac{1}{2} |0, F_{x62}| W_{06}^* - \frac{1}{2} |0, -F_{x62}| W_{62}^* \\ & \quad - \frac{1}{2} |0, F_{x1}| W_1^* + \frac{1}{2} |0, -F_{x1}| W_{00}^* - \frac{1}{2} |0, F_{x61}| W_{61}^* + \frac{1}{2} |0, -F_{x61}| W_{06}^*. \end{aligned} \quad (5.11)$$

The remaining convective term (ρ_{ww}) in Eq. 3.1 can be written similarly. By summing up the three convective terms and using Eqs. 5.7 and 5.9, we obtain the finite-volume expression for z momentum control volume in the following form:

$$\begin{aligned} & \int \left[\frac{\Delta(\gamma_z \rho_{ww})}{\Delta z} + \frac{\Delta(\gamma_x \rho_{wu})}{\Delta x} + \frac{\Delta(\gamma_y \rho_{ww})}{\Delta y} \right] dx dy dz \\ &= a_0^{wc} w_0 - a_1^{wc} w_1 - a_2^{wc} w_2 - a_3^{wc} w_3 - a_4^{wc} w_4 - a_5^{wc} w_5 - a_6^{wc} w_6. \end{aligned} \quad (5.12)$$

where the coefficients are defined by the following equations:

$$\begin{aligned} a_0^{wc} &= \frac{\langle \rho \rangle_6^0 A_{z0} \Delta z_6}{\rho_6 V_6} \left(|0, \bar{F}_{z6}| + \frac{1}{2} |0, -F_{x62}| + \frac{1}{2} |0, -F_{x61}| + \frac{1}{2} |0, -F_{y64}| + \frac{1}{2} |0, -F_{y63}| \right) \\ &+ \frac{\langle \rho \rangle_6^0 A_{z0} \Delta z_0}{\rho_0 V_0} \left(|0, -\bar{F}_{z5}| + \frac{1}{2} |0, F_{x2}| + \frac{1}{2} |0, -F_{x1}| + \frac{1}{2} |0, F_{y4}| + \frac{1}{2} |0, -F_{y3}| \right) \end{aligned} \quad (5.13a)$$

$$a_1^{wc} = \frac{1}{2} \left[0.F_{x1} \left| \Delta z_0 \langle \rho \rangle_{61}^1 A_{z1} / \rho_1 V_1 + 0.F_{x61} \left| \Delta z_6 \langle \rho \rangle_{61}^1 A_{z1} / \rho_{61} V_{61} \right. \right] \right] \quad (5.13b)$$

$$a_2^{wc} = \frac{1}{2} \left[0.-F_{x2} \left| \Delta z_0 \langle \rho \rangle_{62}^2 A_{z2} / \rho_2 V_2 + 0.-F_{x62} \left| \Delta z_6 \langle \rho \rangle_{62}^2 A_{z2} / \rho_{62} V_{62} \right. \right] \right] \quad (5.13c)$$

$$a_3^{wc} = \frac{1}{2} \left[0.F_{y3} \left| \Delta z_0 \langle \rho \rangle_{63}^3 A_{z3} / \rho_3 V_3 + 0.F_{y63} \left| \Delta z_6 \langle \rho \rangle_{63}^3 A_{z3} / \rho_{63} V_{63} \right. \right] \right] \quad (5.13d)$$

$$a_4^{wc} = \frac{1}{2} \left[0.-F_{y4} \left| \Delta z_0 \langle \rho \rangle_{64}^4 A_{z4} / \rho_4 V_4 + 0.-F_{y64} \left| \Delta z_6 \langle \rho \rangle_{64}^4 A_{z4} / \rho_{64} V_{64} \right. \right] \right] \quad (5.13e)$$

$$a_5^{wc} = \left| 0.\bar{F}_{z5} \right| \Delta z_0 \langle \rho \rangle_0^5 A_{z5} / \rho_0 V_0 \quad (5.13f)$$

$$a_6^{wc} = \left| 0.-\bar{F}_{z6} \right| \Delta z_6 \langle \rho \rangle_{66}^6 A_{z6} / \rho_6 V_6. \quad (5.13g)$$

In Eqs. 5.13a-g, the superscript w indicates the w-momentum equation and c indicates convection. The various convective fluxes for the z-momentum control volume are listed in Table 7. The finite-volume expressions for the x- and y-momentum control volumes can be derived similarly. Equation 5.12 can be rewritten in the more general form:

$$\int \left[\frac{\Delta(\gamma, \rho w \phi)}{\Delta z} + \frac{\Delta(\gamma, \rho v \phi)}{\Delta y} + \frac{\Delta(\gamma, \rho u \phi)}{\Delta x} \right] dx dy dz \\ = a_0^{wc} \phi_0 - a_1^{wc} \phi_1 - a_2^{wc} \phi_2 - a_3^{wc} \phi_3 - a_4^{wc} \phi_4 - a_5^{wc} \phi_5 - a_6^{wc} \phi_6. \quad (5.14)$$

Here again, we have employed the general variable ϕ , which can represent either u, v, or w because we are dealing with momentum control volumes.

To demonstrate that the pressure drop occurs at the same location where the density changes, we consider a steady-state one-dimensional flow with a constant flow area and no internal structure. Assuming that convection is dominating, Eq. 3.1 for the z direction becomes

$$\frac{\Delta(\gamma, \rho w w)}{\Delta z} = -\gamma_v \frac{\partial p}{\partial z}. \quad (5.15)$$

Integrating over the z-momentum control volume (Fig. 6) and assuming that w is positive, we obtain from Eq. 5.10

$$\bar{F}_{z6} w_{06} - \bar{F}_{z5} w_5 = -(P_6 - P_0) A_z. \quad (5.16)$$

where A_z is the flow area in the z direction. Substituting Eqs. 5.7 and 5.9 into Eq. 5.16, we obtain

$$(F_{z0} + F_{z6}) F_{z0} / 2 \rho_6 A_z - (F_{z0} + F_{z5}) F_{z5} / 2 \rho_0 A_z = -(P_6 - P_0) A_z. \quad (5.17)$$

For one-dimensional flow with a constant flow area,

$$A_z_0 = A_z_5 = A_z_6 = A_z.$$

Table 7. Convective fluxes for the z-momentum control volume

$\bar{F}_{z5} = \frac{1}{2}(F_{z5} + F_{z0}) = \frac{1}{2}[\langle \rho \rangle_6^0 A z_0 w_0 + \langle \rho \rangle_0^5 A z_5 w_5]$
$\bar{F}_{z6} = \frac{1}{2}(F_{z6} + F_{z0}) = \frac{1}{2}[\langle \rho \rangle_6^6 A z_6 w_6 + \langle \rho \rangle_6^0 A z_0 w_0]$
$F_{z0} = \langle \rho \rangle_{k+1}^k (A z w)_{k+1/2} = \langle \rho \rangle_6^0 A z_0 w_0$
$F_{z1} = \langle \rho \rangle_{i-1, k+1}^{i-1, k} (A z w)_{i-1, k+1/2} = \langle \rho \rangle_{61}^1 A z_1 w_1$
$F_{z2} = \langle \rho \rangle_{i+1, k+1}^{i-1, k} (A z w)_{i+1, k+1/2} = \langle \rho \rangle_{62}^2 A z_2 w_2$
$F_{z3} = \langle \rho \rangle_{j-1, k+1}^{i-1, k} (A z w)_{j-1, k+1/2} = \langle \rho \rangle_{63}^3 A z_{63} w_3$
$F_{z4} = \langle \rho \rangle_{j+1, k+1}^{i-1, k} (A z w)_{j+1, k+1/2} = \langle \rho \rangle_{64}^4 A z_{64} w_4$
$F_{z5} = \langle \rho \rangle_k^{k-1} (A z w)_{k-1/2} = \langle \rho \rangle_0^5 A z_5 w_5$
$F_{z6} = \langle \rho \rangle_{k+2}^{k+1} (A z w)_{k+3/2} = \langle \rho \rangle_{66}^6 A z_6 w_6$
$F_{x2} = \langle \rho \rangle_{i+1}^i (A x u)_{i+1/2} = \langle \rho \rangle_2^0 A x_2 u_2$
$F_{x1} = \langle \rho \rangle_i^{i-1} (A x u)_{i-1/2} = \langle \rho \rangle_0^1 A x_1 u_1$
$F_{x62} = \langle \rho \rangle_{i+1, k+1}^{i, k+1} (A x u)_{i+1/2, k+1} = \langle \rho \rangle_{62}^6 A x_{62} u_{62}$
$F_{x61} = \langle \rho \rangle_{i+1, k+1}^{i-1, k+1} (A x u)_{i-1/2, k+1} = \langle \rho \rangle_6^{61} A x_{61} u_{61}$
$F_{y4} = \langle \rho \rangle_{j+1}^j (A y v)_{j+1/2} = \langle \rho \rangle_4^0 A y_4 v_4$
$F_{y3} = \langle \rho \rangle_j^{j-1} (A y v)_{j-1/2} = \langle \rho \rangle_0^3 A y_3 v_3$
$F_{y64} = \langle \rho \rangle_{j+1, k+1}^{j, k+1} (A y v)_{j+1/2, k+1} = \langle \rho \rangle_{64}^6 A y_{64} v_{64}$
$F_{y63} = \langle \rho \rangle_{j, k+1}^{j-1, k+1} (A y v)_{j-1/2, k+1} = \langle \rho \rangle_6^{63} A y_{63} v_{63}$

$$F_{z0} = \rho_0 A_{z0} w_0 = \rho A_z w,$$

$$F_{z5} = \rho_5 A_{z5} w_5 = \rho A_z w,$$

$$F_{z6} = \rho_6 A_{z6} w_6 = \rho A_z w,$$

and Eq. 5.17 reduces to

$$(\rho w)^2 \left(\frac{1}{\rho_6} - \frac{1}{\rho_0} \right) = - (p_6 - p_0), \quad (5.18)$$

which indicates that the pressure drop occurs at the same location where the density changes. In a similar manner, it can be demonstrated that the same relation holds if w is negative.

5.2 Diffusion Term

5.2.1 Main Control Volume

The integration of diffusion terms over a main control volume (Fig. 7) gives

$$\begin{aligned} & \int \left[\frac{\Delta \left(\gamma_x \Gamma_{\phi} \frac{\partial \phi}{\partial x} \right)}{\Delta x} + \frac{\Delta \left(\gamma_y \Gamma_{\phi} \frac{\partial \phi}{\partial y} \right)}{\Delta y} + \frac{\Delta \left(\gamma_z \Gamma_{\phi} \frac{\partial \phi}{\partial z} \right)}{\Delta z} \right] dx dy dz \\ &= D_2(\phi_2 - \phi_0) - D_1(\phi_0 - \phi_1) + D_4(\phi_4 - \phi_0) - D_3(\phi_0 - \phi_3) + D_6(\phi_6 - \phi_0) - D_5(\phi_0 - \phi_5) \\ &= D_1 \phi_1 + D_2 \phi_2 + D_3 \phi_3 + D_4 \phi_4 + D_5 \phi_5 + D_6 \phi_6 \\ &\quad - (D_1 + D_2 + D_3 + D_4 + D_5 + D_6) \phi_0. \end{aligned} \quad (5.19)$$

Here, D (= effective diffusivity \times flow area/distance between the centers of two control volumes) is the diffusion strength across the surface of the control volume.

To determine the value of D at a surface, we assume that the diffusivity Γ varies continuously from one main control volume to the next and use the following average diffusion strength:

$$D_2 = (A_x)_{1+1/2} (\Gamma_0 + \Gamma_2) / (\Delta x_0 + \Delta x_2). \quad (5.20)$$

Expressions of the diffusion strength for the six surfaces of the main control volume are listed in Table 8.

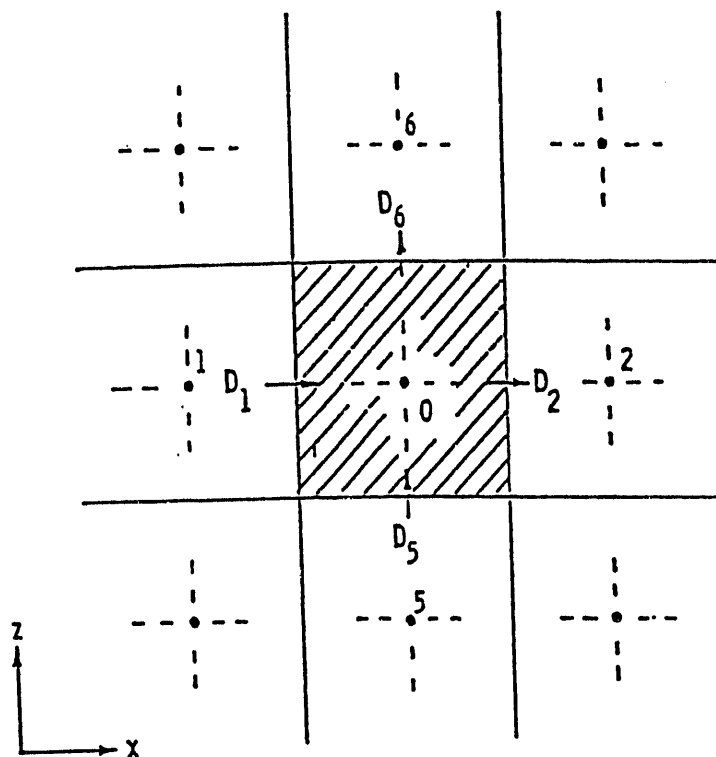


Fig. 7. Diffusion fluxes for the main control volume

Table 8. Diffusion strengths for the main control volume

$$D_1 = (A_x)_{i-1/2} (\Gamma_0 + \Gamma_1) / (\Delta x_0 + \Delta x_1)$$

$$D_2 = (A_x)_{i+1/2} (\Gamma_0 + \Gamma_2) / (\Delta x_0 + \Delta x_2)$$

$$D_3 = (A_y)_{j-1/2} (\Gamma_0 + \Gamma_3) / (\Delta y_0 + \Delta y_3)$$

$$D_4 = (A_y)_{j+1/2} (\Gamma_0 + \Gamma_4) / (\Delta y_0 + \Delta y_4)$$

$$D_5 = (A_z)_{k-1/2} (\Gamma_0 + \Gamma_5) / (\Delta z_0 + \Delta z_5)$$

$$D_6 = (A_z)_{k+1/2} (\Gamma_0 + \Gamma_6) / (\Delta z_0 + \Delta z_6)$$

5.2.2 Momentum Control Volume

Integration of the diffusion terms over the z-momentum control volume (Fig. 8) results in an expression similar to Eq. 5.19:

$$\begin{aligned}
 & \int \left[\frac{\Delta \left(\gamma_x \Gamma_0 \frac{\partial \phi}{\partial x} \right)}{\Delta x} + \frac{\Delta \left(\gamma_y \Gamma_0 \frac{\partial \phi}{\partial y} \right)}{\Delta y} + \frac{\Delta \left(\gamma_z \Gamma_0 \frac{\partial \phi}{\partial z} \right)}{\Delta z} \right] dx dy dz \\
 & = \bar{D}_1 \phi_1 + \bar{D}_2 \phi_2 + \bar{D}_3 \phi_3 + \bar{D}_4 \phi_4 + \bar{D}_5 \phi_5 + \bar{D}_6 \phi_6 \\
 & \quad - (\bar{D}_1 + \bar{D}_2 + \bar{D}_3 + \bar{D}_4 + \bar{D}_5 + \bar{D}_6) \phi_0. \tag{5.21}
 \end{aligned}$$

The only difference is that we now use the momentum control volume diffusion strength \bar{D} , instead of the main control volume diffusion strength D , e.g., for the north face,

$$\bar{D}_6 = \frac{1}{2} \left[(A_z)_k + (A_z)_{k+1} \right] \left(\frac{\Gamma}{\Delta z} \right)_6. \tag{5.22}$$

Expressions of the diffusion strengths \bar{D} for the z momentum control volume are listed in Table 9.

5.3 Unsteady Term

5.3.1 Main Control Volume

Representation of the term $\partial(\gamma_v \rho \phi)/\partial t$ is obtained by assuming that the values ρ_0 and ϕ_0 prevail over the control volume surrounding point 0 (see Fig. 9). Integration of the unsteady terms over the control volume then gives

$$\int \frac{\partial}{\partial t} (\gamma_v \rho \phi) dx dy dz = \frac{(\rho \phi)_0 - (\rho \phi)_0^n}{\Delta t} V_0, \tag{5.23}$$

where $V_0 = \gamma_v \Delta x \Delta y \Delta z$ is the volume of the fluid, the superscript n refers to a known previous time-step value, and the superscript $n+1$ for a new time-step value is omitted for simplicity, i.e., $(\rho \phi)_0$ implies $(\rho \phi)_0^{n+1}$.

5.3.2 Momentum Control Volume

Referring to the z-momentum control volume shown in Fig. 6, and recalling that the momentum of the staggered mesh consists of two parts, i.e.,

$$\begin{aligned}
 M_n &= (M_n)_{v_{n/2}} + (M_n)_{v_{n/2}} \\
 &= \int_{v_{n/2}} \gamma_v \rho w dx dy dz + \int_{v_{n/2}} \gamma_v \rho w dx dy dz, \tag{5.24}
 \end{aligned}$$

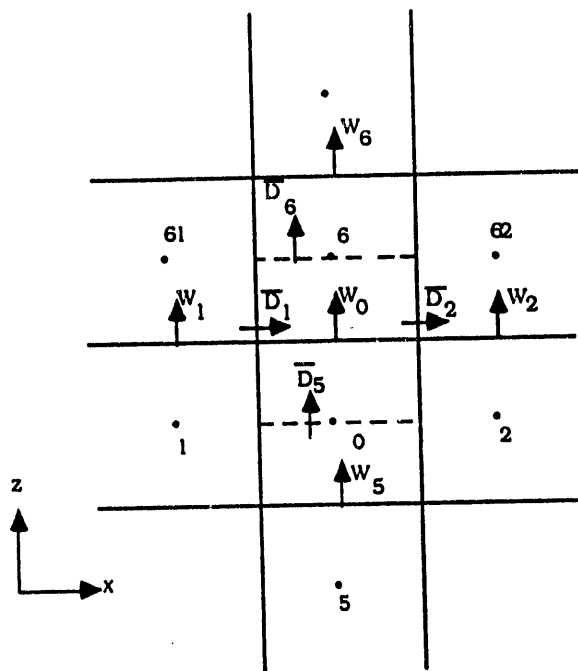


Fig. 8. Diffusion fluxes for the z-momentum control volume

Table 9. Diffusion strengths for the z-momentum control volume

$$\bar{D}_1 = \frac{1}{4} \left[(Ax)_{i-1/2, k} + (Ax)_{i+1/2, k+1} \right] \left[\frac{(\Gamma_0 + \Gamma_1)}{(\Delta x_0 + \Delta x_1)} + \frac{(\Gamma_6 + \Gamma_{61})}{(\Delta x_6 + \Delta x_{61})} \right]$$

$$\bar{D}_2 = \frac{1}{4} \left[(Ax)_{i+1/2, k+1} + (Ax)_{i+1/2, k+1} \right] \left[\frac{(\Gamma_0 + \Gamma_2)}{(\Delta x_0 + \Delta x_2)} + \frac{(\Gamma_6 + \Gamma_{62})}{(\Delta x_6 + \Delta x_{62})} \right]$$

$$\bar{D}_3 = \frac{1}{4} \left[(Ay)_{j-1/2, k} + (Ay)_{j+1/2, k+1} \right] \left[\frac{(\Gamma_0 + \Gamma_3)}{(\Delta y_0 + \Delta y_3)} + \frac{(\Gamma_6 + \Gamma_{63})}{(\Delta y_6 + \Delta y_{63})} \right]$$

$$\bar{D}_4 = \frac{1}{4} \left[(Ay)_{j+1/2, k} + (Ay)_{j+1/2, k+1} \right] \left[\frac{(\Gamma_0 + \Gamma_4)}{(\Delta y_0 + \Delta y_4)} + \frac{(\Gamma_6 + \Gamma_{64})}{(\Delta y_6 + \Delta y_{64})} \right]$$

$$\bar{D}_5 = \frac{1}{2} \left[(Az)_k + (Az)_{k-1} \right] \left[\left(\frac{\Gamma}{\Delta z} \right)_0 \right]$$

$$\bar{D}_6 = \frac{1}{2} \left[(Az)_k + (Az)_{k+1} \right] \left[\left(\frac{\Gamma}{\Delta z} \right)_6 \right]$$

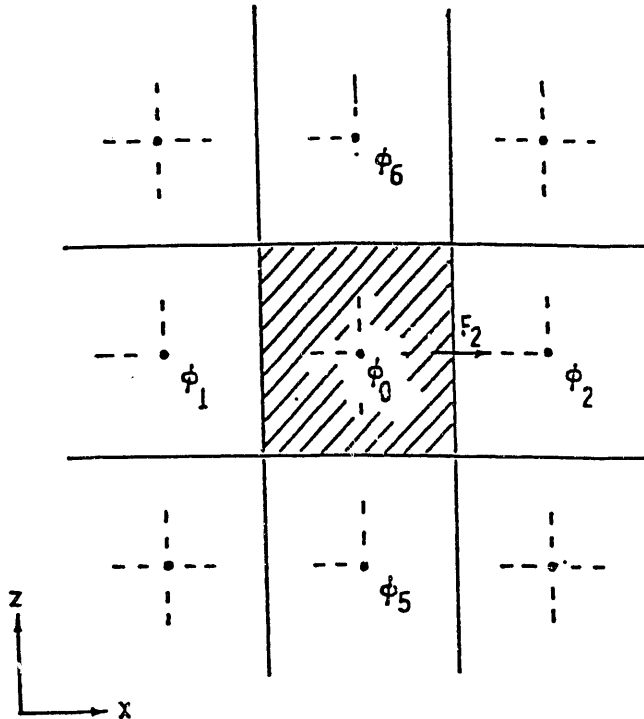


Fig. 9. Control volume for field variables

by integrating the unsteady term over the control volume, we obtain

$$\begin{aligned}
 \int \frac{\partial}{\partial t} (\gamma_v \rho w) dx dy dz &= \int_{V_0/2} \frac{\partial}{\partial t} (\gamma_v \rho w) dx dy dz + \int_{V_0/2} \frac{\partial}{\partial t} (\gamma_v \rho w) dx dy dz \\
 &= \frac{\partial}{\partial t} (M_v)_{V_0/2} + \frac{\partial}{\partial t} (M_v)_{V_0/2} \\
 &= \frac{\partial}{\partial t} \left(\frac{V_0 \rho_0 \bar{w}_{00}}{2} \right) + \frac{\partial}{\partial t} \left(\frac{V_0 \rho_0 \bar{w}_{00}^n}{2} \right) \\
 &= \frac{1}{\Delta t} \left[\frac{V_0}{2} (\rho_0 \bar{w}_{00} - \rho_0^n \bar{w}_{00}^n) + \frac{V_0}{2} (\rho_0 \bar{w}_{00}^n - \rho_0^n \bar{w}_{00}^n) \right]. \quad (5.25a)
 \end{aligned}$$

In deriving Eq. 5.25a, we used Eqs. 5.8b and 5.8f, which were introduced to define volume-averaged velocity \bar{w}^* . Here again, the superscript n refers to the previous time-step value, and the superscript $n+1$ for new a time-step value is omitted for simplicity.

Substituting Eq. 5.9 into Eq. 5.25a and rearranging, we obtain

$$\begin{aligned}
 &\int \frac{\partial}{\partial t} (\gamma_v \rho w) dx dy dz \\
 &= \frac{\Delta z_0 (\rho_0^0 (\Delta z_0 + \Delta z_6))}{2\Delta t} w_0 - \frac{\Delta z_0 [\langle \rho \rangle_6^0]^n (\Delta z_0 + \Delta z_6)}{2\Delta t} w_0^n. \quad (5.25b)
 \end{aligned}$$

In deducing Eq. 5.25b, we have employed the closure relations (Eq. 5.10) described in Sec. 5.1.2.

Note that Eq. 5.25b has two potential limitations: (a) if the density change in the control volume is large, the approximation may be less accurate; (b) if the volume porosity is substantially different from the surface porosity in the momentum control volume, the approximation may also be less accurate. An alternative formulation of the unsteady term as shown in Eq. 5.23 is provided as a user's option. In the alternative formulation, both volume-weighted average porosity and volume-weighted average density are used.

5.4 Source Term

The source term S_ϕ in Eq. 3.1 can, in general, be represented by a linear combination of two terms:

$$S_\phi = S_{c\phi} + S_{p\phi} \phi. \quad (5.26)$$

It is understood that $S_{c\phi}$, $S_{p\phi}$, and ϕ refer to the control volume in question and are assumed uniform in that volume. Clearly, both $S_{c\phi}$ and $S_{p\phi}$ depend on the source term S_ϕ under consideration. When $S_{c\phi}$ is greater than 0 and $S_{p\phi}$ is less than or equal to zero, the linear decomposition of S_ϕ defined by Eq. 5.26 is an effective device for obtaining computational stability and convergence.²²

Integration of the source term over the main control volume gives

$$\int S_\phi dx dy dz = S_{c\phi} V_0 + S_{p\phi} V_0 \bar{\phi}_0. \quad (5.27)$$

where $V_0 = \gamma_v \Delta x \Delta y \Delta z$ is the fluid volume.

Integration of the source term over the z-momentum control volume gives

$$\int S_\phi dx dy dz = S_{c\phi} \bar{V}_0 + S_{p\phi} \bar{V}_0 \bar{\phi}_0. \quad (5.28)$$

where

$$\bar{V}_0 = (\Delta z_0 + \Delta z_6) \left/ \left(\frac{\Delta z_0}{V_0} + \frac{\Delta z_6}{V_6} \right) \right.. \quad (5.29)$$

\bar{V}_0 is the characteristic volume used in the finite-volume integration. It will be made clear in Sec. 5.6 why we employed Eq. 5.29 as the characteristic volume for the integration of the z-momentum control volume.

5.5 General Finite-Volume Equation for the Main Control Volume

Having looked at each term of the general equation separately, we now assemble all terms of Eqs. 5.6, 5.19, 5.23, and 5.27 for the main control volume to obtain the general finite-volume equation.

$$\begin{aligned}
 & \int [(\text{Unsteady}) + (\text{Convection}) - (\text{Diffusion}) - (\text{Source})] dx dy dz \\
 &= \frac{(\rho\phi)_0 - (\rho\phi)_0^n}{\Delta t} V_0 + (|0, -F_1| + |0, F_2| + \dots) \phi_0 \\
 & \quad (\text{Unsteady}) \quad (\text{Convection}) \\
 & - (|0, F_1| \phi_1 + |0, -F_2| \phi_2 + \dots) + (D_1 + D_2 + \dots) \phi_0 \\
 & \quad (\text{Convection}) \quad (\text{Diffusion}) \\
 & - (D_1 \phi_1 + D_2 \phi_2 + \dots) - S_{c\phi} V_0 - S_{p\phi} \phi_0 V_0 = 0. \quad (5.30) \\
 & \quad (\text{Diffusion}) \quad (\text{Source})
 \end{aligned}$$

After some algebra and rearrangement, we obtain

$$\begin{aligned}
 & \phi_0 \left\{ \frac{\rho_0 V_0}{\Delta t} + \alpha [(|0, -F_1| + \dots + |0, F_6|) + (D_1 + \dots + D_6) - S_{p\phi} V_0] \right\} \\
 &= [(|0, F_1| + D_1) \phi_1 + \dots + (|0, -F_6| + D_6) \phi_6] + \left(\frac{\rho_0^n \phi_0^n}{\Delta t} V_0 + S_{c\phi} V_0 \right). \quad (5.31)
 \end{aligned}$$

The discretized form of the continuity equation is obtained by setting $\phi = 1$, $D = 0$, $S_{c\phi} = \dot{m}$, and $S_{p\phi} = 0$ in Eq. 5.31. The result is

$$\frac{\rho_0 \phi_0}{\Delta t} + |0, -F_1| + |0, F_2| + \dots + |0, F_6| = |0, F_1| + \dots + |0, -F_6| + \frac{\rho_0^n}{\Delta t} V_0 + \dot{m} V_0 \quad (5.32)$$

Substituting Eq. 5.32 into Eq. 5.31, we obtain the general finite-volume equation for the main control volume:

$$a_0^\phi \phi_0 = a_1^\phi \phi_1 + \dots + a_6^\phi \phi_6 + b_0^\phi, \quad (5.33)$$

where the coefficients a_0^ϕ , a_1^ϕ , etc. are as given in Table 10.

Finally, it should be noted that the general variable ϕ for the main control volume can represent any nonflow variable such as enthalpy, turbulence kinetic energy, or rate of dissipation of turbulence kinetic energy.

5.6 General Finite-Volume Equation for the z-Momentum Control Volume

The finite-volume expression for the z-momentum equation can be obtained by following the same procedure as for the finite-volume equation of the main control volume, with one exception. The pressure gradient term in the momentum equation is not known a priori. It is determined in accordance with a procedure presented in Sec. 6 and is calculated with the requirement that the velocity field satisfies the continuity equation. For this reason, the pressure-containing term in the finite-volume form of the momentum

Table 10. Fully implicit finite-volume equation for the main control volume and its coefficients

$$a_0^\phi \phi_0 = a_1^\phi \phi_1 + \dots + a_6^\phi \phi_6 + b_0^\phi$$

$a_1^\phi = (O, F_1 + D_1)$	$a_2^\phi = (O, -F_2 + D_2)$
$a_3^\phi = (O, F_3 + D_3)$	$a_4^\phi = (O, -F_4 + D_4)$
$a_5^\phi = (O, F_5 + D_5)$	$a_6^\phi = (O, -F_6 + D_6)$
<hr/>	
$b_0^\phi = \left(\frac{\rho^n \phi^n}{\Delta t} + S_{c\phi} - \dot{m}''' \right)_0 V_0$	
$a_0^\phi = \left(a_1^\phi + a_2^\phi + \dots + a_6^\phi \right) + \left(\frac{\rho_0^n}{\Delta t} - S_{p\phi} \right) V_0$	
<hr/>	

equation is not included it in the source term. Accordingly, the discretized equation for the z-momentum control volume shown in Fig. 6 is written as

$$a_0^w w_0 = a_1^w w_1 + a_2^w w_2 + a_3^w w_3 + a_4^w w_4 + a_5^w w_5 + a_6^w w_6 + b_0^w - d^w (P_6 - P_0), \quad (5.34)$$

where

$$d^w = \bar{V}_0 / \left[\frac{1}{2} (\Delta z_0 + \Delta z_6) \right] \quad (5.35)$$

and \bar{V}_0 is the characteristic volume for the momentum control volume defined by Eq. 5.29. The reason that Eq. 5.35 is written in the form shown is that we want the discretized momentum equation to satisfy the one-dimensional steady-state Bernoulli's equation (with constant density).

The derivation of Eq. 5.29 follows. Referring to Fig. 6, the one-dimensional steady-state Bernoulli equation with constant density can be written as

$$\rho \left(\bar{w}_6^2 - \bar{w}_0^2 \right) / 2 = -(P_6 - P_0) - \frac{\rho g (\Delta z_0 + \Delta z_6)}{2}, \quad (5.36)$$

where \bar{w}_6 and \bar{w}_0 are the average velocities associated with the control volume centered at grid points 6 and 0, respectively. From continuity, we have

$$\rho \bar{w}_6 \frac{V_6}{\Delta z_6} = \rho \bar{w}_0 \frac{V_0}{\Delta z_0} = F_{z0} = \rho A z_0 w_0. \quad (5.37)$$

Substituting Eq. 5.37 into Eq. 5.36, and rearranging lead to the equation

$$\frac{F_{z0}^2}{2\rho} \left[\left(\frac{\Delta z_6}{V_6} \right)^2 - \left(\frac{\Delta z_0}{V_0} \right)^2 \right] = -(P_6 - P_0) - \frac{1}{2} \rho g (\Delta z_0 + \Delta z_6), \quad (5.38)$$

which must be satisfied by the discretized, one-dimensional z -momentum equation.

The one-dimensional momentum equation in the z direction is

$$\frac{\Delta(\gamma_v \rho w w)}{\Delta z} = -\gamma_v \frac{\partial P}{\partial z} - \gamma_v \rho g. \quad (5.39)$$

Integrating over the z -momentum control volume (Fig. 6), and assuming that w is positive, that

$$\int_{V_0} \gamma_v \frac{\partial P}{\partial z} dv = \frac{P_6 - P_0}{\frac{1}{2}(\Delta z_0 + \Delta z_6)} \bar{V}_0,$$

and

$$\int_{V_0} \gamma_v \rho g dv = \gamma_v \rho g \bar{V}_0,$$

we obtain

$$\bar{F}_{z6} W_{06}^* - \bar{F}_{z5} W_5^* = -(P_6 - P_0) \bar{V}_0 / \left[\frac{1}{2}(\Delta z_0 + \Delta z_6) \right] - \gamma_v \rho g \bar{V}_0, \quad (5.40)$$

where \bar{V}_0 is the characteristic volume to be determined.

Substituting Eqs. 5.7 and 5.9 into Eq. 5.40, we get

$$\frac{(F_{z0} + F_{z6}) F_{z0} \Delta z_6}{2\rho_6 V_6} - \frac{(F_{z0} + F_{z5}) F_{z5} \Delta z_0}{2\rho_0 V_0} = -\frac{(P_6 - P_0) \bar{V}_0}{\frac{1}{2}(\Delta z_0 + \Delta z_6)} - \gamma_v \rho g \bar{V}_0. \quad (5.41)$$

For one-dimensional flow with constant density,

$$F_{z0} = F_{z5} = F_{z6},$$

and

$$\rho_0 = \rho_6 = \rho.$$

Therefore, Eq. 5.41 reduces to

$$\frac{F_{z0}^2}{2\rho} \left[\frac{\Delta z_6}{V_6} - \frac{\Delta z_0}{V_0} \right] (\Delta z_6 + \Delta z_0) = -(P_6 - P_0) \bar{V}_0 - \frac{1}{2} \gamma_v \rho g (\Delta z_0 + \Delta z_6) \bar{V}_0. \quad (5.42)$$

Dividing Eq. 5.42 by Eq. 5.38, we obtain

$$\bar{V}_0 = (\Delta z_0 + \Delta z_6) / \left(\frac{\Delta z_0}{V_0} + \frac{\Delta z_6}{V_6} \right) \quad (5.43)$$

Equation 5.43 is identical to Eq. 5.29. Thus, the characteristic volume \bar{V}_0 employed in Eq. 5.35 is the proper volume for integration over the z-momentum control volume, and the resulting finite-volume equation satisfies the one-dimensional Bernoulli equation.

The coefficients a_0^* , a_0^w , and b_0^w in Eq. 5.34 can be evaluated from Eqs. 5.12, 5.21, 5.25, and 5.28. The resulting equation has the same form as Eq. 5.33, except that the contributions of the source that enter a_0^* and b_0^* do not contain the pressure. The effect of the pressure gradient is incorporated in the last term of Eq. 5.34. The coefficients of the momentum equation for the z-momentum control volume are listed in Table 11, where velocity w was replaced by the general variable ϕ . This is to indicate that the x- and y-momentum equations can be derived in a similar manner. Note that in Table 11, the two quantities $S_{C\phi}$ and $S_{P\phi}$ do not contain the mass source term \dot{m}''' . Two different forms of the coefficient a_0^* are given in Table 11. The first form, $a_0^*(1)$, is obtained from the momentum equation only and is referred to as the conservative form because conservation of momentum is satisfied over the control volume. The second form, $a_0^*(2)$, is derived by employing both the momentum and continuity equations even though the latter may not be satisfied during an iteration. Experience indicates that using the continuity equation often helps to speed up convergence during iterations. The second form of the coefficient is referred to as the transport form of the momentum equation and is implemented in COMMIX-PPC.

To derive the transport form of the z-momentum equation, we begin with the discretized continuity equation for Cell 0 and Cell 6, which can be written as

$$(\rho_0 - \rho_0^n) V_0 / \Delta t + F_{z0} - F_{z5} + F_{x2} - F_{x1} + F_{y4} - F_{y3} - \dot{m}_0''' V_0 = 0 \quad (5.44)$$

for Cell 0, and

$$(\rho_6 - \rho_6^n) V_6 / \Delta t + F_{z6} - F_{z0} + F_{x62} - F_{x61} + F_{y64} - F_{y63} - \dot{m}_6''' V_0 = 0 \quad (5.45)$$

for Cell 6. The transport form of the z-momentum equation is obtained from the following relationship:

$$\begin{array}{lcl} \text{transport} & & \text{conservative form } \frac{w_0^*}{2} \times \text{Eq. 5.44} - \frac{w_6^*}{2} \times \text{Eq. 5.45.} \\ \text{form of z-} & = & \text{of z-momentum} \\ \text{momentum} & & \\ \text{equation} & & \end{array} \quad (5.46)$$

Equations 5.44 and 5.45 contain the time-dependent terms, the convective fluxes, and condensation terms. The diffusion terms and the source terms remain the same in the transport form as they are in the conservative form of the z-momentum equation. Thus, all the coefficients are in the conservative and transport forms of the z-momentum equation, with the exception of the coefficient a_0^* , and Eq. 5.46 can be reduced to

$$a_0^*(2) = a_0^*(1) - \frac{w_0^*}{2} \times \text{Eq. 5.44} - \frac{w_6^*}{2} \times \text{Eq. 5.45.} \quad (5.47)$$

After some manipulation and rearrangement, the final forms of $a_0^*(2)$ are identical to those given in Table 11.

Table 11. Coefficients of the fully implicit finite-volume equation for the z-momentum control volume

$$a_0^* \phi_0 = a_1^* \phi_1 + \dots + a_6^* \phi_6 + b_0^* - d_0^* (P_6 - P_0)$$

$$a_1^* = \frac{\langle \rho \rangle_{61}^1 A z_1}{2} \left(|0, F_{x1}| \Delta z_0 / \rho_1 V_1 + |0, F_{x61}| \Delta z_6 / \rho_{61} V_{61} \right) + \bar{D}_1$$

$$a_2^* = \frac{\langle \rho \rangle_{62}^2 A z_2}{2} \left(|0, -F_{x2}| \Delta z_0 / \rho_2 V_2 + |0, -F_{x62}| \Delta z_6 / \rho_{62} V_{62} \right) + \bar{D}_2$$

$$a_3^* = \frac{\langle \rho \rangle_{63}^3 A z_3}{2} \left(|0, F_{y3}| \Delta z_0 / \rho_3 V_3 + |0, F_{y63}| \Delta z_6 / \rho_{63} V_{63} \right) + \bar{D}_3$$

$$a_4^* = \frac{\langle \rho \rangle_{64}^4 A z_4}{2} \left(|0, -F_{y4}| \Delta z_0 / \rho_4 V_4 + |0, -F_{y64}| \Delta z_6 / \rho_{64} V_{64} \right) + \bar{D}_4$$

$$a_5^* = |0, \bar{F}_{z5}| \frac{\Delta z_0 \langle \rho \rangle_0^5 A z_5}{\rho_0 V_0} + \bar{D}_5$$

$$a_6^* = |0, -\bar{F}_{z6}| \frac{\Delta z_6 \langle \rho \rangle_{66}^6 A z_6}{\rho_6 V_6} + \bar{D}_6$$

$$b_0^* = A z_0 \left[\langle \rho \rangle_6^0 \right]^n (A z_0 + A z_6) \phi_0^n / 2 \Delta t + S_{p*} \bar{V}_0$$

$$a_0^*(1) = A z_0 \langle \rho \rangle_6^0 (A z_0 + A z_6) / 2 \Delta t + \frac{\langle \rho \rangle_6^0 A z_0 \Delta z_6}{\rho_6 V_6} \left(|0, \bar{F}_{z6}| + \frac{1}{2} |0, F_{x62}| + \frac{1}{2} |0, -F_{x61}| + \frac{1}{2} |0, F_{y64}| + \frac{1}{2} |0, -F_{y63}| - \frac{\dot{m}_0''}{2} V_6 \right) + \frac{\langle \rho \rangle_6^0 A z_0 \Delta z_0}{\rho_0 V_0} \left(|0, -\bar{F}_{z5}| + \frac{1}{2} |0, F_{x2}| + \frac{1}{2} |0, -F_{x1}| + \frac{1}{2} |0, F_{y4}| + \frac{1}{2} |0, -F_{y3}| - \frac{\dot{m}_6''}{2} V_0 \right)$$

$$+ \bar{D}_1 + \dots + \bar{D}_6 - S_{p*} \bar{V}_0$$

$$a_0^*(2) = \frac{\langle \rho \rangle_6^0 A z_0}{2 \Delta t} \left[\left(\frac{\rho_0^n}{\rho_0} \right) \Delta z_0 + \left(\frac{\rho_6^n}{\rho_6} \right) \Delta z_6 \right] + \frac{\langle \rho \rangle_6^0 A z_0 \Delta z_6}{\rho_6 V_6} \left(|0, -\bar{F}_{z6}| + \frac{1}{2} |0, -F_{x62}| + \frac{1}{2} |0, F_{x61}| + \frac{1}{2} |0, -F_{y64}| + \frac{1}{2} |0, F_{y63}| + F_{z0} \right) + \frac{\langle \rho \rangle_6^0 A z_0 \Delta z_0}{\rho_0 V_0} \left(|0, \bar{F}_{z5}| + \frac{1}{2} |0, -F_{x2}| + \frac{1}{2} |0, F_{x1}| + \frac{1}{2} |0, -F_{y4}| + \frac{1}{2} |0, F_{y3}| - F_{z0} \right) + \bar{D}_1 + \dots + \bar{D}_6 - S_{p*} \bar{V}_0$$

6 Pressure Equation

The pressure in the momentum equation (Eq. 5.34) is unknown and must be determined from the conservation-of-mass equation. In this section, we present the derivation of the pressure equation.

The conservation of mass in Eq. 5.32 for the cell around point 0 (Fig. 9) can be expressed as

$$V_0 \left(\frac{\partial \rho}{\partial t} \right) - (A_x u)_{i-1/2} \langle \rho \rangle_0^1 + (A_x u)_{i+1/2} \langle \rho \rangle_2^0 - (A_y v)_{j-1/2} \langle \rho \rangle_0^3 + (A_y v)_{j+1/2} \langle \rho \rangle_4^0 - (A_z w)_{k-1/2} \langle \rho \rangle_0^5 + (A_z w)_{k+1/2} \langle \rho \rangle_6^0 - \dot{m}_s V_0 = \delta_0. \quad (6.1)$$

Here, $V_0 = \gamma \Delta x \Delta y \Delta z$ is the fluid volume of the main control volume, δ_0 is the mass residual of the continuity equation, $\langle \rho \rangle$ is the upwind density, u , v , and w are the normal velocities at the surface of the control volume, and A is the true flow area, which is the product of superficial surface area and directional surface porosity.

When mass is precisely conserved, the right side of Eq. 6.1 vanishes, i.e., $\delta_0 = 0$. However, because Eq. 6.1 is solved by an iterative procedure, the mass residual δ_0 , in general, may not be zero.

To convert the indirect specification of pressure in the continuity equation to an explicit form, we write the momentum Eq. 5.34 as

$$\phi = \hat{\phi} - d^\phi \Delta(\delta P) \quad (\phi = u, v, w). \quad (6.2a)$$

where

$$\delta P = P^{n+1} - P^n, \quad (6.2b)$$

$$\hat{\phi} = \frac{\sum_{\ell=1}^6 a_\ell^\phi \phi_\ell + b_0^\phi - d^\phi \Delta P^n}{a_0^\phi}. \quad (6.2c)$$

In Eq. 6.2a, δP (instead of P) is used to speed the convergence. This is particularly helpful when the change in pressure is small compared to the absolute pressure of the system.

For example, the z -direction velocity w at the north surface of the main control volume is

$$w_6 = \hat{w}_6 - d_6^w (\delta P_6 - \delta P_0). \quad (6.3a)$$

where

$$\hat{w}_6 = \frac{\alpha \sum_{\ell=1}^6 a_\ell^w w_\ell + b_0^w - d_6^w (P_6^n - P_0^n)}{a_0^w}. \quad (6.3b)$$

$$d_6^w = \frac{2\bar{V}_6^w}{a_0^w(\Delta z_0 + \Delta z_6)}, \quad (6.3c)$$

and

$$\bar{V}_6^w = (\Delta z_0 + \Delta z_6) \left/ \left(\frac{\Delta z_0}{V_0} + \frac{\Delta z_6}{V_6} \right) \right.. \quad (6.3d)$$

Defining \hat{u} , \hat{v} , d , and \bar{V} in a similar manner, the following set of expressions can be derived.

$$u_1 = \hat{u}_1 - d_1^u(\delta P_0 - \delta P_1),$$

$$u_2 = \hat{u}_2 - d_2^u(\delta P_2 - \delta P_0),$$

$$v_3 = \hat{v}_3 - d_3^v(\delta P_0 - \delta P_3),$$

$$v_4 = \hat{v}_4 - d_4^v(\delta P_4 - \delta P_0),$$

and

$$w_5 = \hat{w}_5 - d_5^w(\delta P_0 - \delta P_5), \quad (6.4)$$

where

$$d_1^u = \frac{2\bar{V}_1^u}{a_0^u(\Delta x_0 + \Delta x_1)},$$

$$d_2^u = \frac{2\bar{V}_2^u}{a_0^u(\Delta x_0 + \Delta x_2)},$$

$$d_3^v = \frac{2\bar{V}_3^v}{a_0^v(\Delta y_0 + \Delta y_3)},$$

$$d_4^v = \frac{2\bar{V}_4^v}{a_0^v(\Delta y_0 + \Delta y_4)},$$

and

$$d_5^w = \frac{2\bar{V}_5^w}{a_0^w(\Delta z_0 + \Delta z_5)}. \quad (6.5)$$

The characteristic volumes are defined as

$$\bar{V}_1^u = (\Delta x_0 + \Delta x_1) \left/ \left(\frac{\Delta x_0}{V_0} + \frac{\Delta x_1}{V_1} \right) \right..$$

$$\bar{V}_2^u = (\Delta x_0 + \Delta x_2) \left/ \left(\frac{\Delta x_0}{V_0} + \frac{\Delta x_2}{V_2} \right) \right..$$

$$\bar{V}_3^v = (\Delta y_0 + \Delta y_3) \left/ \left(\frac{\Delta y_0}{V_0} + \frac{\Delta y_3}{V_3} \right) \right..$$

$$\bar{V}_4^v = (\Delta y_0 + \Delta y_4) \left/ \left(\frac{\Delta y_0}{V_0} + \frac{\Delta y_4}{V_4} \right) \right..$$

and

$$\bar{V}_5^w = (\Delta z_0 + \Delta z_5) \left/ \left(\frac{\Delta z_0}{V_0} + \frac{\Delta z_5}{V_5} \right) \right.. \quad (6.6)$$

In Eqs. 6.6, the subscripts 1-6 refer to velocities at the surfaces of the main control volume. Substitution of Eqs. 6.3 and 6.4 into Eq. 6.1 and rearranging yield

$$a_0^p \delta P_0 - \sum_{\ell=1}^6 a_\ell^p \delta P_\ell - b_0^p = \delta_0. \quad (6.7)$$

where the coefficients are as listed in Table 12. These coefficients form a symmetric matrix.

Equation 6.7 is the required pressure equation. It can be solved by using any one of the matrix solvers described in Sec. 11.3.

7 Turbulence Modeling

Currently, two options are available in COMMIX-PPC to account for turbulence effects. One is the constant turbulent viscosity model and the other is the $k-\epsilon$ two-equation model; both are briefly described in the following.

7.1 Constant Turbulent Viscosity Model

The constant turbulent viscosity model, in which the turbulent viscosity and the turbulent conductivity are simply taken to be uniform, is the simplest turbulence model. The value of the turbulent viscosity is a user-prescribed single-input constant. Strictly speaking, the constant-diffusivity model is not a turbulence model. We sometimes find it useful in performing scoping calculations.

It is preferable to prescribe values of turbulent viscosity and turbulent conductivity based on experimental data. If the experimental information is not available, then turbulent viscosity can be estimated with the following equation, suggested by Sha and Launder:²⁵

$$\mu_{\text{tur}} = 0.007 c_\mu \rho U_{\text{max}} \ell. \quad (7.1)$$

where

$$\begin{aligned} c_\mu &= 0.1 & \text{for } Re_{\text{max}} > 2000, \\ c_\mu &= 0.1(0.001 Re_{\text{max}} - 1) & \text{for } 1000 \leq Re_{\text{max}} \leq 2000, \\ c_\mu &= 0 & \text{for } Re_{\text{max}} < 1000. \end{aligned} \quad (7.2)$$

$$U_{\text{max}} = \text{Max}(u, v, w). \quad (7.3)$$

Table 12. Coefficients of the pressure equation
(Eq. 6.7)

$a_1^p = \left(\frac{A_x}{a_0^u} \right)_{i-1/2} \langle \rho \rangle_0^1 \left(\frac{2 \bar{V}_1^u}{\Delta x_0 + \Delta x_1} \right)$
$a_2^p = \left(\frac{A_x}{a_0^u} \right)_{i+1/2} \langle \rho \rangle_2^0 \left(\frac{2 \bar{V}_2^u}{\Delta x_0 + \Delta x_2} \right)$
$a_3^p = \left(\frac{A_y}{a_0^v} \right)_{j-1/2} \langle \rho \rangle_0^3 \left(\frac{2 \bar{V}_3^v}{\Delta y_0 + \Delta y_3} \right)$
$a_4^p = \left(\frac{A_y}{a_0^v} \right)_{j+1/2} \langle \rho \rangle_4^0 \left(\frac{2 \bar{V}_4^v}{\Delta y_0 + \Delta y_4} \right)$
$a_5^p = \left(\frac{A_z}{a_0^w} \right)_{k-1/2} \langle \rho \rangle_0^5 \left(\frac{2 \bar{V}_5^w}{\Delta z_0 + \Delta z_5} \right)$
$a_6^p = \left(\frac{A_z}{a_0^w} \right)_{k+1/2} \langle \rho \rangle_6^0 \left(\frac{2 \bar{V}_6^w}{\Delta z_0 + \Delta z_6} \right)$
$a_0^p = a_1^p + a_2^p + a_3^p + a_4^p + a_5^p + a_6^p$
$b_0^p = -V_0 \left(\frac{\partial \rho}{\partial t} \right)_0 + (A_x \hat{u})_{i-1/2} \langle \rho \rangle_0^1 - (A_x \hat{u})_{i+1/2} \langle \rho \rangle_2^0$
$+ (A_y \hat{v})_{j-1/2} \langle \rho \rangle_0^3 - (A_y \hat{v})_{j+1/2} \langle \rho \rangle_4^0$
$+ (A_z \hat{w})_{k-1/2} \langle \rho \rangle_0^5 - (A_z \hat{w})_{k+1/2} \langle \rho \rangle_6^0 - \dot{m}''' V_0$

$$Re_{max} = \text{Max}(Re_x, Re_y, Re_z) . \quad (7.4)$$

and

$$Re = \frac{u D_h \rho}{\mu} . \quad (7.5)$$

The mixing length ℓ is given by

$$\ell = C_\ell D_h , \quad (7.6)$$

with the coefficient

$$C_\ell = 0.4 , \quad (7.7)$$

and D_h is the hydraulic diameter.

If information about the turbulent conductivity λ_{tur} is not available, the following approximation may be used:

$$\lambda_{\text{tur}} = \frac{C_p \mu_{\text{tur}}}{\sigma_h} = \frac{C_p \mu_{\text{tur}}}{0.8 [1 - \exp(-6 \times 10^{-5} \text{Re} \text{Pr}^{1/3})]} \quad (7.8)$$

where σ_h is the turbulent Prandtl number, Re is the characteristic Reynolds number, and $\text{Pr} = C_p \mu / \lambda$ is the molecular Prandtl number. Equation 7.8 was proposed by Nijssing and Eifler.²⁶

7.2 k- ϵ Two-Equation Turbulence Model

The derivations of the transport equations for k and ϵ are well documented in the literature, e.g., Sha and Launder,²⁵ Launder and Spalding,²⁷ and Arpaci and Larsen.²⁸ Here, we only briefly summarize the results. The turbulence kinetic energy k is defined by

$$k = \frac{1}{2} \overline{(u'^2 + v'^2 + w'^2)} \quad (7.9)$$

and the dissipation rate is defined by

$$\epsilon = \nu \overline{\frac{\partial u_i}{\partial x_j} \frac{\partial u_i}{\partial x_j}} \quad (7.10)$$

Here, u' , v' , and w' denote the fluctuation velocity components in the coordinate directions x_1 , x_2 , and x_3 respectively, ν is the molecular-kinematic viscosity, i and j are the indices from 1 to 3, and the overbars denote time averaging.

7.2.1 Transport Equation for k

The transport equation for turbulence kinetic energy k can be written as

$$\rho \frac{\partial k}{\partial t} + \rho u_j \frac{\partial k}{\partial x_j} = -\rho \overline{u_i u_j} \frac{\partial u_i}{\partial x_j} + \overline{\rho' u_i} g_i - \mu \overline{\frac{\partial u_i}{\partial x_j} \left(\frac{\partial u_i}{\partial x_j} + \frac{\partial u_j}{\partial x_i} \right)} \quad \text{A} \quad \text{B} \quad \text{C}$$

$$+ \frac{\partial}{\partial x_j} \left[\mu \left(\frac{\partial k}{\partial x_j} + \frac{\overline{u_i u_j}}{\partial x_i} \right) - \rho \frac{\overline{u_i u_i u_j}}{2} - \rho \overline{u_i} \delta_{ij} \right]. \quad \text{D} \quad (7.11)$$

The four groups of terms on the right-hand side are

A: source due to mean shear,

B: buoyancy interactions,

C: loss of k through viscous dissipation, and

D: diffusive transport of k and randomizing action of the pressure/strain correlation.

It is evident that Eq. 7.11 requires closure. The prevailing practice is to rewrite Eq. 7.11 in the following form:

$$\rho \frac{\partial k}{\partial t} + \rho u_j \frac{\partial k}{\partial x_j} = P_k + G_k - \rho \epsilon + \frac{\partial}{\partial x_j} \left[\left(\frac{\mu_{\text{tur}}}{\sigma_k} + \mu_{\text{lam}} \right) \frac{\partial k}{\partial x_j} \right]. \quad (7.12)$$

in which

$$P_k = \mu_{\text{tur}} \left[\frac{\partial u_i}{\partial x_j} \left(\frac{\partial u_i}{\partial x_j} + \frac{\partial u_j}{\partial x_i} \right) \right] \quad (7.13)$$

is the source due to mean shear, and

$$G_k = - \frac{\mu_{\text{tur}}}{\rho \sigma_h} \frac{\partial p}{\partial T} \left(\frac{\partial T}{\partial x_j} g_j \right) \quad (7.14)$$

is the source due to thermal buoyancy. It is commonly recommended that the turbulence Prandtl number σ_h be assigned a value of 0.9. The term containing σ_k in Eq. 7.12 represents the diffusion of k , and σ_k is called the turbulence Prandtl number for k . Launder et al.²⁹ have recommended that σ_k be assigned the value 1.0.

7.2.2 Transport Equation for ϵ

The transport equation for ϵ is discussed in detail by Daly and Harlow,³⁰ Hanjalic and Launder,³¹ and Lumley and Khajeh-Nouri.³² At the present time, the only feasible approach toward devising a useful ϵ equation is to employ physical intuition and intelligent dimensional analysis. The resulting ϵ equation usually contains several empirical coefficients that require adjustment to account for prominent behaviors of different shear flows. The equation proposed by Jones and Launder³³ and by Daly and Harlow³⁰ is

$$\rho \frac{\partial \epsilon}{\partial t} + \rho u_j \frac{\partial \epsilon}{\partial x_j} = C_1 \frac{\epsilon}{k} (P_k + G_k) - C_2 \frac{\rho \epsilon^2}{k} + \frac{\partial}{\partial x_j} \left[\left(\frac{\mu_{\text{tur}}}{\sigma_\epsilon} + \mu_{\text{lam}} \right) \frac{\partial \epsilon}{\partial x_j} \right]. \quad (7.15)$$

In Eq. 7.15, the source terms P_k and G_k have the same form as Eq. 7.13 and Eq. 7.14, the second term on the right accounts for energy dissipation, and the last term represents diffusion, in which σ_ϵ is the turbulence Prandtl number for ϵ and its recommended value²⁸ is 1.3. The choice of the coefficient of the production term C_1 is usually based on near-wall turbulence, whereas the coefficient C_2 is determined from the decay-of-grid turbulence. The values of C_1 and C_2 recommended by Launder et al.³⁴ are 1.44 and 1.92, respectively.

7.2.3 Sequence of Steps in the $k-\epsilon$ Two-Equation Turbulence Model

In the $k-\epsilon$ two-equation turbulence model, the transport equations for the turbulence kinetic energy k (Eq. 7.12) and for the dissipation rate of turbulence kinetic energy ϵ (Eq. 7.15) are solved first. Then, the turbulent viscosity μ_{tur} is determined from the relation

$$\mu_{\text{tur}} = \left(\frac{C_D \rho k^2}{\epsilon} \right). \quad (7.16)$$

where, C_D is a constant with the recommended value 0.09. The turbulent thermal conductivity λ_{tur} is determined from the equation

$$\lambda_{\text{tur}} = \frac{C_p \mu_{\text{tur}}}{\sigma_h}. \quad (7.17)$$

In turbulent flows, the turbulent diffusivities in the governing conservation equation (3.1) are time-averaged quantities. By combining them with their respective molecular counterparts, we can write

$$\mu = \mu_{\text{eff}} = \mu_{\text{lam}} + \mu_{\text{tur}} \quad (7.18)$$

and

$$\lambda = \lambda_{\text{eff}} = \lambda_{\text{lam}} + \lambda_{\text{tur}}. \quad (7.19)$$

where, the subscripts lam and tur stand for laminar (molecular) and turbulent properties, respectively.

The Prandtl's mixing-length hypothesis is a special case of the $k-\epsilon$ two-equation turbulence model. We shall now proceed to demonstrate that this is indeed the case. For steady-state, one-dimensional flow near a wall, the effects of convection and diffusion are usually negligible; turbulence production is balanced by dissipation. Hence, Eq. 7.12 reduces to

$$\mu_{\text{tur}} \left(\frac{\partial u}{\partial y} \right)^2 = \rho \epsilon. \quad (7.20)$$

Combining Eq. 7.16 and Eq. 7.20 gives

$$\mu_{\text{tur}}^2 \left(\frac{\partial u}{\partial y} \right)^2 = C_D \rho^2 k^2. \quad (7.21)$$

Because

$$\tau_{\text{tur}} = \mu_{\text{tur}} \frac{\partial u}{\partial y}, \quad (7.22)$$

Eq. 7.21 can be written as

$$\tau_{\text{tur}} = C_D^{1/2} \rho k, \quad (7.23)$$

which states that the turbulent shear stress is directly proportional to the turbulence kinetic energy in local equilibrium turbulence. This important relationship is supported by numerous experiments on flows near walls.

From dimensional considerations,²⁷ the dissipation rate ϵ can be expressed as

$$\epsilon = C_D^{3/4} k^{3/2} / \ell. \quad (7.24)$$

Substituting Eqs. 7.16 and 7.24 into Eq. 7.20 and after rearrangement, one obtains

$$C_D^{1/2} k = \left(\frac{\partial u}{\partial y} \right)^2 \ell^2. \quad (7.25)$$

Eliminating k between Eqs. 7.23 and 7.25 gives

$$\tau_{\text{tur}} = \rho \ell^2 \left(\frac{\partial u}{\partial y} \right)^2. \quad (7.26)$$

which is the original form given by the Prandtl's mixing-length hypothesis. Thus, the mixing-length hypothesis can be deduced from the transport equation for the turbulence kinetic energy upon neglecting the contributions from convection and diffusion. Its application is limited to local equilibrium turbulent flows that usually occur near walls. Consequently, as we shall soon see, the results of a local equilibrium turbulence model play an important role in the development of the wall function to be described in Sec. 7.4.

7.3 Boundary Conditions for Turbulence Transport Equations

There are three types of boundaries: 1. a line or a surface (plane) of symmetry, 2. inlet and outlet boundaries, and 3. a solid wall. The first two boundaries are discussed here, and a solid-wall boundary is discussed in Sec. 7.4.

7.3.1 Symmetry Boundary

The simplest boundary is the line or plane of symmetry; at a symmetry line or plane, the normal velocity is zero. The gradients of scalar quantities k and ϵ normal to the symmetry line or plane also vanish.

7.3.2 Inlet and Outlet Boundaries

At the outlet plane (free boundary), the gradient of turbulence quantities is assumed to be zero. Thus, at the outlet plane,

$$\frac{\partial k}{\partial z} = 0,$$

and

$$\frac{\partial \epsilon}{\partial z} = 0, \quad (7.27)$$

where z represents flow direction at the outlet.

The inlet plane requires special treatment. Both the inlet turbulence kinetic energy k_{in} and the inlet dissipation rate ϵ_{in} should be obtained from measurements if available. If measurements are not available at the inlet plane, the following procedure may be used to estimate k_{in} and ϵ_{in} . If the inlet velocity u_{in} is uniform,

$$k_{in} = 0.001 u_{in}^2 \quad (7.28)$$

and

$$\epsilon_{in} = C_D k_{in}^{3/2} / \ell_{in}, \quad (7.29)$$

where ℓ_{in} is a length scale at the inlet. It is usually assumed that ℓ_{in} is equal to the smaller of $0.42 y$ and 0.1δ , where y denotes the distance to the nearest wall and δ is the width of the shear layer. If u_{in} is not uniform but the profile of the mean velocity at the inlet plane is known, k_{in} can be estimated from

$$k_{in} = 3 \ell_{in}^2 \left[\left(\frac{\partial u_{in}}{\partial y} \right)^2 + \left(\frac{\partial u_{in}}{\partial z} \right)^2 \right]. \quad (7.30)$$

where u_{in} is the mean velocity component in the main flow (x) direction. The inlet dissipation rate ϵ_{in} is again estimated by using Eq. 7.29.

Note that k_{in} and ϵ_{in} are user-specified input parameters in COMMIX-PPC. If the user does not specify k_{in} and ϵ_{in} , COMMIX-PPC assumes that the inlet k and ϵ are negligibly small ($k = 10^{-16}$ and $\epsilon = 10^{-10}$).

7.4 Wall-Function Treatment

In the immediate vicinity of a solid wall, there is a large variation in the values of turbulence properties. Therefore, to predict the correct values of momentum flux, energy flux, and the gradients of k and ϵ , a special procedure is followed, called the wall-function treatment. In this procedure, we implicitly account for steep variation near a wall and avoid the need for a fine mesh. This approach fits well with COMMIX because, in most engineering applications, one rarely has the luxury of resolving the fine details in a boundary layer that are due primarily to the high cost of computation with a fine-mesh system.

In the literature, there are several different treatments of wall function.³⁵ It appears that, at the present time, no single wall-function treatment can claim superiority in both generality and accuracy under a variety of condition. In view of this, we have developed the wall-function model in COMMIX-PPC based on the following guidelines:

1. Simplicity.
2. Minimizing numerical difficulties.

3. Wide range of applicability.

The first two guidelines are self-explanatory. In a general-purpose code such as COMMIX, one may frequently have to deal simultaneously with laminar and turbulent flows at different locations in a system. Also, during a transient simulation, different flow regimes may occur at the same location but at different times. Thus, in COMMIX-PPC, provision is made to calculate flows with local Reynolds numbers ranging from very small (laminar) to very large (highly turbulent), even though the accuracy of the results may deteriorate in a certain range of the relevant parameters (such as Reynolds number). This is what we mean by a wide range of applicability in Guideline 3.

There are basically two approaches in treating the cells adjacent to walls. The first is that both k and ϵ are calculated algebraically for the cells next to the walls, and therefore, the transport equations for k and ϵ are not solved. The second approach is to calculate ϵ algebraically and solve the transport equation for k for cells adjacent to walls. In COMMIX-PPC, we have adopted the first approach, i.e., both k and ϵ are solved algebraically, because of simplicity (Guideline 1).

There are also two types of wall-function models; a two-layer model and a three-layer model. In COMMIX-PPC, the simpler two-layer wall-function model is adopted with minor modification.

7.4.1 A Wall-Function Model

Figure 10 illustrates the wall-function model used in COMMIX-PPC, where P is the node adjacent to the wall, y_p is the distance from P to the wall, and y_ℓ is the thickness of the viscous sublayer. When $y_p > y_\ell$, the node P is in the fully turbulent region; when $y_p < y_\ell$, the node P is in the laminar sublayer. The distance y_p is fixed when the user completes modeling the geometry (and mesh system). The thickness of the viscous sublayer y_ℓ , however, is not constant and often cannot be easily determined beforehand. Hence, provision is made in COMMIX-PPC to accommodate both situations.

When $y_p > y_\ell$, the first node is in the fully turbulent zone (Fig. 10). The velocity at node P is given by the law of the wall in the fully turbulent region

$$u_p^+ = \frac{1}{K} \ln(E y_p^+), \quad (7.31)$$

where

$$u_p^+ = u_p/u_\tau, \quad (7.32)$$

$$u_\tau = (\tau_w/\rho)^{1/2}, \quad (7.33)$$

$$y^+ = yu_\tau/\nu, \quad (7.34)$$

E is a constant equal to 9.0, K is the von Karman constant ($K = 0.42$), and ν is the kinematic viscosity.

The turbulence kinetic energy k at node P can be calculated by using Eq. 7.23, which is rewritten as

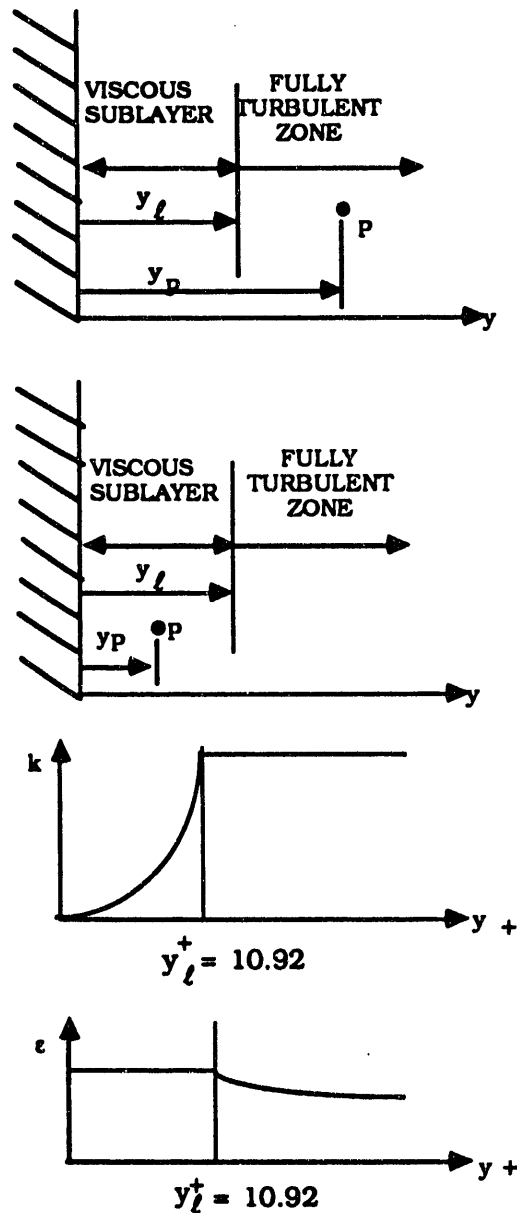


Fig. 10. Two-layer wall-function model
($y_p > y_l$)

$$k_p^3 = u_\tau^2 / C_D^{1/2} . \quad (7.35)$$

for which the approximation that $\tau_{\text{tur}} = \tau_w$ was used. The turbulence dissipation rate ϵ at node P is calculated by using an equation similar to Eq. 7.24, i.e.,

$$\begin{aligned} \epsilon_p &= C_D^{3/4} k_p^{3/2} / (K y_p) \\ &= u_\tau^3 / (K y_p) . \end{aligned} \quad (7.36)$$

because $\ell_p = K y_p$.

When $Y_P \leq Y_\ell$, the node P is in the viscous sublayer (Fig. 10). The velocity at node P is given by the law of the wall in the viscous sublayer

$$u_p^+ = y_p^+. \quad (7.37)$$

which can be rewritten as

$$u_\tau = (v u_p / y_p)^{1/2}. \quad (7.37a)$$

The turbulence kinetic energy at node P is calculated from

$$k_p = k_\ell (y_p / y_\ell)^2. \quad (7.38)$$

where k_ℓ is the turbulence kinetic energy at $y = y_\ell$. If we assume that Eq. 7.24, which is valid for local equilibrium turbulence, applies at the edge of the laminar sublayer ($y = y_\ell$), then Eq. 7.38 becomes

$$k_p = u_\tau^2 (y_p / y_\ell)^2 / C_D^{1/2}. \quad (7.38a)$$

Note that the assumption of local equilibrium at the edge of the laminar sublayer may not be strictly valid. It is known²⁸ that local equilibrium applies in the region $30 < y^+ < 50$. The main reason that the assumption was adopted was to simplify the calculation. The present model also assumes that the turbulence kinetic energy k is constant outside the laminar sublayer (Fig. 10). This assumption greatly simplifies the numerical calculation (Guideline 1) because no extrapolation is needed.

The turbulence dissipation rate ε at node P, which is calculated by using Eq. 7.35 and by assuming that the dissipation rate in the viscous sublayer is constant and equal to that at $y = y_\ell$, is defined as

$$\varepsilon_p = u_\tau^3 / k y_\ell. \quad (7.39)$$

The assumption of constant ε in the viscous sublayer is in agreement with most wall-function models in the literature. The assumption that ε_p is equal to ε at $y = y_\ell$ is different from assumptions in the literature. The reason for making the last assumption is to make ε continuous so that numerical difficulties associated with discontinuous functions can be avoided (Guideline 2).

7.4.2 Evaluating k and ε for Cells Adjacent to Walls

In the computer code, the following paths are followed to determine the proper values of k and ε for cells adjacent to the wall. The key is to determine whether the node adjacent to a wall is in the viscous sublayer or in the turbulent zone. The relevant scaling parameter is the frictional velocity u_τ , which appears in the equations for k , ε , and the velocity distribution given by the law of the wall in Sec. 7.4.1.

The preliminary step is to evaluate the dimensionless thickness of the viscous sublayer y_ℓ^+ . This is accomplished by matching the velocity at the edge of the viscous sublayer ($y = y_\ell$) to that from the law of the wall. Because $u_\ell^+ = y_\ell^+$,

$$y_t^+ = \frac{1}{K} \ln(E y_t^+), \quad (7.40)$$

where

$$y_t^+ = y_t u_t / v. \quad (7.41)$$

with $K = 0.42$, and $E = 9$. It should be noted that y_t^+ depends only on the constants K and E . When the values of K and E just cited are used, $y_t^+ = 10.92$. We then proceed to calculate k_p and ϵ_p as follows:

Step 1 – Calculate y_t based on a guessed value of u_t

The value of u_t can be estimated by either the viscous sublayer relationship (Eq. 7.37a), or the local equilibrium turbulence relationship (Eq. 7.35). In the code, we take the larger of the two as the guessed value of u_t , i.e.,

$$u_t^2 = \max\left(\frac{v u_p}{y_p}, C_D^{1/2} k_p\right). \quad (7.42)$$

Then, y_t is calculated from

$$y_t = v y_t^+ / u_t = 10.92 \frac{v}{u_t}.$$

Step 2 – Compute k_p and ϵ_p

If $y_p > y_t$, the node P is in the turbulent zone, and the frictional velocity u_t is recomputed iteratively by using the law of the wall in the turbulent zone,

$$u_t = K u_p / \ln(E y_p u_t / v). \quad (7.43)$$

Next, k_p and ϵ_p are calculated according to Eqs. 7.35 and 7.36, respectively, i.e.,

$$k_p = u_t^2 / C_D^{1/2}$$

$$\epsilon_p = u_t^3 / K y_p.$$

If $y_p \leq y_t$, the node P is in the viscous sublayer, and the friction velocity u_t is recomputed by using Eq. 7.37a. Thus,

$$u_t = (v u_p / y_p)^{1/2}.$$

Next, k_p and ϵ_p are calculated according to Eqs. 7.38a and 7.39, respectively, i.e.,

$$k_p = u_t^2 (y_p / y_t)^2 / C_D^{1/2}$$

$$\epsilon_p = u_t^3 / K y_t.$$

The algebraically computed k_p and ϵ_p of the cells adjacent to the wall are then used in the solution of the transport equations of k and ϵ for other cells. If the results do not satisfy the convergence criteria, Steps 1 and 2 are repeated until convergence is reached.

7.5 Solution Procedure for Calculating Turbulent Flows

The procedure for calculating turbulent flows is similar to that described in Sec. 11, except that two additional transport equations for k and for ϵ must be solved. This is accomplished after solving the pressure equation and before solving the component mass conservation equation. A fully implicit solution procedure for calculating turbulent flows is summarized in Table 13.

7.6 Discussion

Eight constants are employed in the $k-\epsilon$ two-equation turbulence model. Listed in Table 14, they are the default values used in COMMIX-PPC. Some of these values may be slightly different from those used in other $k-\epsilon$ two-equation turbulence models. If users wish to use values other than those listed in Table 14, they can readily do so (see input preparation described in Volume II).

The wall-function model described in Sec. 7.4 is simpler than most other models in the literature. We have thoroughly tested this model against data for fully developed pipe flow and for two-dimensional sudden-expansion associated with backward-facing steps.³⁶ The results indicate that the current $k-\epsilon$ two-equation turbulence model compares favorably with the data from fully developed pipe flow at high Reynolds numbers, but is less favorable for the backward-facing step, particularly near the reattachment zone. These observations are in agreement with the assessment of other two-equation turbulence models.³⁷

The $k-\epsilon$ two-equation turbulence model has also been tested against data from a circular buoyant jet.³⁶ Both the calculated centerline velocity and centerline temperature distributions compare favorably with data for a densimetric Froude number of 5. The buoyant jet is a free shear flow and therefore is not affected by the wall-function model.

Finally, it should be noted that the $k-\epsilon$ two-equation turbulence model described in this chapter is, strictly speaking, only valid for turbulence at very high Reynolds numbers. Even though the code will perform calculations for flows at lower Reynolds numbers, the results are less reliable and must be examined and interpreted very carefully. The $k-\epsilon$ two-equation turbulence model does not automatically degenerate to that for low Reynolds flows, which is the inherent limitation of most turbulence models. Users must be aware of this limitation. Our assessment is that this model does have some generality in treating a variety of turbulent flows encountered in engineering systems, even though the accuracy may vary from one type of flow to another.

**Table 13. Fully implicit (SIMPLEST-ANL) solution sequence
for turbulent flows**

1. Calculate velocity-pressure relation coefficients from the previous iterate values of u , v , w , and μ_{eff} :

$$\hat{\phi}, d^*; (\phi = u, v, w).$$

2. Calculate pressure equation coefficients using $\hat{\phi}, d^*$:

$$a_0^p, a_\ell^p, b_0^p.$$

3. Solve pressure equation for new-time, new-iterate pressure δP :

$$a_0^p \delta P_0 = \sum a_\ell^p \delta P_\ell + b_0^p.$$

4. Calculate new-time, new-iterate velocities u , v , w from velocity-pressure relations:

$$\phi = \hat{\phi} - d^* \Delta \delta P; (\phi = u, v, w).$$

5. Calculate coefficients for k and ϵ equations using new-time new-iterate velocities:

$$a_0^k, a_\ell^k, b_0^k; a_0^\epsilon, a_\ell^\epsilon, b_0^\epsilon$$

6. Solve k and ϵ equations for new-time, new-iterate k and ϵ :

$$a_0^k k_0 = \sum a_\ell^k k_\ell + b_0^k; a_0^\epsilon \epsilon_0 = \sum a_\ell^\epsilon \epsilon_\ell + b_0^\epsilon$$

7. Calculate new-time, new-iterate μ_{eff} and λ_{eff} :

$$\mu_{\text{tur}} = C_D \rho k^2 / \epsilon, \lambda_{\text{tur}} = C_P \mu_{\text{tur}} / \sigma_h$$

$$\mu_{\text{eff}} = \mu_{\text{lam}} + \mu_{\text{tur}}, \lambda_{\text{eff}} = \lambda_{\text{lam}} + \lambda_{\text{tur}}$$

8. Solve mass fraction x_k from component conservation equation.

$$(a_0^x x_0)_k = \left(\sum_\ell a_\ell^x x_\ell \right)_k + (b_0^x)_k$$

9. Calculate partial steam pressure, saturation temperature, and mixture enthalpy.

$$P_s, T_s, h.$$

10. Check for convergence of u , v , w , h , k , ϵ , x_k ; if not converged, return to Step 1.

Table 14. Summary of constants employed in the $k-\epsilon$ two-equation turbulence model

Symbol	Value	Appearance (Equation)
σ_h	0.9	7.11
σ_k	1.0	7.11
σ_ϵ	1.3	7.15
C_1	1.44	7.15
C_2	1.92	7.15
C_D	0.09	7.16
K	0.42	7.31 and 7.35
E	9.0	7.31 and 7.39

8 One-Dimensional Formulation for Condenser Tube-Side Flow

Because the flow in the tube side is essentially unidirectional along the tube axis, one-dimensional calculations can be used. The flow is also single phase. The governing equations and their finite-volume formulations are as follows:

8.1 Governing Equations

Continuity equation

$$\frac{\partial \rho}{\partial t} + \frac{\partial}{\partial x}(\rho u) = 0. \quad (8.1)$$

Momentum equation

$$\frac{\partial}{\partial t}(\rho u) + \frac{\partial}{\partial x}(\rho uu) = -\frac{\partial P}{\partial x} + \rho g_x - R_x. \quad (8.2)$$

Energy equation

$$\frac{\partial}{\partial t}(\rho h) + \frac{\partial}{\partial x}(\rho uh) = \dot{q}_w'''. \quad (8.3)$$

where R_x is the tube-wall resistance per unit volume, and \dot{q}_w''' is the wall heat flux per unit volume.

Thus, wall friction is incorporated as a sink in the momentum equation and heat transfer at the tube wall is treated as a source in the energy equation. In the latter, both conduction and dissipation in fluid are neglected.

8.2 Finite-Volume Formulation

8.2.1 Control Volume

In common with shell-side analysis, the staggered-grid system was used for tube-side computation. All dependent nonflow variables are stored at the center of a cell, and flow velocities are stored at the surface of the cell.

Figure 11 shows the control volume for nonflow variables. It is constructed around a grid point $0(i)$, which has grid points $1(i-1)$ and $2(i+1)$ as its west and east neighbors. This control volume, also called the main control volume, will be used for calculating the nonflow variables, such as temperature and pressure.

Because the velocities are calculated for the surface of the cells, the control volume for the fluid velocity at the east surface of the main control volume is that of a cell shifted half a cell length from the main control volume, as shown in Fig. 12. The pressure difference between the two adjacent grid points (0 and 2) drives the flow. The staggered control volume is used for the momentum equation.

8.2.2 Finite-Volume Equations for Continuity, Momentum, and Energy Conservation

8.2.2.1 Continuity Equation

Figure 13 shows the control volume for the continuity equation, in which F is the mass flux across the control surface.

Upon integrating Eq. 8.1 over the control volume, we obtain

$$\frac{(\rho_i - \rho_i^n)V_i}{\Delta t} + F_{i+1/2} - F_{i-1/2} = 0. \quad (8.4)$$

where $V_i = A \Delta x_i$ is the fluid volume, A is the cross-sectional area of the tube, superscript n refers to known old time-step values, and the superscript $n+1$ refers to new time-step values. The latter is omitted for simplicity.

The mass flux $F_{i+1/2}$ and $F_{i-1/2}$ in Eq. 8.4 can be expressed as

$$\begin{aligned} F_{i+1/2} &= \langle \rho \rangle_{i+1}^i (uA)_{i+1/2} = \rho_i (uA)_{i+1/2} & (\text{If } u_{i+1/2} > 0) \\ &= \rho_{i+1} (uA)_{i+1/2} & (\text{If } u_{i+1/2} < 0) \end{aligned} \quad (8.5)$$

and

$$\begin{aligned} F_{i-1/2} &= \langle \rho \rangle_i^{i-1} (uA)_{i-1/2} = \rho_{i-1} (uA)_{i-1/2} & (\text{If } u_{i-1/2} > 0) \\ &= \rho_i (uA)_{i-1/2} & (\text{If } u_{i-1/2} < 0). \end{aligned} \quad (8.6)$$

Here, the upwind-difference scheme is used. A location-value superscript is used for positive velocity and a location-value subscript is used for negative velocity.

Equations 8.5 and 8.6 can also be written as

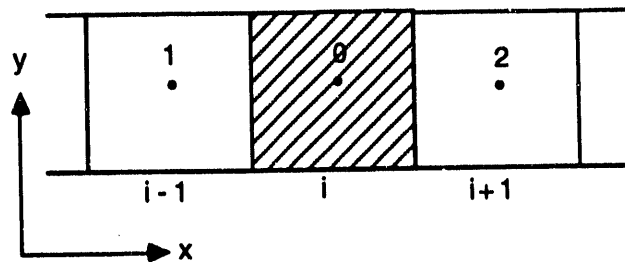


Fig. 11. Control volume for nonflow variables

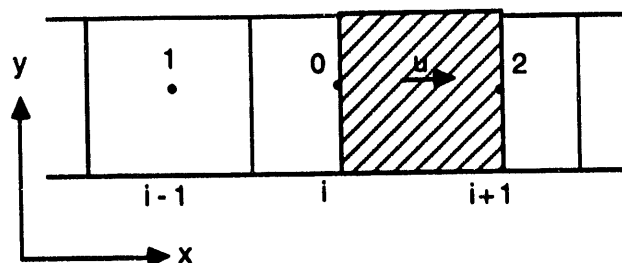


Fig. 12. Control volume for flow velocities

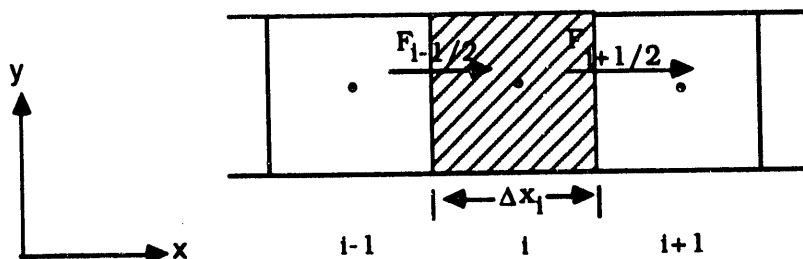


Fig. 13. Control volume for the continuity equation

$$\langle \rho \rangle_{i+1}^i (uA)_{i+1/2} = |0, (uA)_{i+1/2}| \rho_i - |0, -(uA)_{i+1/2}| \rho_{i+1} \quad (8.7)$$

and

$$\langle \rho \rangle_i^{i-1} (uA)_{i-1/2} = |0, (uA)_{i-1/2}| \rho_{i-1} - |0, -(uA)_{i-1/2}| \rho_i \quad (8.8)$$

The symbol $|x_1, x_2|$ denotes the maximum of the two real numbers x_1 and x_2 .

8.2.2.2 Momentum Equation

The finite-volume formulation for the momentum equation can be obtained by integrating Eq. 8.2 over the staggered control volume, as shown in Fig. 14.

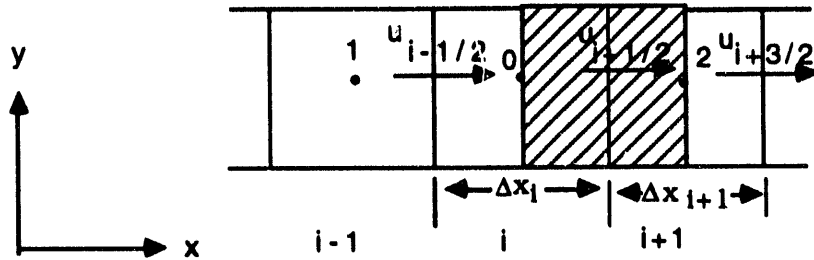


Fig. 14. Control volume for the momentum equation

Transient Term

$$\int \frac{\partial}{\partial t} (\rho u) dV = \frac{[(\rho u)_{i+1/2} - (\rho u)_{i+1/2}^n]}{\Delta t} V_{i+1/2}, \quad (8.9)$$

where

$$\rho_{i+1/2} = \frac{\rho_{i-1} \Delta x_i + \rho_{i+1} \Delta x_{i+1}}{\Delta x_i + \Delta x_{i+1}} \quad (8.10)$$

$$V_{i+1/2} = \frac{A}{2} (\Delta x_i + \Delta x_{i+1}) \quad (8.11)$$

Convective Term

$$\int \frac{\partial}{\partial x} (\rho u u) dV = [0, F_{i+1}] u_o - [0, -F_{i+1}] u_2 - [0, F_i] u_1 + [0, -F_i] u_o. \quad (8.12)$$

where

$$\begin{aligned} F_{i+1} &= \frac{1}{2} [\langle \rho \rangle_{i+1}^1 (Au)_{i+1/2} + \langle \rho \rangle_{i+2}^{i+1} (Au)_{i+3/2}] \\ &= \frac{1}{2} [0, (Au)_{i+1/2} | \rho_1 - 0, -(Au)_{i+1/2} | \rho_{i+1} + 0, (Au)_{i+3/2} | \rho_{i+1} - 0, -(Au)_{i+3/2} | \rho_{i+2}] \end{aligned} \quad (8.13)$$

$$\begin{aligned} F_i &= \frac{1}{2} [\langle \rho \rangle_i^{i-1} (Au)_{i-1/2} + \langle \rho \rangle_{i+1}^i (Au)_{i+1/2}] \\ &= \frac{1}{2} [0, (Au)_{i-1/2} | \rho_{i-1} - 0, -(Au)_{i-1/2} | \rho_i + 0, (Au)_{i+1/2} | \rho_i - 0, -(Au)_{i+1/2} | \rho_{i+1}] \end{aligned} \quad (8.14)$$

Pressure Term

$$\int -\frac{\partial P}{\partial x} dV = -\frac{P_{i+1} - P_i}{\frac{1}{2} (\Delta x_i + \Delta x_{i+1})} V_{i+1/2} = -(P_{i+1} - P_i) A. \quad (8.15)$$

Gravity Term

$$\int \rho g_x dV = (\rho V)_{i+1/2} g_x. \quad (8.16)$$

Wall Friction Term

$$-\int R_x dV = -(R_x V)_{i+1/2}. \quad (8.17)$$

where

$$R_{x_{i+1/2}} = C_1 \frac{f}{D} \rho_{i+1/2} |u_{i+1/2}^n| u_{i+1/2} = F_R u_{i+1/2}. \quad (8.18)$$

with

$$F_R = C_1 \frac{f}{D} \rho_{i+1/2} |u_{i+1/2}^n|. \quad (8.19)$$

Using Eqs. 8.9, 8.12, 8.15–8.19, we can write the finite-volume form of the momentum equation as

$$a_o^u u_{i+1/2} = a_1^u u_{i-1/2} + a_2^u u_{i+3/2} + b_o^u - (P_{i+1} - P_i) A. \quad (8.20)$$

where

$$a_o^u = \frac{(\rho V)_{i+1/2}}{\Delta t} + |O.F_{i+1}| + |O.-F_i| + F_R V_{i+1/2}. \quad (8.21)$$

$$a_1^u = |O.F_i|. \quad (8.22)$$

$$a_2^u = |O.-F_{i+1}|. \quad (8.23)$$

and

$$b_o^u = (\rho V)_{i+1/2} g_x + \frac{(\rho^n u^n v^n)_{i+1/2}}{\Delta t}. \quad (8.24)$$

Dividing Eq. 8.20 by a_o^u and rearranging, one obtains

$$u_{i+1/2} = \hat{u}_{i+1/2} - du_{i+1/2} (P_{i+1} - P_i). \quad (8.25)$$

where

$$\hat{u}_{i+1/2} = \frac{a_1^u u_{i-1/2} + a_2^u u_{i+3/2} + b_o^u}{a_o^u}. \quad (8.26)$$

$$du_{i+1/2} = \frac{A}{a_o^u}. \quad (8.27)$$

8.2.2.3 Energy Equation

The finite-volume equation for the conservation of energy is obtained by integrating Eq. 8.3 over the main control volume (Fig. 15).

Transient Term

$$\int \frac{\partial(\rho h)}{\partial t} dV = \frac{[(\rho h)_i - (\rho h)_i^n]}{\Delta t} V_i. \quad (8.28)$$

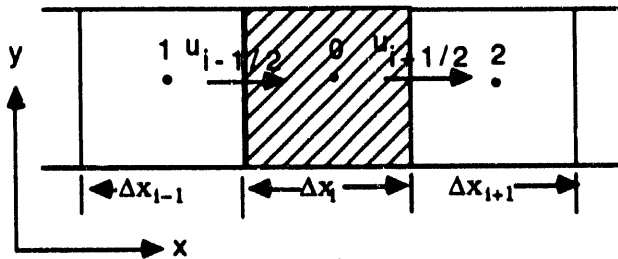


Fig. 15. Control volume for the energy equation

Convective Term

$$\begin{aligned}
 \int \frac{\partial}{\partial x} (\rho u h) dV &= (Au)_{i+1/2} \langle \rho h \rangle_{i+1}^i - (Au)_{i-1/2} \langle \rho h \rangle_i^{i-1} \\
 &= \left| 0 \cdot (Au)_{i+1/2} \rho_i h_i \right| - \left| 0 \cdot -(Au)_{i+1/2} \rho_{i+1} h_{i+1} \right| \\
 &\quad - \left| 0 \cdot (Au)_{i-1/2} \rho_{i-1} h_{i-1} \right| + \left| 0 \cdot -(Au)_{i-1/2} \rho_i h_i \right|. \tag{8.29}
 \end{aligned}$$

Wall Heat Flux Term

$$\int \dot{q}_w'' dV = (\dot{q}_w'' V)_i = \dot{q}_{wi}'' V_i. \tag{8.30}$$

The evaluation of \dot{q}_{wi}'' is discussed in Sec. 9.

Combining Eqs. 8.27–8.32, we obtain the finite-volume equation

$$a_o^h h_i = a_1^h h_{i-1} + a_2^h h_{i+1} + b_o^h. \tag{8.31}$$

where

$$a_o^h = \frac{(\rho V)_1}{\Delta t} + \left| 0 \cdot (Au)_{i+1/2} \rho_i \right| + \left| 0 \cdot -(Au)_{i-1/2} \rho_i \right|, \tag{8.32}$$

$$a_1^h = \left| 0 \cdot (Au)_{i-1/2} \right|. \tag{8.33}$$

$$a_2^h = \left| 0 \cdot -(Au)_{i+1/2} \right|. \tag{8.34}$$

and

$$b_o^h = \frac{(\rho h)_1^n V_i}{\Delta t} + \dot{q}_{wi}'' V_i. \tag{8.35}$$

8.2.3 Pressure Equation

The pressures P_{i+1} and P_i appearing in the momentum equation (8.25) are not known a priori and are determined from the conservation-of-mass equation.

$$\text{Let } P = P^n + \delta P, \quad (8.36)$$

where δP is the pressure increment relative to the old time pressure value P^n .

Using Eq. 8.36, we can rewrite Eq. 8.25 as

$$u_{i+1/2} = \hat{u}_{i+1/2} - (du)_{i+1/2} (\delta P_{i+1} - \delta P_i). \quad (8.37)$$

where

$$\hat{u}_{i+1/2} = \hat{u}_{i+1/2} - (du)_{i+1/2} (P_{i+1}^n - P_i^n). \quad (8.38)$$

Upon substituting Eq. 8.37 into Eq. 8.4 and rearranging, we obtain the pressure equation

$$a_o^P \delta P_i = a_1^P \delta P_{i-1} + a_2^P \delta P_{i+1} + b_o^P. \quad (8.39)$$

where

$$a_o^P = a_1^P + a_2^P. \quad (8.40)$$

$$a_1^P = \langle \rho \rangle_i^{i-1} A (du)_{i-1/2}. \quad (8.41)$$

$$a_2^P = \langle \rho \rangle_{i+1}^i A (du)_{i+1/2}. \quad (8.42)$$

and

$$b_o^P = \langle \rho \rangle_i^{i-1} A \hat{u}_{i-1/2} - \langle \rho \rangle_{i+1}^i A \hat{u}_{i+1/2} - \frac{V_i}{\Delta t} (\rho_i - \rho_i^n). \quad (8.43)$$

9 Auxiliary Relations and Supplementary Physical Models

To broaden the scope of COMMIX-PPC applications and to more accurately account for the phenomena relevant to thermal-hydraulic simulation, several supplementary physical models have been incorporated into COMMIX-PPC.

9.1 Rigorous Fluid-Property Routines

There are two fluid-property packages in COMMIX-PPC. One is for liquid water, the other, for water vapor. These two packages are formulated in a modular fashion so they can be readily replaced by any other property package, if desired. The input description for the use of these packages is given in Volume II of this report.

9.2 Simplified Fluid-Property Option

Besides the rigorous fluid-property packages, a simplified option is available to the user. This option includes both fluid and solid properties. Enthalpy, density, thermal conductivity, viscosity, and the saturation pressure of steam are expressed in the following functional form:

$$h = C_{0h} + C_{1h}T + C_{2h}T^2 + C_{3h}P,$$

$$\rho = C_{0\rho} + C_{1\rho}T + C_{2\rho}P / (T + 273.15),$$

$$k = C_{0k} + C_{1k}T + C_{2k}T^2,$$

$$\mu = C_{0\mu} + C_{1\mu}T + C_{2\mu} / (T + 273.15),$$

and

$$P_s = \exp(C_{0p} + C_{1p}T + C_{2p}T^2). \quad (9.1)$$

In the foregoing equation, T is temperature in degrees C, P is pressure in Pascals, and C₀, C₁, C₂, and C₃ are constant coefficients to be specified by the user. The default values for these constants are zero. We have found that the simplified option is quite useful in many applications because it takes very little time to prepare and input the coefficients into Eq. 9.1. It should be noted that for liquids and solids, the pressure dependence of a property does not apply, and the corresponding coefficients should be set to zero. A detailed description of inputting the simplified property option is given in Volume II of this report.

9.3 Heat Transfer Correlations

9.3.1 Heat Transfer Correlation for Condensation of a Steam/Air Mixture in a Power Condenser

As a steam/air mixture flows past a bank of condensing tubes in a power condenser, noncondensable air tends to accumulate at the interface between the metal surface and the condensate film. Depending on the surface properties and contamination of the metal surface, the noncondensable air tends to adhere to the surface and is, in general, not completely removed by the flow of the condensate film. Condensation also takes place at the interface between the condensate film and the steam/air mixture and, here again, the air also tends to accumulate. Because air is a poor conductor, its accumulation at both interfaces could significantly retard the overall condensation rate. The physical process is complicated, and at the present stage of understanding, we resort to empirical correlations and approximate analysis.

The deposition of dirt and the formation of scale on the inside surface of the tube are also important considerations. In practice, their effect is accounted for by introducing a fouling resistance. Accordingly, the overall heat transfer coefficient for the condensation of a steam/air mixture in a power plant condenser is commonly expressed by^{5,7,8}

$$\frac{1}{U_0} = \frac{1}{h_a} + \frac{1}{h_c} + R_w + R_f + \frac{D_0}{D_1 h_{cw}}, \quad (9.2)$$

where

U_0 = overall heat transfer coefficient, $\text{W}/\text{m}^2\cdot\text{K}$,

h_a = heat transfer coefficient to account for resistance due to the presence of noncondensable air, $\text{W}/\text{m}^2\cdot\text{K}$,

h_c = film heat transfer coefficient between liquid film and uncontaminated tube surface, $\text{W}/\text{m}^2\cdot\text{K}$,

R_w = thermal resistance of tube wall, $\text{m}^2\cdot\text{K}/\text{W}$,

R_f = thermal resistance to account for fouling due to scale formation and dirt deposition on tube wall, $\text{m}^2\cdot\text{K}/\text{W}$,

h_{cw} = tube-side heat transfer coefficient due to flow of cooling water, $\text{W}/\text{m}^2\cdot\text{K}$,

D_0 = outer diameter of the tube, m,

and

D_1 = inner diameter of the tube, m.

Figure 16 shows the component parts of the various resistances. The two resistances due to the presence of an air layer at the tube surface and at the interface between the condensate film and the steam/air mixture are combined into one, namely $1/h_a$. In Fig. 16, T_s is the temperature of the steam/air mixture, T_{cs} is the exterior temperature of the condensate film, T_{wo} is the temperature of the outside tube wall, T_{wi} is the temperature of the inside tube wall, and T_{cw} is the bulk temperature of the cooling water.

9.3.2 Heat Transfer Coefficient due to Presence of Noncondensable Air (h_a)

The heat transfer coefficient due to the presence of air can be evaluated from³⁸

$$h_a = a \frac{D_m}{D_0} Re_m^{0.5} \left(\frac{P_m}{P_a} \right)^{0.6} P_m^{1/3} \left(\frac{\rho_s h_{fg}}{T_s} \right)^{2/3} (T_s - T_{cs})^{1/3} \text{ W}/\text{m}^2\cdot\text{K} \quad (9.3)$$

where

a = empirical constant, 0.82.

D_m = molecular diffusivity, m^2/s ,

P_m = pressure of steam/air mixture, Pa,

P_a = partial pressure of air, Pa,

ρ_s = density of steam, kg/m^3 ,

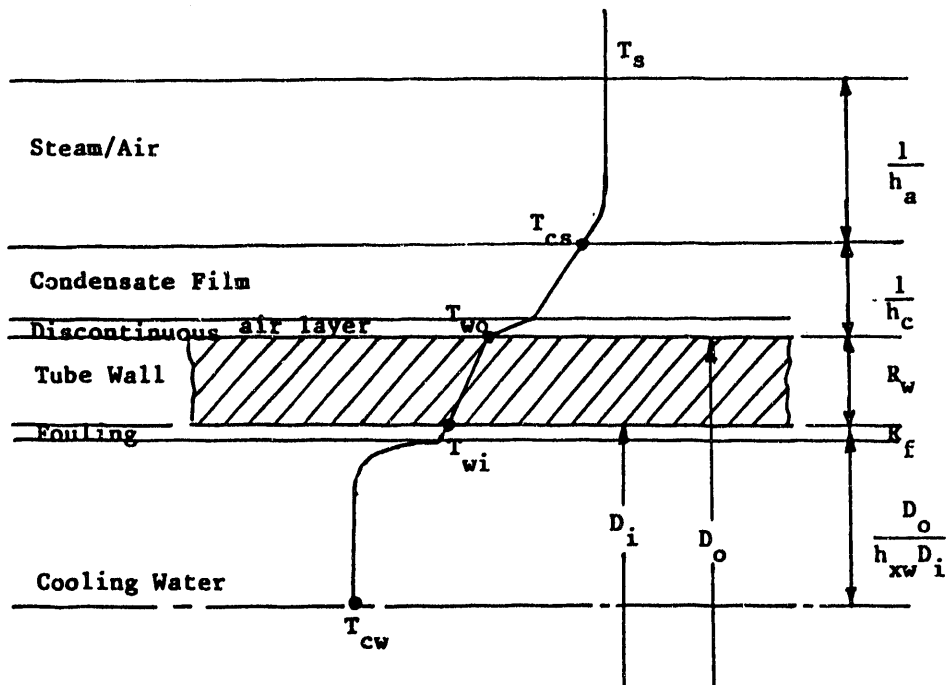


Fig. 16. Component parts of thermal resistances for condensation of a steam/air mixture

T_s = saturation temperature of steam, K,

T_{cas} = vapor/condensate interface temperature, °C,

h_{fg} = latent heat, J/kg,

$$Re_m = \frac{G_m D_o}{\mu_m} = \text{Reynolds number}, \quad (9.3a)$$

G_m = mass flux of mixture flow, kg/m²•sec,

and

μ_m = mixture viscosity, kg/m•s.

9.3.3 Heat Transfer Coefficient of Film Condensation for a Tube Bank (h_c)

The heat transfer coefficient for pure steam condensing on horizontal tubes, modified by the effects of inundation, subcooling, and vapor shear, can be expressed by

$$h_c = h_N \cdot f_i \cdot f_s \cdot f_v, \quad (9.4)$$

where h_N is the heat transfer coefficient for laminar film condensation of pure steam on the outside of a single horizontal tube, and f_i , f_s , and f_v are the correction factors that account for the effects of inundation, subcooling, and vapor shear, respectively.

An expression for h_N , averaged over the entire surface of a horizontal tube, was originally derived by Nusselt.³⁹ It is

$$h_n = 0.725 \left[\frac{\rho_\ell(\rho_\ell - \rho_g) g k_\ell^3 h_{fg}}{\mu_\ell D_o (T_{cs} - T_{wo})} \right]^{1/4} \quad (9.5)$$

where

ρ_ℓ = density of the liquid, kg/m^3 .

ρ_g = density of the vapor, kg/m^3 .

g = gravitational force, 9.8 m/s^2 .

k_ℓ = thermal conductivity of liquid, $\text{W/m/}^\circ\text{C/s}$.

μ_ℓ = viscosity of the liquid, kg/m/s .

h_{fg} = latent heat of condensation J/kg .

$C_{p\ell}$ = specific heat of the liquid, $\text{W/kg}^\circ\text{C}$.

T_{cs} = vapor - condensate interface temperature, $^\circ\text{C}$.

T_{wo} = surface temperature of the outside wall, $^\circ\text{C}$.

and

D_o = outside diameter of the tube, m .

9.3.3.1 Inundation Effect (f_I)

For the condensation of vapor on a vertical bank of horizontal tubes, as shown in Fig. 17, where the condensate flowing from a tube is assumed to fall upon the next lower row of tubes, Nusselt³⁹ obtained the following expression for the average heat transfer coefficient over n tube rows:

$$\bar{h} = 0.725 \left[\frac{g \rho_\ell (\rho_\ell - \rho_g) k_\ell^3 h_{fg}}{n D_o \mu_\ell (T_{cs} - T_{wo})} \right]^{1/4} \quad (9.6)$$

Comparing Eqs. 9.5 and 9.6, one sees that the correction factor f_I is

$$f_I = n^{-1/4}. \quad (9.7)$$

Nusselt's result is generally considered to be too conservative. Clearly, the inundation effect varies with tube layout. Bundles with tubes in line in the vertical direction will show a greater inundation effect than those with tubes in a staggered arrangement, because the condensate will tend to hit tube sides rather than tube tops (Fig. 18).

An empirical relationship proposed by Short and Brown⁴⁰ for the inundation effect is

$$f_I = 1.24 n^{-1/4}. \quad (9.8)$$

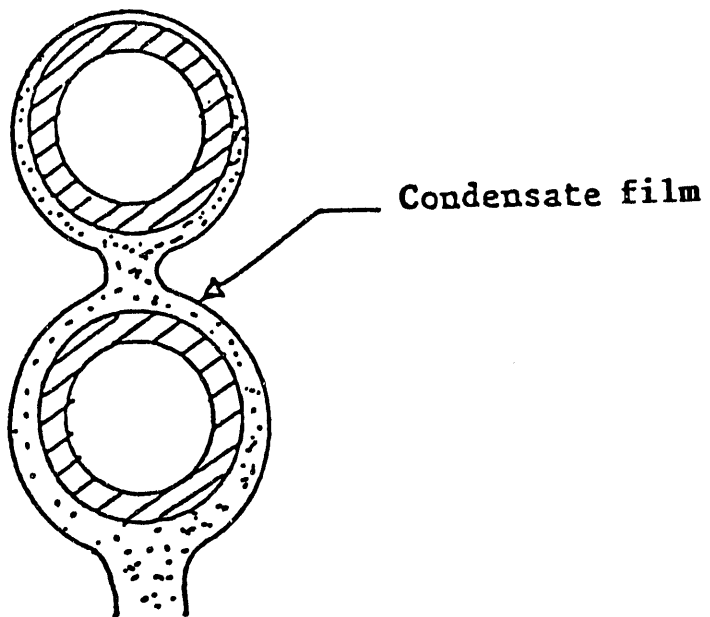


Fig. 17. Condensate film on horizontal tubes

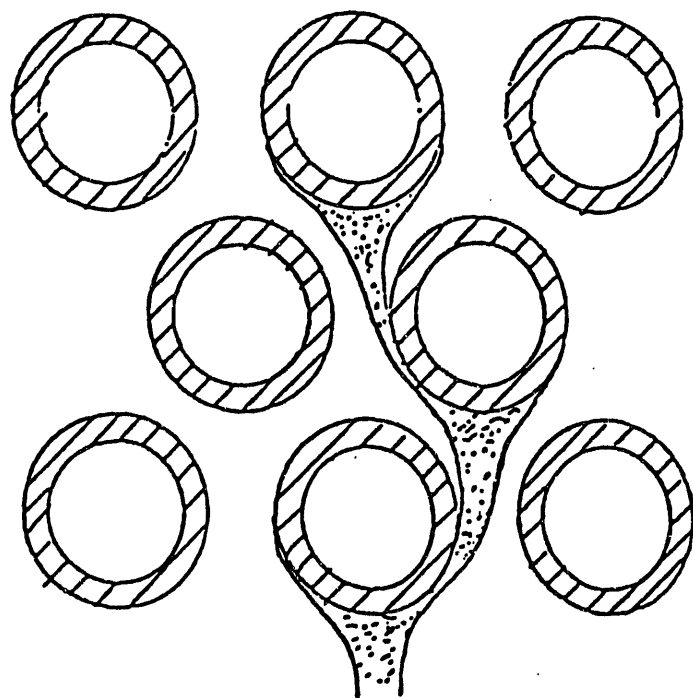


Fig. 18. Condensate film on staggered tubes

9.3.3.2 Condensate Subcooling Effect (f_s)

Because the liquid film on the tube surface is subcooled, Chen⁴¹ suggested that it is possible for additional condensation to occur on the subcooled liquid layer around the tubes; his analysis led to the following expression:

$$f_s = 1 + 0.2 \frac{C_{p\ell}(T_{cs} - T_{wo})}{h_{fg}}(n - 1), \quad (9.9)$$

which is a good approximation when $\frac{(n - 1)C_{p\ell}(T_{cs} - T_{wo})}{h_{fg}} < 2$.

Rosenhow⁴² proposed that h_{fg} in Eq. 9.5 be replaced by

$$h_{fg} = h_{fg} + 0.68 C_{p\ell} (T_{cs} - T_{wo}) \quad (9.10)$$

to obtain good agreement with experimental data.

In a power condenser, the latent heat (h_{fg}) is two orders of magnitude greater than the sensible heat, $C_{p\ell} (T_{cs} - T_{wo})$. Hence, the subcooling effect is of less significance when compared with the effects of condensate inundation and shear of flowing vapor.

9.3.3.3 Vapor Shear Effect (f_v)

Vapor shear influences the condensation heat transfer over tube bundles in three ways. First, at high vapor velocity, there is increasing tendency for the film flow to become turbulent. Second, vapor shear will reduce the thickness of the flowing condensate film due to its acceleration in the direction of vapor flow. Third, a higher vapor velocity will alter the flow path of the condensate that is falling on the tube rows.

The vapor shear correction factor suggested by Berman and Tumanov⁴³ is incorporated in the COMMIX-PPC code:

$$f_v = 1 + 0.0095 Re_m^{11.8/\sqrt{N_u}}, \quad (9.11)$$

where Re_m is defined in Eq. 9.3a and N_u is the Nusselt number defined as

$$N_u = \frac{h_N D_0}{k_\ell}. \quad (9.12)$$

9.3.4 Thermal Resistance of the Tube Wall (R_w)

The thermal resistance of the tube wall is expressed as

$$R_w = \frac{D_0 \ln(D/D_i)}{k_w}, \quad \frac{m^2 \cdot K}{W}, \quad (9.13)$$

where

D_o = tube outside diameter, m

D_i = tube inside diameter, m

k_w = thermal conductivity of the tube material, W/m•K.

9.3.5 Thermal Resistance of the Fouling Layer (R_f)

Fouling is an extremely complex phenomenon in condensers. The fouling characteristics are functions of various parameters:

- Geometry and material of the heat transfer surface.
- Temperature of the fouling fluid and the deposit.
- Flow velocity.
- Characteristics of the fouling fluid.

Condensers in which sea water is used for cooling are subject to biofouling, corrosion fouling, and fouling due to deposition of suspended particles or precipitation of salts.

Fouling deposits are usually poor thermal conductors; therefore, because they accumulate on heat transfer surfaces, there is a reduction in condenser efficiency and performance.

Thus, the thermal resistance due to a fouling layer in the condenser tube varies. A value of R_f from 0.00005 to 0.00014 m²•K/W was used by Eissenberg and Noritake⁴⁴ in seawater distillation plants.

9.3.6 Heat Transfer Coefficient for the Flow of Cooling Water Inside a Tube

The Dittus-Boelter⁴⁵ correlation, used to calculate the turbulent heat transfer coefficient between tube wall and cooling water, is

$$h_{cw} = 0.023 \frac{k_f}{D_i} Re^{0.8} Pr^{0.4} . \quad (9.14)$$

9.4 Structure/Fluid Momentum Interaction

As described previously, the solid structures in the system under study interact with fluid and influence momentum distribution. In the porous-medium formulation employed in COMMIX-PPC, these interactions are modeled with distributed resistances that appear in the source term of the momentum equations (Table 1). This section describes how the distributed resistance, also known as force structure, is determined, and how a wide range of generality and flexibility is provided in COMMIX-PPC.

In COMMIX-PPC, the frictional pressure drop due to stationary solid structures is expressed in the following general form:

$$\Delta p = c_1 \frac{L}{D} \rho v^2 f . \quad (9.15)$$

where L (Δx , Δy , or Δz) is the length of the cell and D is the hydraulic diameter.

The friction factor f is a function of the Reynolds number and is assumed to be of the form

$$f = a_{\text{lam}} \text{Re}^{b_{\text{lam}}} + c_{\text{lam}} \quad (\text{As } \text{Re} \rightarrow 0, c_{\text{lam}} \rightarrow 0) \quad (9.16)$$

for $\text{Re} \leq \text{Re}_{\text{tr}}$ and

$$f = a_{\text{tur}} \text{Re}^{b_{\text{tur}}} + c_{\text{tur}} \quad (9.17)$$

for $\text{Re} > \text{Re}_{\text{tr}}$. Here, Re is the Reynolds number, and a , b , and c are constants. The subscripts lam , tur , and tr stand for laminar, turbulent, and transition. COMMIX has the flexibility of permitting as many correlations as the user desires. Each correlation requires seven input numbers: a_{lam} , b_{lam} , c_{lam} , a_{tur} , b_{tur} , c_{tur} , and Re_{tr} . The Reynolds number Re is defined by

$$\text{Re} = \frac{VD\rho}{\mu} , \quad (9.18)$$

where V is the local flow velocity, D is the hydraulic diameter, ρ is the density, and μ is the viscosity. The product ρV is the local mass flux.

In Eq. 9.15, the values of c_1 and D depend on the geometry and type of structure and must be provided by the user. There may be more than one type of structure in a flow domain of interest. Partially submerged structures usually have different geometries and require different values for parameters c_1 and D . In COMMIX, we have provided this flexibility; details are given in Volume II of this report.

The resistance to flow due to internal structure would depend on the orientation of the structure relative to the general flow direction. Accordingly, a directional distributed resistance R , expressed in pressure drop per unit length, is introduced. It is defined by

$$R = \frac{\Delta D}{L} = c_1 \rho \frac{v|v|}{D} f . \quad (9.19)$$

Equation 9.19 is used in COMMIX-PPC to account for frictional pressure drop. To simplify the specification of the manner that a fluid cell interacts with a structure, a specific input arrangement has been implemented in COMMIX; details are presented in Volume II. A collection of resistance correlations commonly needed by COMMIX users is presented in a recent report⁴⁶ and is also included in the appendix of Volume II of this report.

Occasionally, the COMMIX-PPC user may find that the desired correlation is not of a form directly suitable for input into COMMIX. When this occurs, the user may approximate the correlation to fit the input form, or implement the new correlation into the code.

9.5 Shell-Side and Tube-Side Thermal Coupling

9.5.1 Introduction

As described earlier, solid structures, partially or totally submerged in a fluid, interact with the fluid and influence momentum distribution. They influence temperature distribution when the temperature of the solid structure is different from that of the fluid. The structure/thermal interaction in COMMIX-PPC is modeled by distributed heat sources. Such interaction consists primarily of heat transfer between a structure and surrounding fluid and, indirectly, heat transfer within the solid structure.

In COMMIX-PPC, the condenser tubes are modeled as thermal structures. The tubes interact with a steam/air mixture on the shell side and with cooling water on the tube side. When a mixture of steam and air flows over tube surfaces, steam condenses on the tube surface and releases latent heat to the tube. This latent heat is then transferred to the tube side and raises the temperature of the cooling water.

COMMIX-PPC has modeled the thermal structure in a more generalized way so that it can be used for other engineering calculations, such as those used in the nuclear industry. It has the following features:

- The model considers all internal structures.
- A structure can be planar, cylindrical, or spherical with either one surface (e.g., solid cylinder or sphere) or two surfaces (plane or annular cylinder) thermally interacting with surrounding fluid. The axis of the structure can be aligned with any of the three coordinate axes.
- Each structure can consist of more than one type of material, each separated by a gap.

A generalized way of modeling thermal structure is presented in the Appendix. In this section, the thermal coupling between the shell-side and tube-side fluids will be described. The heat transfer and temperature distribution within the tube wall is calculated by solving the one-dimensional heat conduction equation in the radial direction. This assumes that heat conduction in the other two directions is negligible. The rate of heat transfer from a steam/air mixture to a tube is the distributed heat source. Because the energy equation is not solved for a steam/air mixture, this distributed heat source is then used to calculate the steam condensation rate.

9.5.2 Geometrical Description

Figure 19 shows a condenser tube with its axis aligned in the x-direction and its length extending over a number of computational cells with partition Δx . Each Δx partition of the tube is referred to as a thermal-structure element. Each element interacts with only one fluid cell. Each element has its own temperature distribution as it interacts with surrounding fluid cells. Each element has two surfaces, outer and inner. The outer surface

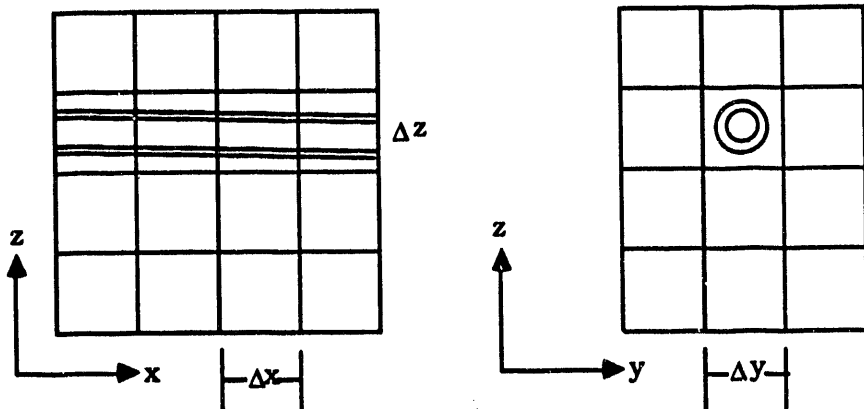


Fig. 19. Condenser tube (thermal structure) in a flow domain

interacts thermally with the steam/air mixture and the inner surface interacts thermally with the cooling water. Each element can consist of any number of tubes.

9.5.3 Governing Equation

The transient one-dimensional heat conduction equation is

$$\rho C_p \frac{\partial T}{\partial t} = \frac{1}{A} \frac{\partial}{\partial r} (-Aq), \quad (9.20)$$

where ρ and C_p are the density and specific heat of the tube, q is the radial heat flux per unit area, and A is the local cross-sectional area.

9.5.4 Finite-Difference Formulation

Figure 20 shows the cross section of the thermal-structure element under consideration. Each element is divided into a desired number of equal partitions. Let Δr be the partition size and L be the total number of partition cells.

9.5.4.1 Internal Cells ($\ell = 2, 3, \dots, L-1$)

Consider the energy balance of cell ℓ as shown in Fig. 21. The integrated energy equation for the structure in the control volume of cell ℓ gives

$$\frac{\rho C_p V_\ell}{\delta t} (T_\ell - T_\ell^n) = A_\ell q_\ell - A_{\ell+1} q_{\ell+1}. \quad (9.21)$$

Here, V_ℓ is the cell volume. The heat flux q_ℓ can be expressed in terms of the overall heat transfer coefficient U_ℓ or its reciprocal and a temperature difference:

$$q_\ell = U_\ell (T_{\ell-1} - T_\ell^n) = \frac{1}{R_\ell} (T_{\ell-1} - T_\ell^n). \quad (9.22)$$

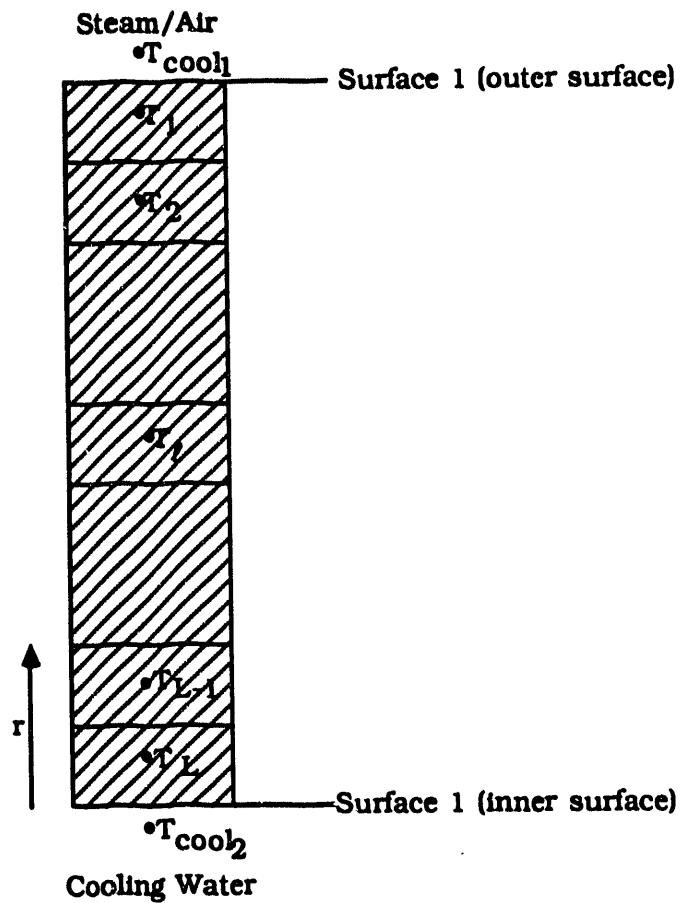


Fig. 20. Cross section of thermal-structure element

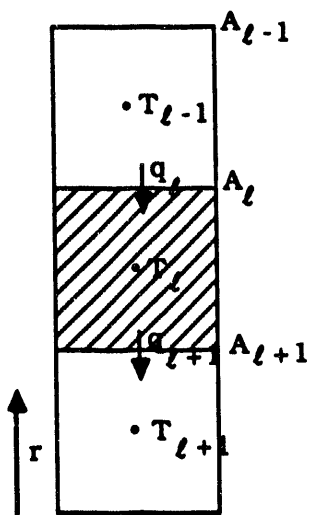


Fig. 21. Energy Balance of a partition cell ℓ

where

$$U_\ell = \frac{1}{R_\ell} = \frac{1}{\left(\frac{\Delta r}{2\lambda}\right)_{\ell-1} + \left(\frac{\Delta r}{2\lambda}\right)_\ell}. \quad (9.23)$$

Here, λ is thermal conductivity, T^n and T are temperatures at time t and $(t + \delta t)$, respectively.

Upon substituting Eq. 9.22 into Eq. 9.21 and rearranging, we obtain

$$(a_\ell + b_\ell + b_{\ell+1})T_\ell = b_\ell T_{\ell-1} + b_{\ell+1} T_{\ell+1} + d_\ell, \quad (9.24)$$

where

$$a_\ell = \rho C_p V_\ell / \delta t, \quad (9.25)$$

$$b_\ell = A_\ell U_\ell = A_\ell / R_\ell, \quad (9.26)$$

$$b_{\ell+1} = A_{\ell+1} U_{\ell+1} = A_{\ell+1} / R_{\ell+1}, \quad (9.27)$$

and

$$d_\ell = a_\ell T_\ell^n. \quad (9.28)$$

In Eq. 9.24, a_ℓ is related to the tube heat capacity, b_ℓ and $b_{\ell+1}$ are related to the heat transfer area and heat transfer coefficients, and d_ℓ is related to a_ℓ and T_ℓ^n .

9.5.4.2 Outer Surface Cell ($\ell = 1$)

For the case of Cell 1 (Fig. 22), adjacent to the coolant T_{cool} , the finite-difference energy equation is

$$\frac{\rho C_p V_1}{\delta t} (T_1 - T_1^n) = U_1 A_1 (T_{cool_1} - T_1) - U_2 A_2 (T_1 - T_2). \quad (9.29)$$

where

$$U_1 = \frac{1}{R_1} = \frac{1}{\frac{1}{h_1} + \left(\frac{\Delta r}{2x}\right)_1} \quad (9.30)$$

and

$$U_2 = \frac{1}{R_2} = \frac{1}{\left(\frac{\Delta r}{2\lambda}\right)_1 + \left(\frac{\Delta r}{2\lambda}\right)_2}. \quad (9.31)$$

Here, h_1 is the convective heat transfer coefficient between fluid and tube wall, and can be evaluated from Eq. 9.2 as

$$\frac{1}{h_1} = \frac{1}{h_a} + \frac{1}{h_c}. \quad (9.32)$$

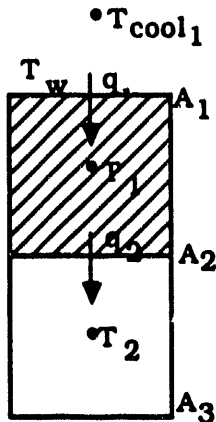


Fig. 22. Energy balance of Cell 1

Upon substituting Eqs. 9.30 and 9.31 into Eq. 9.29 and rearranging, we obtain

$$(a_1 + b_1 + b_2)T_1 = b_1 T_{cool_1} + b_2 T_2 + d_1. \quad (9.33)$$

where

$$a_1 = \frac{\rho C_p V_1}{\delta t}, \quad (9.34)$$

$$b_1 = A_1 U_1 = \frac{A_1}{h_1 + \left(\frac{\Delta x}{2\lambda}\right)_1}, \quad (9.35)$$

$$b_2 = A_2 U_2. \quad (9.36)$$

and

$$d_1 = a_1 T_1^n. \quad (9.37)$$

Here, a_1 , b_1 , and d_1 have the same meaning as a_ℓ , b_ℓ , and d_ℓ , in Eqs. 9.25–28. Note that b_1 includes the convective contribution.

9.5.4.3 Inner Cell ($\ell = L$)

For the case of Cell L (Fig. 23), adjacent to coolant T_{cool_2} , the finite-difference energy equation is

$$\frac{\rho C_p V_\ell}{\delta t} (T_L - T_L^n) = U_L A_L (T_{L-1} - T_L) - U_{L+1} A_{L+1} (T_L - T_{cool_2}). \quad (9.38)$$

where

$$U_L = \frac{1}{\left(\frac{\Delta x}{2\lambda}\right)_{L-1} + \left(\frac{\Delta x}{2\lambda}\right)_L}, \quad (9.39)$$

and

$$U_{L+1} = \frac{1}{h_2 + \left(\frac{\Delta x}{2\lambda}\right)_L}. \quad (9.40)$$

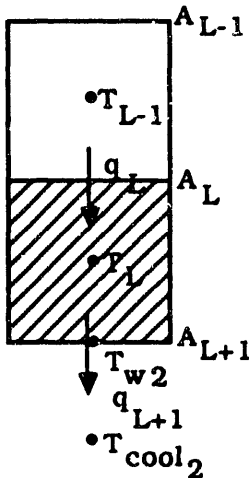


Fig. 23. Energy balance of Cell L

Here, h_2 is the convective heat transfer coefficient, which, from Eq. 9.2, can be defined as

$$\frac{1}{h_2} = R_f + \frac{D_0}{D_1 h_{cw}}. \quad (9.41)$$

Upon substituting Eqs. 9.39 and 9.40 into Eq. 9.38 and rearranging, we obtain

$$(a_L + b_L + b_{L+1})T_L = b_L T_{L-1} + b_{L+1} T_{cool2} + d_L, \quad (9.42)$$

where

$$a_L = \frac{\rho C_p V_L}{\delta t}, \quad (9.43)$$

$$b_L = A_L U_L, \quad (9.44)$$

$$b_{L+1} = A_{L+1} U_{L+1}, \quad (9.45)$$

and

$$d_L = a_L T_L^n. \quad (9.46)$$

Here, a_L , b_L , b_{L+1} , and d_L have the same meaning as a_ℓ , b_ℓ , $b_{\ell+1}$, and d_ℓ , defined in Eqs. 9.25–9.28. Note that b_{L+1} includes the convective contribution.

We can see from the formulations of the preceding section that there are L equations for L unknown temperatures.

- Outside Surface Cell ($\ell = 1$)

$$(a_1 + b_1 + b_2) T_1 = b_2 T_2 + b_1 T_{cool1} + d_1 \quad (9.47a)$$

- Internal cell ($\ell = 2, 3, \dots, L-1$)

$$(a_\ell + b_\ell + b_{\ell+1}) T_\ell = b_\ell T_{\ell-1} + b_{\ell+1} T_{\ell+1} + d_\ell \quad (9.47b)$$

- Inner cell ($\ell = L$)

$$(a_L + b_L + b_{L+1}) T_L = b_L T_{L-1} + b_{L+1} T_{\text{cool}_2} + d_L. \quad (9.47c)$$

Equations 9.47 can be rewritten as

$$C_1 T_1 = b_2 T_2 + A_1 \quad (\ell = 1) \quad (9.48)$$

$$C_\ell T_\ell = b_{\ell+1} T_{\ell+1} + A_\ell \quad (\ell = 2, \dots, L-1) \quad (9.49)$$

$$C_L T_L = b_{L+1} T_{\text{cool}_2} + A_L \quad (\ell = L), \quad (9.50)$$

where

$$A_\ell = d_\ell + \frac{b_\ell A_{\ell-1}}{C_{\ell-1}} \quad (\ell = 2, \dots, L), \quad (9.51)$$

$$C_\ell = a_\ell + b_\ell + b_{\ell+1} - \frac{b_\ell^2}{C_{\ell-1}} \quad (\ell = 2, \dots, L), \quad (9.52)$$

$$a_1 = d_1 + b_1 T_{\text{cool}_1}. \quad (9.53)$$

and

$$C_1 = a_1 + b_1 + b_2. \quad (9.54)$$

The inside-surface cell temperature is first calculated from Eq. 9.50. The remaining temperatures are then computed by using Eqs. 9.48 and 9.49.

9.5.5 Heat Transfer to Adjacent Fluid

Once the temperature distribution in a structure element is determined, the rate of heat transfer to the adjacent fluid can be computed from

$$\dot{q}_1 = A_1 U_1 (T_{\text{cool}_1} - T_1) \quad \text{for the outside surface} \quad (9.55)$$

$$\dot{q}_{L+1} = A_{L+1} U_{L+1} (T_L - T_{\text{cool}_2}) \quad \text{for the inside surface.} \quad (9.56)$$

9.5.6 Steam Condensation Rate

The steam condensation rate per unit volume (\dot{m}''') is computed from

$$\dot{m}''' = \frac{\dot{q}}{h_{fg} V_f}, \quad (9.57)$$

where h_{fg} is latent heat and V_f is the volume of the computational fluid cell.

10 Initial and Boundary Conditions

10.1 Initial Conditions

Generally, before the solution sequence can begin, values of all variables must be assigned. In COMMIX-PPC, we can accomplish this by either

- Continuing a previous run via the restart capability (recommended for all but the first run), or
- Specifying the initial distribution throughout the interior points and boundary of the space under consideration.

When the initialization is not a restart, we must specify initial pressure, temperature, velocity, mass fraction, and turbulence parameters for the entire computation domain. The assignment of these initial values and their subsequent input into the code are generally tedious. In COMMIX, several simplified input procedures are provided for the initialization of velocity, pressure, temperature, mass fraction, and turbulence parameters. These procedures are described in Volume II of this report.

10.2 Boundary Conditions

This section describes the boundary conditions for mass, momentum, and energy equations. The boundary conditions for turbulence-transport equations have already been described in Sec. 7.4. The surface fluxes are in a direction normal to the local surface and pointing into the fluid from the boundary surface.

10.2.1 Fluid Velocity Boundary Conditions

The most common physical boundaries in an engineering system are solid impervious surface, inlet, symmetry, and outlet. To accommodate all possible fluid velocity conditions at these boundaries, seven boundary condition options (summarized in Table 15) are provided in the COMMIX code. In the following, these options are described in mathematical terms; in Volume II their implementation in the input data is described.

1. Constant Fluid Velocity

This boundary condition implies that normal fluid velocity v_n is constant. This option is applicable to an inlet surface with constant inlet fluid velocity. It is also applicable to a stationary solid surface as a special case of zero normal fluid velocity.

2. Transient Fluid Velocity

This option is applicable when the inlet velocity varies with time, e.g.,

$$v_n = v_0 f(t) .$$

(10.1)

Table 15. Fluid velocity boundary options

Boundary/Suitable Option	Option No.	Remarks
Solid Impervious Surface		
Constant velocity	1	Specify normal velocity $v_n = 0$
Inlet		
Constant velocity	1	Specify inlet velocity
Transient velocity	2	Specify inlet velocity and appropriate transient function
Surface of Symmetry		
Free Slip	3	Axis through origin in cylindrical coordinate is a surface of symmetry
Outlet		
Continuous mass flow	4	General outlet condition
Continuous momentum	5	Suitable when areas are equal
Continuous velocity	6	Suitable when areas and densities are equal
Uniform velocity	7	Suitable when outlet is finely divided (Fig. 24)

Here,

v_n = surface-normal fluid velocity at time, t ,

v_0 = surface-normal fluid velocity at time, $t = 0$,

and

$f(t)$ = dimensionless function of time.

3. Free Slip

The free-slip option is used when the shear stress at the surface vanishes and

$$v_n = 0.0 . \quad (10.2)$$

This option is applicable to a symmetry boundary. For a cylindrical coordinate system in COMMIX, the z axis passing through the origin is considered a symmetry boundary with zero surface area.

4. Continuous Mass Flow at Outlet

This option is for an outlet surface, as illustrated in Fig. 24, in which ℓ and m are the outlet boundary cells and $\ell+1$ and $m-1$ are the neighboring cells. The

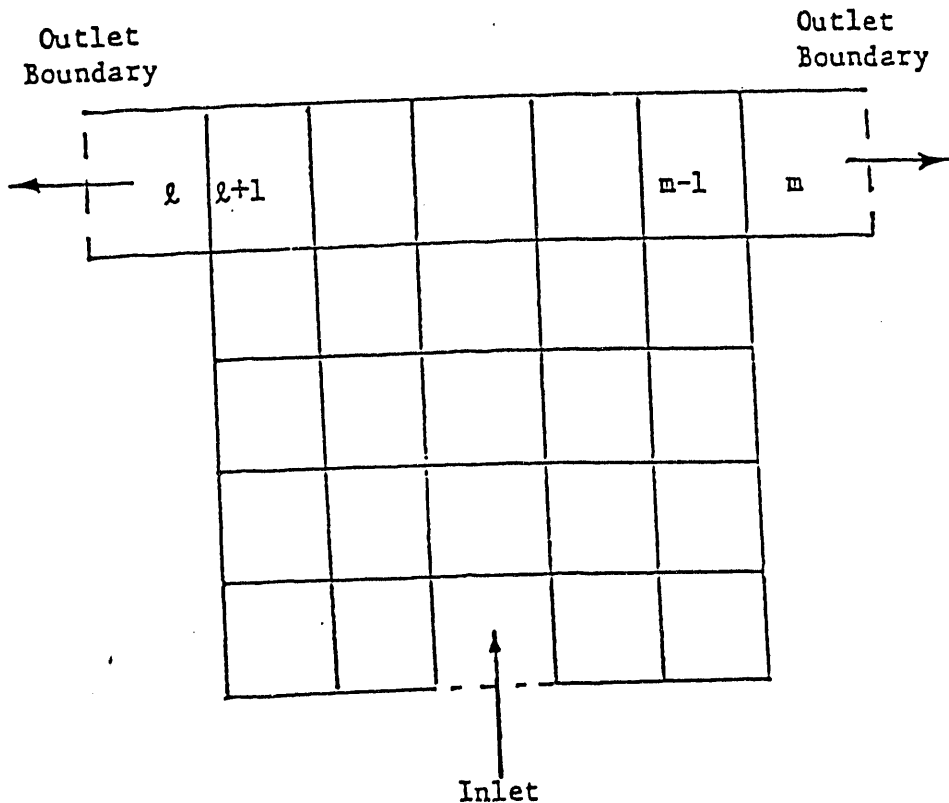


Fig. 24. Near-boundary cells

continuous mass flow at the outlet implies that the normal surface velocity must be such as to balance the mass flow, i.e.,

$$(v_n)_{l-1/2} = [(\rho A)_{l+1/2} u_{l+1/2} + (\rho_l - \rho_l^n) v_l / \Delta t] / (\rho A)_{l-1/2}. \quad (10.3a)$$

and

$$(v_n)_{m+1/2} = [-(\rho A)_{m-1/2} u_{m-1/2} + (\rho_m - \rho_m^n) v_m / \Delta t] / (\rho A)_{m+1/2}. \quad (10.3b)$$

The sign difference between Eqs. 10.3a and 10.3b is in conformity with the COMMIX convention that surface-normal is directed into the flow domain.

5. Continuous Momentum Flow at Outlet

When an outlet area is the same as the neighboring surface area, Eq. 10.3a simplifies to

$$(v_n)_{l-1/2} = [(\rho u)_{l+1/2} + (\rho_l - \rho_l^n) \Delta x / \Delta t] / \rho_{l-1/2}. \quad (10.4)$$

It is called continuous momentum flow at outlet because it has the appearance of equating neighboring and outlet momentum fluxes.

6. Continuous Velocity at Outlet

If we have equal areas and equal densities, Eq. 10.3a simplifies to

$$(v_n)_{t-1/2} = (u)_{t+1/2} . \quad (10.5)$$

This option is called continuous velocity at outlet because the outlet velocity and the velocity of the neighboring cells are equal.

7. Uniform Velocity at Outlet

The uniform velocity at outlet option of the boundary condition sets the normal velocity for all surface elements at the same value. This value is computed in such a way that the total mass flow through a surface is the same as that obtained from the boundary condition of continuous mass flow outlet. Mathematically,

$$(v_n) = \sum [(\rho A u)_{t+1/2} + (\rho_t - \rho_t^n) v / \Delta t] / \sum (\rho A_{t-1/2}). \quad (10.6)$$

Here, the summation is taken over all elements of a surface. This option is suitable when an outlet is very finely divided, as shown in Fig. 25.

10.2.2 Temperature Boundary Conditions

The five options of temperature boundary condition available in COMMIX-PPC are briefly described here and summarized in Table 16.

1. Constant Temperature

This option is for a constant-temperature surface. The temperature associated with each surface element is set initially and remains unchanged throughout the calculation, as shown in Fig. 26. The surface heat flux is calculated from the relation

$$\dot{q} = UA(T_w - T_f) . \quad (10.7)$$

where the subscripts w and f refer to the solid surface element and boundary fluid cell, respectively, and

$$U = \frac{1}{\frac{1}{h} + \frac{\Delta L}{2\lambda_w}} , \quad (10.8)$$

in which h is the heat transfer coefficient, λ is the conductivity of the wall material, and ΔL is the wall thickness. Calculation of the overall heat transfer coefficient U requires input on wall thickness, suitable correlation for h, and thermal conductivity of wall material λ .

If the Biot number $h\Delta L/2\lambda_w \ll 1$, the overall heat transfer coefficient becomes equal to h.

If an inlet surface has a constant temperature, as shown in Fig. 27, the surface heat flux is calculated from the Fourier relation

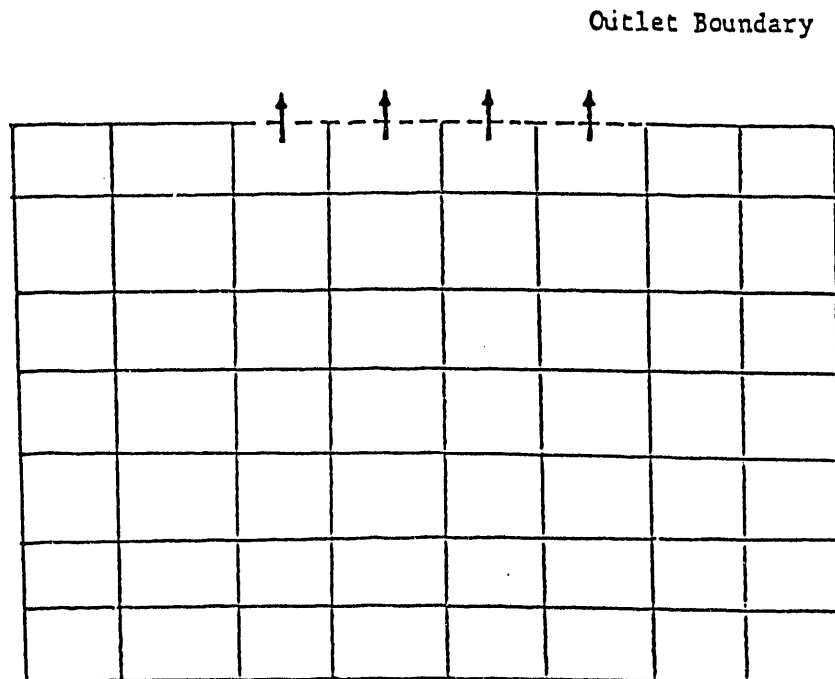


Fig. 25. Model suitable for uniform velocity at outlet option

Table 16. Suitable temperature boundary options

Boundary/Option	Option No.	Remarks
Solid Surface		
Constant temperature	1	$T_w = \text{constant}$
Transient temperature	2	$T_w = T_0 f(t)$
Constant heat flux	3	$q_w = \text{constant}$
Transient heat flux	4	$q_w = q_0 f(t)$
Adiabatic	5	$q_w = 0$
Inlet		
Constant temperature	1	$T_w = \text{constant}$
Transient temperature	2	$T_w = T_0 f(t)$
Outlet		
Adiabatic	5	$q_w = 0$
Surface of Symmetry		
Adiabatic	5	$q_w = 0$

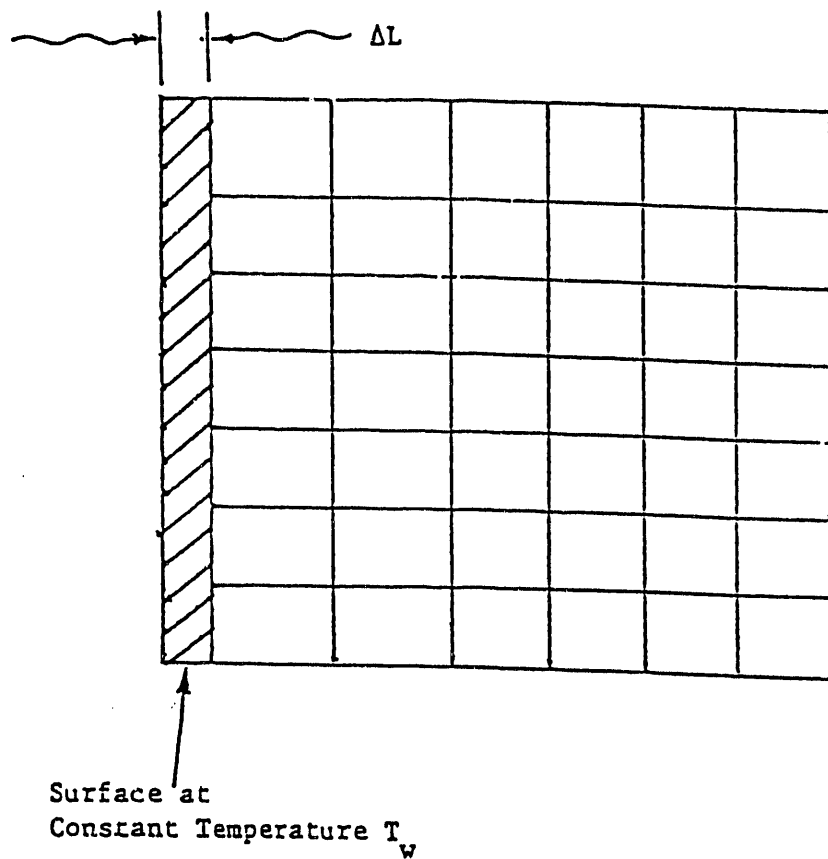


Fig. 26. Constant-temperature boundary

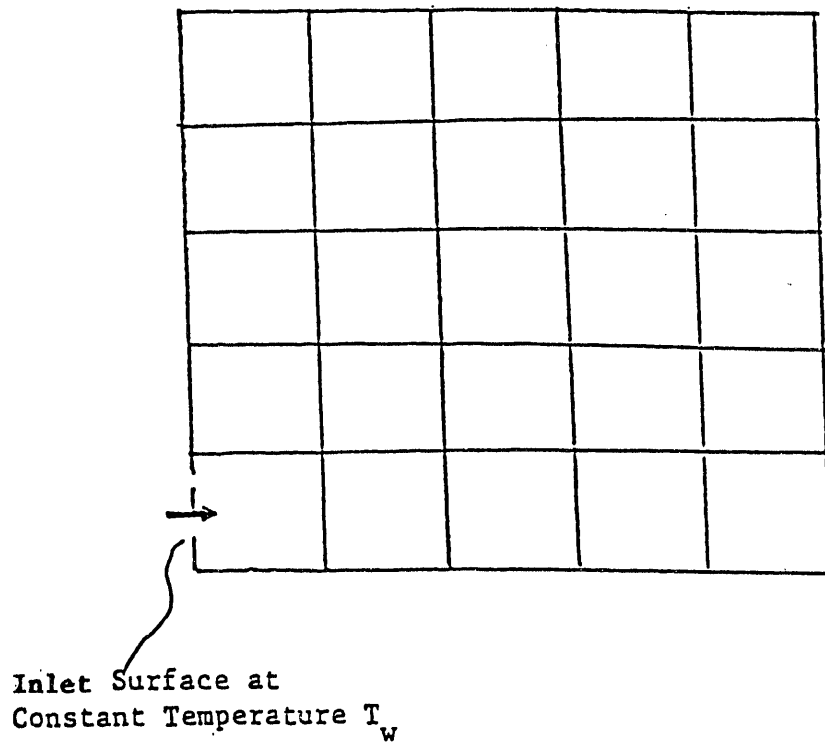


Fig. 27. Nonconvective constant-temperature boundary

$$\dot{q} = \frac{\lambda_{\text{eff}} A (T_w - T_f)}{\frac{\Delta x_f}{2}}. \quad (10.9)$$

Here, λ_{eff} is the effective thermal conductivity of the fluid in the adjacent internal cell and can be calculated from Eq. 7.19, Δx_f is the distance between the surface and the boundary cell center, and the subscripts w and f stand for wall (surface element) and adjacent internal cell, respectively.

2. Transient Temperature

This option is for a surface whose temperature varies with time, e.g.,

$$T_w = T_0 f(t), \quad (10.10)$$

where

T_w = surface temperature at time t ,

T_0 = surface temperature at time = 0,

and

$f(t)$ = a dimensionless function of time.

We calculate the surface-element heat flux with the procedure described for the constant-temperature boundary option.

3. Constant Heat Flux

In this option, the heat flux associated with each surface element is set initially and remains unchanged throughout the calculation. Although the surface heat flux remains fixed, its temperature is evaluated by using Eq. 10.7 or 10.9.

4. Transient Heat Flux

This option is useful when the surface heat flux has a known variation with time, e.g.,

$$\dot{q} = \dot{q}_0 f(t), \quad (10.11)$$

where

\dot{q} = surface heat flux at time t ,

\dot{q}_0 = surface heat flux at time $t = 0$,

and

$f(t)$ = a dimensionless function of time.

Once the surface heat flux is known for any given time t , the surface temperature can be calculated from Eq. 10.7 or 10.9.

5. Adiabatic Surface

The adiabatic boundary option is used when the heat flux $q = 0$. In this option, the normal heat flux at all elements of a surface is initialized to zero and it remains at zero. The surface-element temperature is set equal to the temperature of the neighboring internal cell.

10.2.3 Pressure Boundary Conditions

Currently, two options for pressure boundary condition are provided in COMMIX-PPC:

- Constant pressure, and
- Transient pressure.

The pressure boundary is specified for cells adjacent to the surface. This option is usually used in conjunction with the continuous-mass-flow boundary condition.

If the velocity boundary condition is specified for an inlet surface, the pressure boundary option is not used, because surface pressure does not enter into any calculation.

It is important to note that the pressure boundary condition in COMMIX-PPC refers to the pressure at the boundary of adjacent fluid cells. Therefore, it is recommended that the geometry be modeled in such a way that the pressure boundary is applied to

- A surface with one surface element, or
- A surface that is normal to the direction of gravity and has parallel flow.

as shown in Fig. 28.

When the constant-pressure boundary option is used, the pressures of all internal cells adjacent to a surface are set to a prescribed value. These values then remain unchanged during the calculation.

For a transient pressure over a surface, the pressures of all internal cells adjacent to that surface are calculated from

$$P_m = P_{m0} f(t) . \quad (10.12)$$

where

P_m = pressure of the adjacent cell m and time t ,

P_{m0} = pressure of adjacent cell m at time = 0,

and

$f(t)$ = a dimensionless function of time.

The implementation of these options in the input is explained in Volume II.

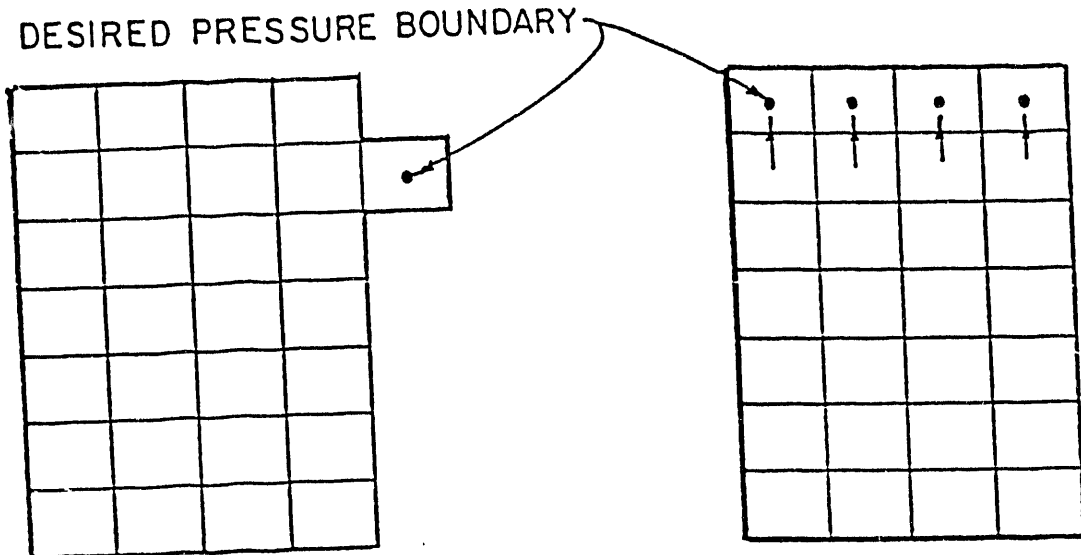


Fig. 28. Recommended surface arrangements for pressure boundary condition

10.3 Additional Options

The boundary conditions described in Sec. 10.2 are generally for uniform conditions at the boundary surfaces. If the distribution of the parameter in question is not uniform, this parameter can be specified by using the boundary surface-element initialization procedure in COMMIX-PPC. For example, if the inlet velocity is not uniform, the velocity can be specified individually for each surface element at the inlet plane by using the variable VELB. Similarly, if the heat flux on a given surface is not uniform, the heat flux can be specified individually for each surface element by using the variable QBN. Other variables such as mass flow rate, mass fraction, enthalpy, temperature, density, turbulence kinetic energy, and dissipation rate of turbulence kinetic energy are included in the procedure for boundary surface-element initialization, which overrides the procedures described in Sec. 10.2. Quite frequently, a combination of two procedures is used to achieve better accuracy in specifying boundary conditions. The boundary surface-element initialization procedure provides greater flexibility not only in specifying the nonuniform boundary conditions previously described, but also for others not described in Sec. 10.2. For example, if the user wishes to specify uniform mass flow at the inlet and because this option is not provided in Table 15, the user can specify uniform mass flow at the inlet plane by using the boundary surface-element initialization procedure. A detailed description of this procedure is given in Volume II of this report.

11 Solution Procedures

11.1 Introduction

COMMIX-PPC performs thermal-hydraulic calculations by marching in time. The values of the dependent variables at a given time-step n are known and the values of the dependent variables at time-step $n+1$ are calculated. By repeating this procedure, the thermal-hydraulic variables for the desired time span are determined. The overall flow chart of the program is shown in Fig. 29.

The same procedure is followed for steady-state calculations. We start with an initial guess and continue the marching-in-time process until the changes in values of all dependent variables of two successive time steps are lower than specified. The size of the time step for the implicit steady-state calculation can be many times larger than the Courant time-step criterion.

In COMMIX-PPC, two options are provided for the size of the time step:

- The user-desired time-step size (details of this input are given in the Input Description in Volume II), and
- The automatic time-step option.

In the automatic time-step option, the time-step size is evaluated on the basis of the Courant condition

$$\Delta t = C_1 \Delta t_C . \quad (11.1)$$

where C_1 is the user-prescribed coefficient and Δt_C is the time-step size evaluated from the Courant condition. The Courant time-step size is defined as the minimum time required for fluid to be convected through a cell. In COMMIX, each computational cell is examined with respect to flow in all three component directions for the determination of the Courant time-step size. The fully implicit solution sequence is used in COMMIX-PPC. Details are described in Section 11.2.

11.2 Fully Implicit (SIMPLEST-ANL) Solution Sequence

The fully implicit solution sequence, named SIMPLEST-ANL, is based on a modification of the SIMPLE/SIMPLER procedures developed at the Imperial College in England. SIMPLEST/ANL requires less computer storage than SIMPLER and has comparable or better computing efficiency. Because it relieves many of the time-step size limitations and permits use of larger time steps, it is most suitable for steady-state and transient calculations.

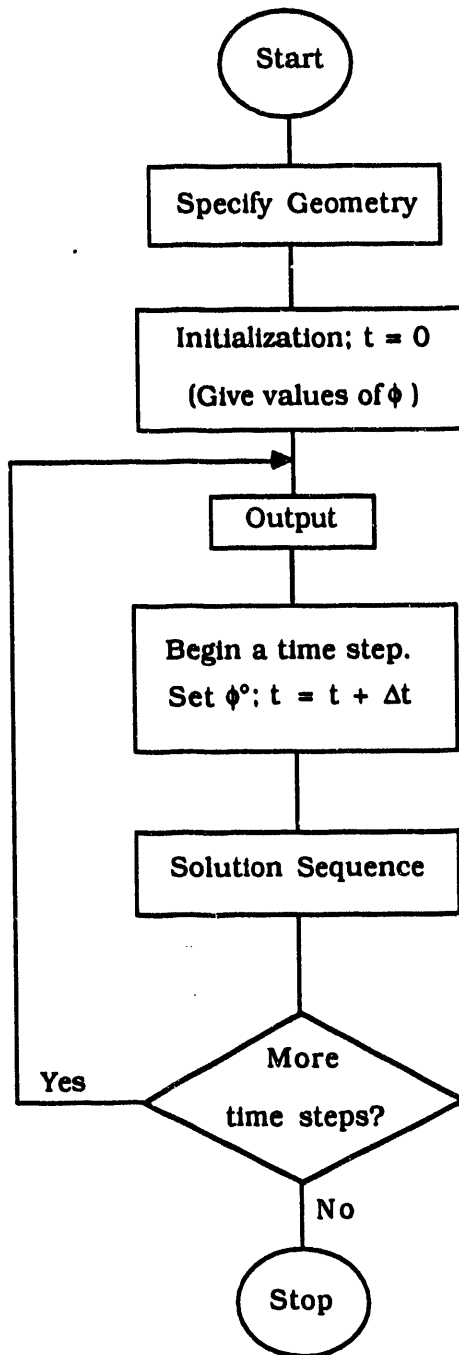


Fig. 29. COMMIX-PPC flow chart

The procedure is called fully implicit because the new-time values of all variables prevail during any time step. An iterative procedure is therefore needed. Each outer* iteration loop yields a better estimate of advanced-time values of all variables. When the

*Here, *outer iteration loop* is used to distinguish it from the inner iterative loops used for the solution of a specific variable equation, e.g., the iterative loop (successive overrelaxation procedure or the preconditioned conjugate gradient method) used for the solution of pressure equations is considered an inner iterative loop.

change in all variable values becomes smaller as one proceeds from one outer iteration to the next, the iterative process is considered converging and the last outer iterated values are used for the advanced time-variable values. The solution sequence for the fully implicit formulation is the seven-step iterative process shown in Table 17.

11.3 Matrix Solvers

Three matrix solvers are available in COMMIX-PPC to solve the discretized equations. They are the successive overrelaxation (SOR) method, the direct matrix inversion method (DMIM), and the Preconditioned Conjugate Gradient (PCG) method. All are incorporated in COMMIX-PPC in a modular fashion so that the user has the flexibility of choosing any one of the solvers for the pressure equation because the resulting matrix is symmetric. Either SOR or DMIM can be selected for the scalar transport equations.

Of the three matrix solvers, SOR and PCG are iterative solvers, whereas DMIM is a direct solver and requires no iteration. It should be noted that the solution procedures require the solving of several sets of algebraic equations by one or a combination of the three matrix solvers.

11.3.1 Successive Overrelaxation Iterative Scheme

The SOR iteration scheme uses one pass through the computational cell domain. As each cell is visited, the residual of the ϕ -equation to be solved is computed, using the most recent values of the surrounding ϕ 's. In this way, an updated value of ϕ is used if the neighboring cell has been visited earlier in the pass, and a previously iterated value of ϕ is used if the neighboring cell is to be visited later. Immediately after the residual of the ϕ equation for a cell under consideration is computed, the ϕ is adjusted in that cell before the computation proceeds to the next cell in the pass.

After all cells have been visited, the convergence is checked and if it has been achieved, the iterative process terminates; if convergence has not been achieved, another single-pass iteration is performed.

The SOR scheme requires the relaxation parameter ω to be between 0 and 2. Generally, convergence can be achieved in fewer iterations than in the Jacobi scheme. Because ω can have values greater than 1.0, it is termed overrelaxation. The optimum value of the relaxation parameter is generally geometry- and problem-dependent; it is usually between 1.4 and 1.8, and hence the name *overrelaxation*.

11.3.2 Direct Matrix Inversion Method

The DMIM is a collection of routines for solving the $n \times n$ system of linear algebraic equations when the coefficient matrix is large and sparse. The direct method is based on Gaussian elimination without pivoting. The coefficient matrix can be symmetric or nonsymmetric. The routines of the direct matrix inversion method decompose the coefficient matrix into triangular factors and then successively solve the triangular systems.

Table 17. Fully implicit (SIMPLEST-ANL) solution sequence

1. Calculate velocity-pressure relation coefficients from the previous iterates of u , v , and w :

$$\hat{\phi}, d^*; (\phi = u, v, w).$$

2. Calculate pressure equation coefficients using $\hat{\phi}, d^*$:

$$a_0^p, a_\ell^p, b_0^p.$$

3. Solve pressure equation for new-time, new-iterate pressure δP :

$$a_0^p \delta P_0 = \sum a_\ell^p \delta P_\ell + b_0^p.$$

4. Calculate new-time, new-iterate velocities u , v , w from velocity-pressure relations:

$$\phi = \hat{\phi} - d^* \Delta \delta P; (\phi = u, v, w).$$

5. Calculate component mass fraction equation coefficients using new-time, new-iterate velocities:

$$a_0^x, a_\ell^x, b_0^x.$$

6. Solve component mass fraction equation for new-time mass fraction x :

$$a_0^x x_0 = \sum a_\ell^x x_\ell + b_0^x.$$

7. Calculate the steam partial pressure, the saturation temperature, and mixture enthalpy:

$$P_s, T_s, h.$$

8. Check for convergence of u , v , w , h , x ; if convergence criterion is not satisfied, return to Step 1.

The routine takes advantage of the sparse coefficient matrix by solving the triangular systems without storing or operating on zero entries. The advantage of DMIM is that it is a direct solver and no iteration is involved. Both symmetric and nonsymmetric matrices can be solved. However, as the number of computation cells is increased, both the storage and the work increase rapidly and other methods (SOR and PCG) may become more economical and efficient.

11.3.3 Preconditioned Conjugate Gradient Method

A number of PCG-like methods have been reported in the literature.⁴⁷ The PCG method uses an iterative procedure that computes a sequence of approximate solutions of a system of linear algebraic equations. In COMMIX-PPC, it solves the symmetric, positive-definite systems, requires no estimates of scalar parameters, and is relatively inexpensive

per step. These properties make the conjugate gradient method more robust, easier to implement, and more rapidly convergent than other iterative methods for solving symmetric, positive-definite problems. The convergence of the conjugate gradient method can be improved by preconditioning techniques.⁴⁶ Consider a linear system of the form

$$Mx = b, \quad (11.2)$$

where M is the coefficient matrix, and x and b are column vectors whose components are x_i, b_i ($i = 1, 2, \dots, n$). In broad terms, preconditioning consists of solving the following system:

$$Q^{-1} Mx = Q^{-1} b, \quad (11.3)$$

where Q is an approximation of M so that Eq. 11.3 is in some sense easier to solve than Eq. 11.2. The preconditioning technique employed in COMMIX-PPC is the incomplete factorization of M . More detailed descriptions of the conjugate gradient methods and the preconditioning techniques can be found in Ref. 47.

11.3.4 Discussion

As described previously, the user has the flexibility of choosing any one or a combination of the three matrix solvers to solve the pressure equations and the scalar transport (energy, turbulence kinetic energy, etc.) equations. Table 18 summarizes the properties of these matrix solvers and the type of equations each solver is suitable for. The pressure equations in COMMIX-PPC are made symmetric and therefore can be solved by all three matrix solvers. The transport equations are nonsymmetric and therefore not suitable for PCG, but can be solved by either the SOR or the DMI method. Practically speaking, the DMIM is more efficient for relatively small numbers of computational cells; it becomes less efficient when the number of computational cells is greater than 1000. When the number of computational cells exceeds 2000, the PCG and SOR methods are more efficient and economical than the DMIM. As a rough guide, the DMIM should be used for all equations if the number of computational cells is less than 1000. If the number of computational cells is greater than 2000, the PCG method should be used to solve the pressure equations and the SOR method should be used to solve the scalar transport equations.

11.4 Iteration Criteria

As has already been pointed out, SIMPLEST-ANL is a fully implicit scheme and requires iteration. Thus, iteration criteria are needed to determine if iteration should proceed or be stopped before advancing to a next time step. This is what we referred to earlier as the outer iteration loop.

The seventh step listed in the fully implicit scheme (Table 17) is to check for convergence. The changes from one iteration to the next are checked against the convergence criteria for all ϕ 's. The iteration criteria are considered satisfied when

$$\frac{|\phi_{\text{new}} - \phi_{\text{old}}|_{\text{max}}}{\phi_{\text{old}}} < \epsilon_3,$$

Table 18. Properties of the three matrix solvers in COMMLX-PPC

Matrix Solver	Coefficient Matrix	Scheme	Suitable for	
			Pressure Eqs.	Transport Eqs.
SOR	Symmetric/Nonsymmetric	Iterative	Yes	Yes
DMIM	Symmetric/Nonsymmetric	Direct	Yes	Yes
PCG	Symmetric	Iterative	Yes	No

$$\begin{aligned}
 \frac{|u^{new} - u^{old}|_{max}}{V_{max}} &< \varepsilon_3, \\
 \frac{|v^{new} - v^{old}|_{max}}{V_{max}} &< \varepsilon_3, \text{ and} \\
 \frac{|w^{new} - w^{old}|_{max}}{V_{max}} &< \varepsilon_3
 \end{aligned} \tag{11.4}$$

simultaneously. Here, V_{max} is the maximum magnitude of the velocity, ε_3 is a user input convergence parameter, and the superscripts "new" and "old" refer to current and previous iterate values. If any one of these convergence criteria is not met, the sequence is repeated from Step 1. The solution proceeds through the sequence until it converges or the specified maximum number of iterations has been performed. Here, ϕ refers to the general scalar transport variable (such as enthalpy, turbulence kinetic energy, etc.).

Iteration criteria are also needed for the inner iteration loop if an iterative matrix solver is selected. The inner iteration loop solves the individual pressure and scalar transport equations within a given time step. If either the SOR or PCG method is selected, we will need a mass convergence criterion for the pressure equation and some other criteria for the scalar transport equations.

In theory, the pressure equation (Eq. 6.7) is considered solved when mass residue δ is equal to 0 for all cells. Because Eq. 6.7 is solved iteratively, this will, in general, never be true. Instead, a nonzero mass residual δ is computed for every cell and a maximum is determined as $|\delta|_{max}$. The iterative process continues until either a maximum specified number of iterations has been performed or the maximum mass residual falls below the convergence criterion.

$$|\delta|_{max} < \text{convergence criterion.} \tag{11.5}$$

The mass convergence criterion is calculated with the relation

$$\text{Convergence criterion} = \varepsilon_1 \cdot \left[\left(\frac{\rho \gamma_1 u_1}{\gamma_v \Delta x_1} \right)_{max} \right] + \varepsilon_2. \tag{11.6}$$

where ϵ_1 and ϵ_2 are the input convergence constants and subscript i stands for three coordinates.

The convergence criteria for the scalar transport equations in the inner iteration loop within a given time step are

$$\frac{h_{ijk}^{m+1} - h_{ijk}^m}{h_{\max}^m - h_{\min}^m} \leq \epsilon_5,$$

$$\frac{k_{ijk}^{m+1} - k_{ijk}^m}{k_{\max}^m - k_{\min}^m} \leq \epsilon_6,$$

and

$$\frac{\epsilon_{ijk}^{m+1} - \epsilon_{ijk}^m}{\epsilon_{\max}^m - \epsilon_{\min}^m} \leq \epsilon_6, \quad (11.7)$$

where the superscripts m and m+1 represent the previous and the current iterative values, respectively, the subscripts max and min represent the maximum and minimum values of the variable in the entire computational domain, and the subscript ijk indicates the change in value of the variable from one iteration to the next and is evaluated at the same location. The convergence criteria expressed by Eq. 11.7 mean that if the change in value of a variable from one iteration to the next at any location divided by the maximum variation of that variable in the computational domain is equal to or smaller than some prespecified number ϵ , the solution is considered convergent and no more iteration is required. Again, these criteria apply only to iterative matrix solvers such as SOR and PCG. These iteration criteria are not needed for the DMIM.

Table 19 summarizes the convergence criteria for the iterative scheme (fully implicit) and the iterative matrix solvers (SOR and PCG) and provides the default values of convergence parameters employed in COMMIX-PPC.

Table 19. Convergence criteria for the iterative scheme (fully implicit) and the iterative matrix solvers (SOR and PCG) used in COMMIX-PPC

Convergence Parameter	Default Value	Iteration Loop	Description
ϵ_1	10^{-4}	Inner	Mass convergence for pressure equations
ϵ_2	10^{-6}	Inner	Mass convergence for pressure equations
ϵ_3	5×10^{-5}	Outer	All transport variables
ϵ_6	10^{-5}	Inner	Turbulence parameters k and ϵ

12 Summary and Discussion

12.1 Major Features of COMMIX-PPC

The important features of COMMIX-PPC have already been explained. Some are unique and distinct from other computer codes. Five of these unique features, which significantly expand COMMIX-PPC capabilities and increase its flexibility, are reiterated below.

- Porous-medium formulation
- Geometry modeling
- Matrix solvers
- Multicomponent capability
- Shell-tube-side thermal coupling.

12.1.1 Porous-Medium Formulation

In COMMIX, volume porosity, directional surface porosity, distributed resistance, and distributed heat source (or sink) are used to model the fluid dynamic and thermal characteristics of a system involving complex geometry. The use of directional surface porosity is relatively new. It has greatly facilitated the modeling of flow and heat transfer in anisotropic media and has improved the resolution and accuracy of numerical modeling.

The porous-medium formulation has its foundation built on local volume-averaging of the governing partial differential conservation equations. The resulting equations are more general. If the directional surface porosity is set to equal the volume porosity, the equations reduce to those for the conventional porous-medium formulation. Furthermore, if the volume porosity and the directional surface porosity are set to unity, and the distributed resistances and heat sources are set to zero, then the equations simplify to those of the continuum formulation. Therefore, we may say that the continuum formulation is a subset of the conventional porous-medium formulation which, in turn, is a subset of the present porous-medium formulation.

The porous-medium formulation has provided a wider range of applicability of the COMMIX code and has been successfully used to treat irregular geometries that are often encountered in engineering applications. With some modification, COMMIX-PPC has the capability to analyze in great detail

- A single-component system, such as a
 - fuel assembly
 - reactor plenum
 - piping network,

as well as

- A multicomponent system, such as a
 - reactor vessel
 - downcomer and lower plenum,
 - cold leg, high-pressure injection system, downcomer.

12.1.2 Geometry Modeling

Unique features related to geometry modeling are

- *Identification of a computational cell by a cell number instead of its (i,j,k) location.* All "do loops" are performed with the cell number as an index instead of the conventional directional indices i,j,k. Consequently, the storage requirement depends only on the total number of computational cells and not on the dimension of IMAX x JMAX x KMAX. This is illustrated in Fig. 30 for the grid arrangement in a two-dimensional piping system. The storage requirement reduces from 56 for the conventional (i,j,k) method of cell identification to 14 when the present scheme is used.
- *Use of surface arrays to store boundary values at the boundary surface.* This eliminates the need for fictitious boundary cells to store boundary values.
- *Extra surface to model irregular geometry.* An irregular surface is one that is at an angle to a grid plane. It is an additional surface to the six, or normal, surfaces (parallel to grid planes) of a computational cell. Heat transfer in the energy equation and shear stress in the momentum equation pertaining to this seventh irregular surface are properly accounted for in COMMIX-PPC.

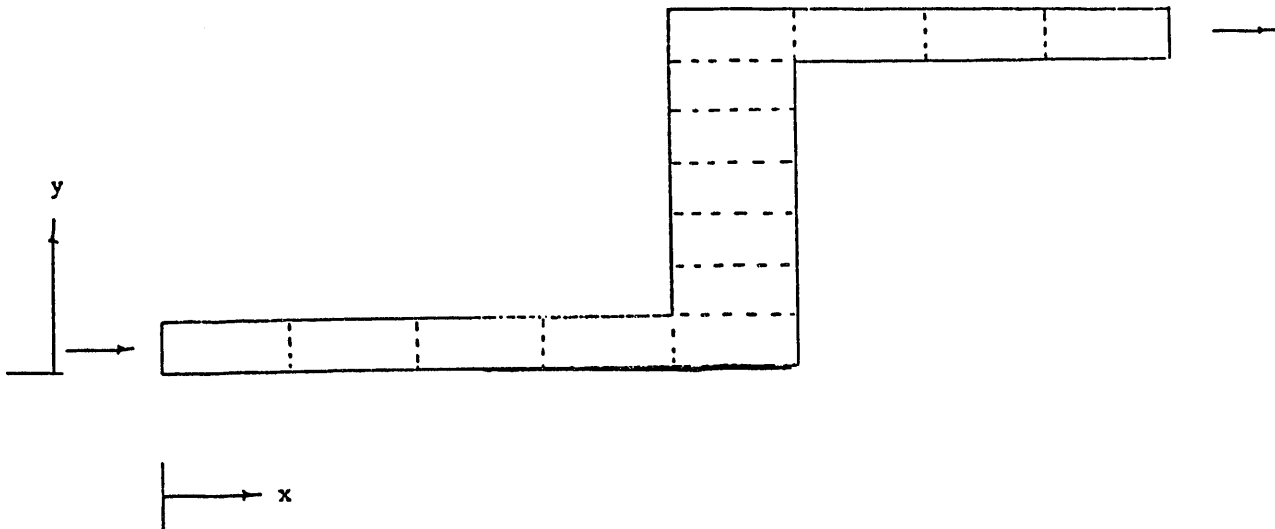
12.1.3 Matrix Solvers

Three matrix solvers are provided in COMMIX-PPC. They are the

- Successive overrelaxation (SOR) method
- Direct Matrix Inversion Method (DMIM)
- Preconditioned conjugate gradient (PCG) method.

These matrix solvers are used for the individual discretized equations (pressure and scalar transport equations) in the inner iteration loop.

The SOR method and the DMIM are suitable for both symmetric and nonsymmetric matrices, whereas the PCG method is limited to symmetric matrices only. Thus, the SOR method and the DMIM are applicable to both the pressure and the scalar transport equations, whereas the PCG method is limited to the pressure equation only. Both the SOR and the PCG methods are iterative, whereas the DMIM is a direct solver and does not involve iteration. In general, if the number of computational cells is less than 1,000, the DMIM should be used. On the other hand, if the number of computational cells is greater than 2,000, the SOR or PCG method should be selected.



IMAX = 8

JMAX = 7

Total number of cells = 14

Conventional storage requirements = $8 \times 7 = 56$

Storage Requirement in COMMIX-1C = 14

Fig. 30. Grid arrangement in a two-dimensional piping system, illustrating storage requirements in COMMIX-PPC

The three matrix solvers significantly increase the flexibility and efficiency of COMMIX-PPC for the numerical computation of a wide range of engineering problems.

12.1.4 Multicomponent Capability

A multicomponent capability has been incorporated into the COMMIX-PPC code and this capability is necessary because the shell side consists, in general, of a mixture of steam and air. The distributions of steam and air inside a condenser are essential for the evaluation of the performance of a condenser. The presence of air has a significant impact on the local heat transfer rate. The steam is assumed in the saturated state with its bulk temperature determined solely by its partial pressure in the mixture. This assumption is quite reasonable for condenser operation and greatly simplifies calculation.

12.1.5 Shell-Tube-Side Thermal Coupling

Tube-side fluid flow and heat transfer have been developed and incorporated into the COMMIX-PPC code. The use of one-dimensional conservation equations of mass, momentum, and energy for tube-side flows greatly reduces the complexity and computer running time without sacrificing accuracy. It also facilitates the handling of thermal coupling between the condensation of vapor on the shell side and forced convection of a single-phase liquid in the tube side.

12.2 Code Application and Validation

The COMMIX-PPC computer code has been applied to the Maansan nuclear power plant for calculating condenser performance. The calculation is based on data provided by the Taiwan Power Company. The data contain the boundary conditions at the inlets and outlets of the shell and tube sides. The inlet and outlet pressure and temperature of tube-side flow are measured, whereas the inlet steam pressure and temperature are calculated based on measured tube-side information and the designed values of steam mass flow rate, feed water pump turbine exhaust flow conditions, tube-side mass flow rate, and the overall heat transfer coefficient. The actual air leakage to the condenser is not known. The velocity, pressure, and temperature distribution are also not available.

Because the appropriate experimental data are not available, validation of the COMMIX-PPC computer code is not possible. Hopefully, we may be able to obtain experimental data to validate COMMIX-PPC through cooperation with industrial vendors and government agencies.

12.3 Future Developments

Future developments of COMMIX-PPC will include the following:

- *Tracking down condensates.* In the present COMMIX-PPC, the liquid condensate is discarded once steam is condensed. The effects of the motion of the condensate on the fluid dynamic and heat transfer in the condenser are thus neglected. Neglecting the presence of condensate, in general, underestimates the pressure drop. Developing a two-phase model to track down the liquid fluid and study its effects on condenser performance is needed.
- *Validating all heat transfer correlations.* We are seeking available condenser experimental data to validate all the heat transfer correlations that are used in the COMMIX-PPC computer code.
- *Quantifying the turbulent viscosity and mass diffusivity.* In the present COMMIX condenser calculation, constant values of turbulent viscosity and mass diffusivity are used. To improve the accuracy of COMMIX-PPC calculations, the two-equation turbulence model will be used to quantify turbulent viscosity and diffusivity.
- *Developing an efficient numerical scheme.* The current converging rate is slow. An efficient and new solution scheme must be developed to speed up the calculation.
- *Improving input and output processing.* COMMIX-PPC is a very large computer code. Consequently, input preparation and output processing often become tedious. Currently, due to the separation of shell- and tube-side flow formulations, the graphic capability for the tube-side is no longer operational. Further developments and efforts are needed to make COMMIX-PPC a more user-friendly computer program.

Acknowledgments

This work is a result of international cooperation. The authors thank E. Lin, P. C. Chen, S. C. Cheng, Y. H. Cheng, T. K. Lee, C. K. Fwu, C. C. Jao, and M. W. Lin of Taiwan Power Company for supporting and sponsoring this work. We also thank Professors B. T. Chao and S. L. Soo of the University of Illinois at Urbana-Champaign for their stimulating discussions and constructive comments.

References

1. E. J. Barsnoss, *Calculation of the Performance of Surface Condenser by Digital Computer*, Am. Soc. Mech. Eng., Paper No. 63-PWR-2 (1963).
2. D. Chisholm, B. D. J. Osment, M. W. McFarlane, and M. H. Chondhury, *The Performance of an Experimental Condenser*, Proc. 3rd. Int. Heat Transfer Conference, Vol. I, pp. 179-185 (1966).
3. J. L. Wilson *The Design of Condensers by Digital Computers*, Inst. Chem. Eng. Symposium Series No. 35, Inst. Chem. Eng., London, pp. 3.21-3.27 (1972).
4. B. J. Davidson and M. Rowe, *Simulation of Power Plant Condenser Performance by Computational Methods*, Proc. Workshop on Modern Developments in Marine Condensers, Hemisphere Publ. Corp., New York, pp. 17-49 (1981).
5. D. Chisholm, *Modern Developments in Marine Condensers: Non-condensable Gases: An Overview*, Power Condenser Heat Transfer Technology, Hemisphere Publ. Corp., New York, pp. 95-109 (1981).
6. S. Al-Sanea, N. Rhodes, D. G. Tatchell, and T. S. Wilkinson, *A Computer Model for Detailed Calculation of the Flow in Power Station Condensers*, Condensers: Theory and Practice, Inst. Chem. Eng. Symposium Series, No. 75, Pergamon Press, New York, pp. 70-88 (1983).
7. H. L. Hopkins, J. Longhead, and C. J. Monks, *A Computerized Analysis of Power Condenser Performance Based upon an Investigation of Condensers*, Condensers: Theory and practice, Inst. Chem. Eng. Symposium Series, No. 75, Pergamon Press, New York, pp. 152-171 (1983).
8. C. Caremoli, *Numerical Computation of Steam Flow in Power Plant Condensers*, Condensers: Theory and Practice, Inst. Chem. Eng. Symposium Series, No. 75, Pergamon Press, New York, pp. 89-96 (1983).
9. W. T. Sha, H. M. Domanus, R. C. Schmitt, J. J. Oras, and E. I. H. Lin, *A New Approach for Rod-Bundle Thermal-Hydraulic Analysis*, Proc. Int. Mtg. on Nuclear Power Reactor Safety, Brussels, Belgium (Oct. 1978), Nucl. Technol., **46**, pp. 268-290 (Dec. 1979).

10. H. M. Domanus, R. C. Schmitt, W. T. Sha, and V. L. Shah, *COMMIX-1A: A Three-Dimensional Transient Single-Phase Computer Program for Thermal Hydraulic Analysis of Single and Multicomponent Systems: Vol. I User's Manual, and Vol. II Assessment and Verification*, NUREG/CR-2896, Argonne National Laboratory Report ANL-82-25 (Dec. 1983).
11. Analytical Thermal Hydraulic Research Program, *COMMIX-1B: A Three-Dimensional Transient Single-Phase Computer Program for Thermal Hydraulic Analysis of Single- and Multicomponent Systems: Vol. I Equations and Numerics, Vol. II User's Manual*, NUREG/CR-4348, Argonne National Laboratory Report ANL-85-42 (Sept. 1985).
12. H. M. Domanus, Y. S. Cha, T. H. Chien, R. C. Schmitt, and W. T. Sha, *COMMIX-1C: A Three-Dimensional, Transient, Single-Phase Computer Program for Thermal-Hydraulic Analysis of Single-Component and Multicomponent Engineering Systems, Vol. I*, NUREG/CR-5649, Argonne National Laboratory Report ANL-90/33 (Nov. 1990).
13. W. T. Sha and B. T. Chao, *Conservation Equations for Finite Control Volume Containing Single-Phase Fluid with Fixed, Dispersed Heat Generating (or Absorbing) Solids*, NUREG/CR-0945, Argonne National Laboratory Report ANL-CT-79-42 (July 1979).
14. W. T. Sha and J. C. Slattery, *Local Volume-Time Averaged Equations of Motion for Dispersed, Turbulent, Multiphase Flows*, NUREG/CR-1491, Argonne National Laboratory Report ANL-80-51 (Nov. 1980).
15. W. T. Sha and B. T. Chao, *Local Volume-Averaged Transport Equations for Single-Phase Flow in Regions Containing Fixed, Dispersed, Heat-Generating (or Absorbing) Solids*, NUREG/CR-1969, Argonne National Laboratory Report ANL-80-124 (April 1981).
16. W. T. Sha, *A New Porous Media Approach for Thermal Hydraulic Analysis*, Trans. Am. Nucl. Soc. **39**, pp. 510-512 (Nov. 1981).
17. W. T. Sha, B. T. Chao, and S. L. Soo, *Local Volume-Averaged Transport Equations for Multiphase Flow in Regions Containing Distributed Solid Structures*, NUREG/CR-2354, Argonne National Laboratory Report ANL-81-69 (Dec. 1981).
18. W. T. Sha, B. T. Chao, and S. L. Soo, *Time Averaging of Local Volume-Averaged Conservation Equations of Multiphase Flow*, NUREG/CR-3434, Argonne National Laboratory Report ANL-83-49 (July 1983).
19. W. T. Sha, B. T. Chao, and S. L. Soo, *Time-Averaging of Local Volume-Averaged Conservation Equations of Multiphase Flow*, Proc. AIChE/ASME National Heat Transfer Conf., Seattle (July 25-29, 1983).
20. W. T. Sha, B. T. Chao, and S. L. Soo, *Porous-Media Formulation for Multiphase Flow with Heat Transfer*, Nucl. Eng. Des. **82**, pp. 93-106 (Oct. 1984).
21. W. T. Sha, B. T. Chao, and S. L. Soo, *Time- and Volume-Averaged Conservation Equations for Multiphase Flow, Part One: System without Internal Solid Structures*, NUREG/CR-3989, Argonne National Laboratory Report ANL-84-66 (Dec. 1984).

22. S. V. Patankar, *Numerical Heat Transfer and Fluid Flow*, Numerical Heat Transfer, Vol. 2, McGraw-Hill, New York, pp. 143-146 (1979).
23. J. C. Slattery and R. B. Bird, *AIChE J.*, **4**, pp. 137-142 (1958).
24. A. Padilla, Jr. and D. S. Rowe, *A Donor Flow Formulation for Momentum Flux Differencing*, *Trans. Am. Nucl. Soc.* **46**, pp. 851-852 (1984).
25. W. T. Sha and B. E. Launder, *A General Model for Turbulent Momentum and Heat Transport in Liquid Metals*, Argonne National Laboratory Report ANL-77-78 (1979).
26. R. Nijssing and W. Eifler, *Temperature Fields in Liquid Metal Cooled Assemblies*, *Prog. Heat Mass Transfer* **7**, p. 115 (1973).
27. B. E. Launder and D. B. Spalding, *Lectures in Mathematical Models of Turbulence*, Academic Press, London (1972).
28. V. S. Arpaci and P. S. Larsen, *Convective Heat Transfer*, Prentice-Hall, Englewood Cliffs, NJ (1974).
29. B. E. Launder, G. J. Reese, and W. Rodi, *Progress in the Development of a Reynolds-Stress Turbulent Closure*, *J. Fluid Mech.* **68**, pp. 537-566 (1975).
30. B. J. Daley and F. H. Harlow, *Transport Equation in Turbulence*, *Physics of Fluids* **13**, pp. 2634-2649 (1970).
31. K. Hanjalic and B. E. Launder, *A Reynolds-Stress Model of Turbulence and its Application to Asymmetric Shear Flows*, *J. Fluid Mech.* **52**, pp. 609-638 (1972).
32. J. J. Lumley and B. J. Khajeh-Nouri, *Computational Modeling of Turbulent Transport*, *Adv. Geophysics* **18A**, pp. 169-192 (1974).
33. W. P. Jones and B. E. Launder, *The Prediction of Laminarization with a Two-Equation Model of Turbulence*, *Int. J. Heat Mass Transfer Trans.*, **15**, pp. 301-313 (1982).
34. B. E. Launder, A. Morse, W. Rodi, and D. B. Spalding, *The Prediction of Free Shear Flows—A Comparison of the Performance of Six Turbulent Models*, Proc. of NASA Conference on Free Turbulent Shear Flows, Vol. 1., NASA SP320, Langley (1973).
35. M. Ciofalo and M. W. Collins, *$k-\epsilon$ Predictions of Heat Transfer in Turbulent Recirculation Flows Using an Improved Wall Treatment*, Numerical Heat Transfer, Part B, **15**, pp. 21-49 (1989).
36. Y. S. Cha, H. M. Domanus, and W. T. Sha, *Validation and Assessment of the $k-\epsilon$ Two-Equation Turbulence Model in the COMMIX Code*, Argonne National Laboratory Report ANL/ATHRP-42 (Feb. 1990).
37. The 1980-1981 AFOSR-FTTM-Stanford Conference on Complex Turbulent Flows, S. J. Kline, B. J. Cantwell, and G. M. Lilley, eds, published by Thermosciences Division, Mechanical Engineering Dept., Stanford University, Stanford, CA (1982).

38. L. D. Berman and S. N. Fuks, *Mass Exchange in Horizontal Tube Condenser with Steam Containing Air*, *Teploenergetika*, **5**(8), pp. 66-74 (1958).
39. W. Nusselt, *Die oberflächen Kondensatoren des Wasserdampfes*, *Z. Ver. Deutsch. Ing.*, **60**, pp. 541-569 (1916).
40. B. E. Short and H. E. Brown, *Condensation of Vapours on Vertical Banks of Horizontal Tubes*, *Proc. General Discussion Heat Transfer, Inst. Mech. Eng.*, pp. 27-31 (1951).
41. M. M. Chen, *An Analytical Study of Laminar Film Condensation, Part 1. Flat Plates, and Part 2. Single and Multiple Horizontal Tubes*, *Trans. ASME, Sec. C*, **83**, pp. 48-60 (1961).
42. M. H. Rosenhow, *Heat Transfer and Temperature Distribution in Laminar-Film Condensation*, *Trans. ASME*, **78**, pp. 1546-1648 (1956).
43. L. D. Berman and Y. A. Tumanov, *Condensation Heat Transfer in a Vapour Flow over a Horizontal Tube*, *Teploenergetika*, **9**(10), pp. 77-83 (1962).
44. D. M. Eissenberg and H. M. Noritake, *Computer Model and Correlations for Prediction of Horizontal-Tube Condenser performance in Seawater Distillation Plants*, ORNL-TM-2972 (1970).
45. F. W. Dittus and L. M. K. Boelter, *Heat Transfer in Automobile Radiation of Tubular Type*, U. California-Berkeley Pubs. Eng., Vol. 2, pp. 443-461 (1930).
46. W. T. Sha and V. L. Shah, *Some Resistance Correlations for COMMIX Users*, Argonne National Laboratory Report ATHRP-13 (1983).
47. H. C. Elman, *Iterative Methods for Large, Sparse, Nonsymmetric Systems of Linear Equations*, Ph.D. Dissertation, Yale University (May 1982).

Appendix: Structure/Fluid Thermal Interaction

A.1 Introduction

Solid structures partially or totally submerged in a fluid interact with the fluid and influence momentum distribution. They influence temperature distribution when the temperature of the solid structures is different from that of the fluid. The structure/fluid thermal interaction in COMMIX-PPC is modeled by distributed heat sources. Such interaction consists primarily of heat transfer between a structure and surrounding fluid and, indirectly, heat transfer within the solid structure.

The transfer of heat to fluid from a structure is calculated by solving the one-dimensional heat conduction equation for the structure. This assumes that heat conduction in the other two directions is negligible.

The following features are found in the COMMIX thermal-structure model:

- The model considers all internal structures. The input determines the total number of structures.
- A structure can be planar, cylindrical, or spherical, with either one surface (e.g., solid cylinder or sphere) or two surfaces (plane or annular cylinder) thermally interacting with the surrounding fluid. The axis of the structure can be aligned with any of the three coordinate axes.
- Each structure can consist of more than one type of material, each separated by a gap.
- Temperature dependence of thermal conductivity and specific heat of structures are incorporated.
- The effects of gaps in a structure element are accounted for in the model. The gap width and heat transfer coefficient across a gap are input parameters.
- The heat source in a structure element is considered in the heat conduction equation. The heat source can be transient.
- Each structure is divided into a desired number of axial elements. A set of discretization equations is obtained for each element through the use of proper boundary conditions. The equations are solved by using the Tri-Diagonal Matrix Algorithm. The temperature variations in the element and heat transfer from the element to fluid are calculated.

A.2 Thermal Structure Modeling

A.2.1 Geometrical Description

To explain the geometrical features of the model, we consider a cylindrical structure with its axis aligned in the z direction and its length extending over a number of Δz partitions (k levels) as shown in Fig. A.1. Although the description and subsequent formulation are for cylindrical-type structures, the model in COMMIX-PPC is also applicable to spherical and slab-type geometries.

Each Δz partition of the structure is referred to as a thermal-structure element. Each element has its own internal temperature distribution as it interacts with surrounding fluid cells. Each element has two surfaces, outer and inner. The outer surface interacts thermally with surrounding fluid. The inner surface can either be adiabatic or interact with fluid, as shown in Fig. A.2. Each element may interact with no more than one fluid cell per element, as illustrated in Fig. A.3.

Figure A.4 shows the cross section of a typical structure element. The outside surface is designated as Surface 1 and the inside as Surface 2. Each element can be made up of more than one material. In Fig. A.4, there are three materials. Each material region can be subdivided into several partitions as shown.

A.2.2 Governing Equation

The transient one-dimensional heat conduction equation is

$$\rho c_p \frac{\partial T}{\partial t} = \frac{1}{A} \frac{\partial}{\partial r} (-Aq) + \dot{q}''' . \quad (\text{A.1})$$

Here, ρ and c_p are the density and specific heat of the material, \dot{q}''' is the heat source per unit volume, q is the radial heat flux per unit area, and A is the local cross-sectional area.

A.2.3 Finite-Difference Formulation

Figure A.5 shows the cross section of a typical structure element under consideration. Each element is divided into a number of material regions and each material region is subdivided into several partitions. Let Δr be the partition size and L be the total number of partition cells.

Consider the energy balance of cell ℓ shown in Fig. A.6. The integrated energy equation for the structure in the control volume of cell ℓ gives

$$\frac{\rho c_p V_\ell}{\delta t} (T_\ell - T_\ell^n) = -(A_{\ell+1} q_{\ell+1} - A_\ell q_\ell) + \dot{q}''' V_\ell . \quad (\text{A.2})$$

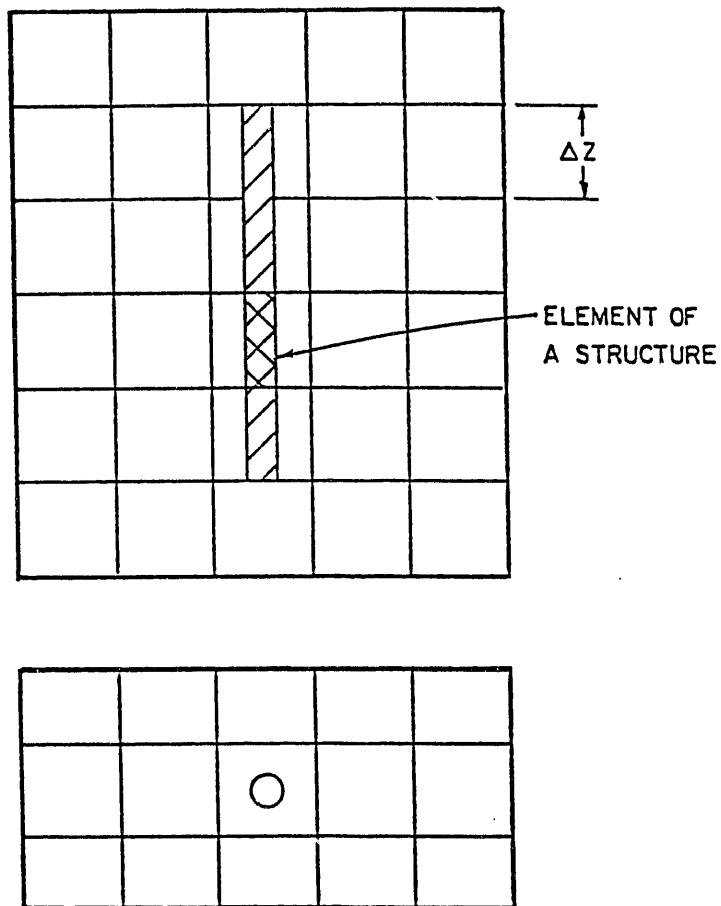


Fig. A.1. Flow domain, showing cylindrical structure

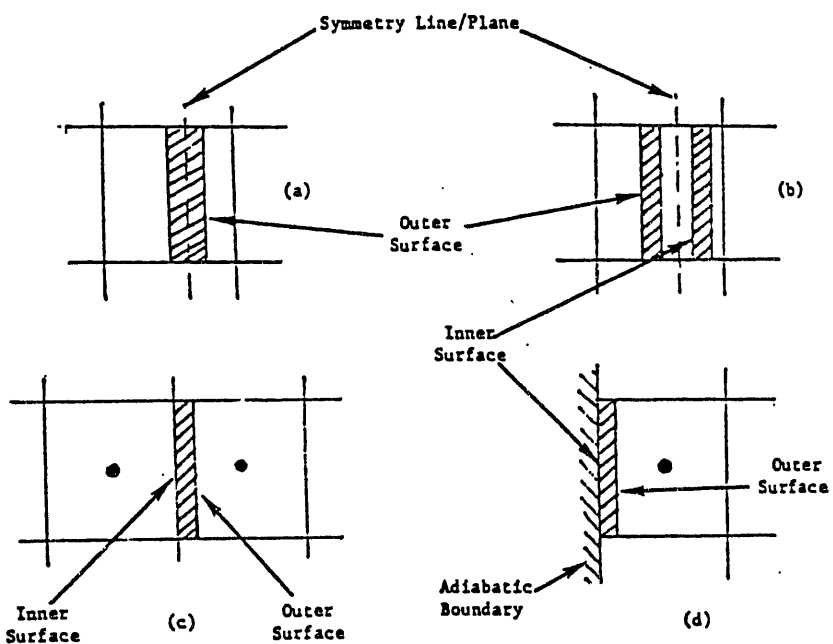


Fig. A.2. Element of thermal structure, showing outer and inner surfaces

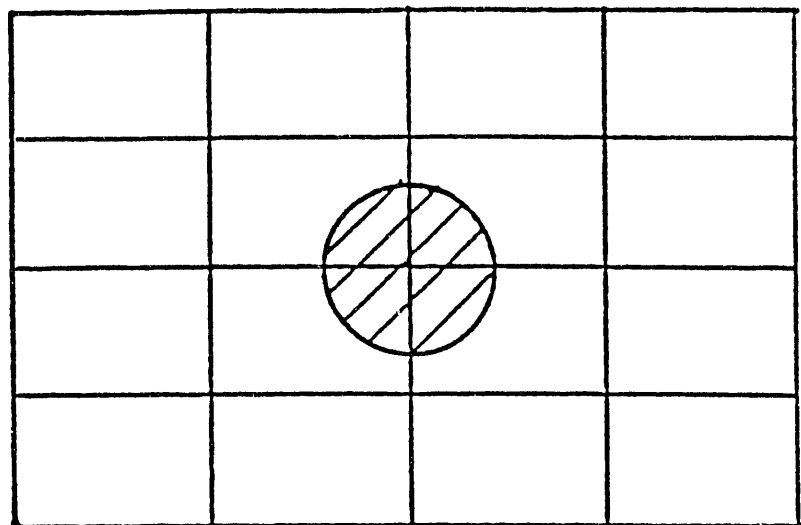


Fig. A.3. Four quarter-cylindrical structures, each interacting with one fluid cell

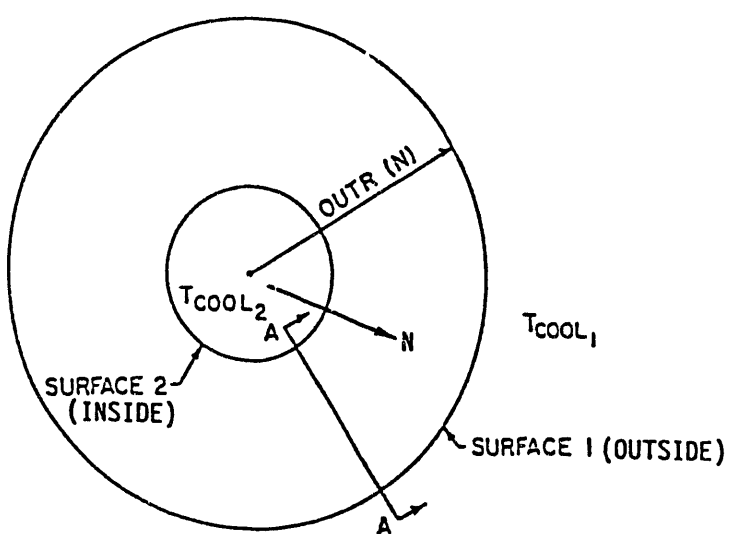
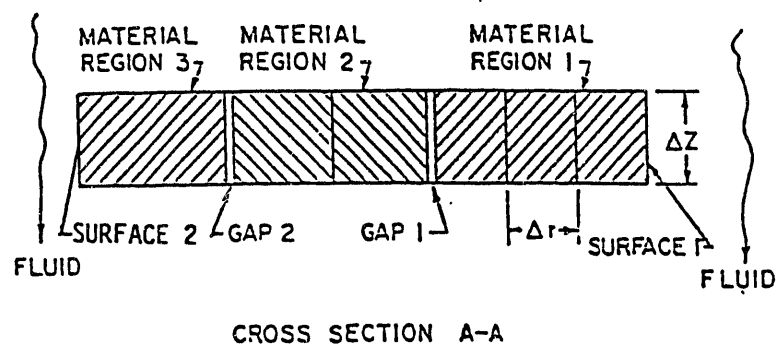


Fig. A.4. Typical structure element, showing material regions and gaps

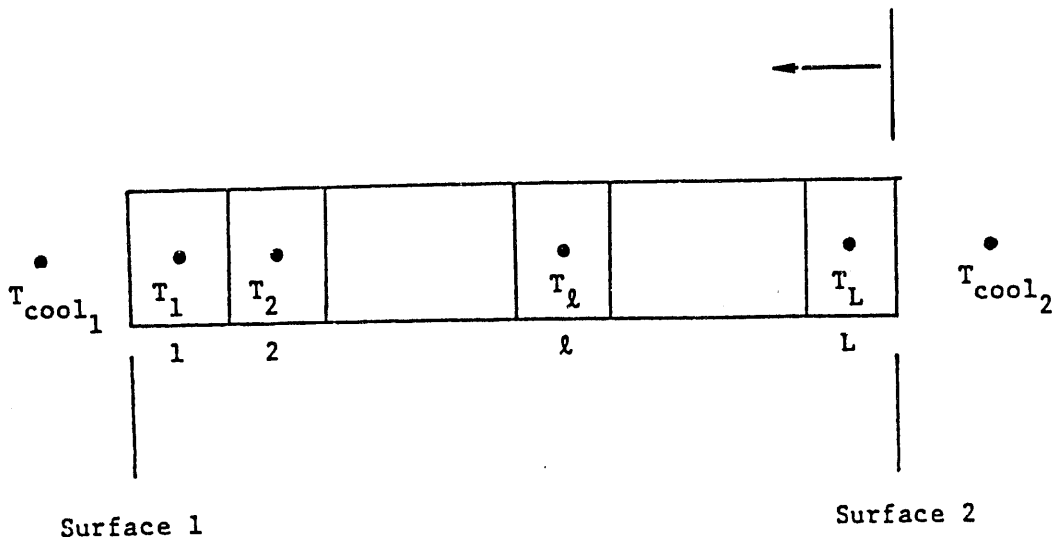
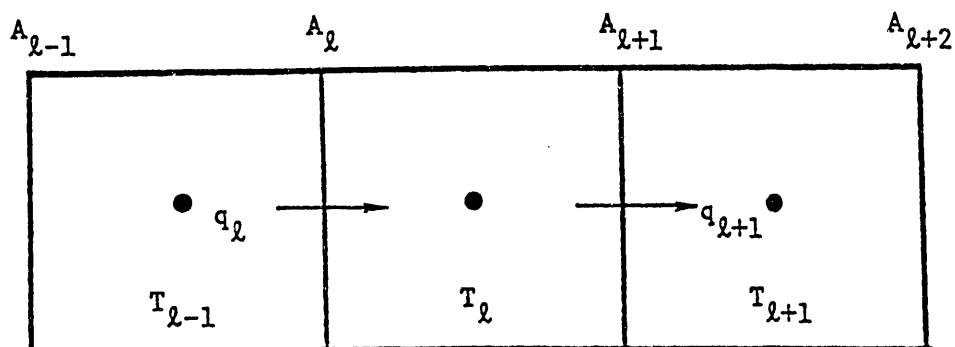


Fig. A.5. Cross section of a thermal-structure element

Fig. A.6. Energy balance of a partition cell ℓ

Here, V_ℓ is the cell volume. The heat flux q_ℓ can be expressed in terms of the overall heat transfer coefficient (conductance) U_ℓ or its reciprocal R_ℓ , the overall thermal resistance, and a temperature difference

$$q_\ell = U_\ell (T_{\ell-1} - T_\ell) = (T_{\ell-1} - T_\ell)/R_\ell. \quad (\text{A.3})$$

$$U_\ell = \frac{1}{R_\ell} = \begin{cases} \frac{1}{(\frac{\Delta r}{2\lambda})_{\ell-1} + (\frac{\Delta r}{2\lambda})_\ell} & \text{for conduction between two solid cells of same material,} \end{cases} \quad (\text{A.4})$$

$$U_\ell = \frac{1}{R_\ell} = \begin{cases} \frac{1}{h + (\frac{\Delta r}{2\lambda})_\ell} & \text{for conduction and convection between a fluid cell and a solid cell (this is only when convection takes place on a surface whose normal is in the r-direction)} \end{cases} \quad (\text{A.5})$$

$$U_\ell = \frac{1}{R_\ell} = \begin{cases} \frac{1}{(\frac{\Delta r}{2\lambda})_{\ell-1} + \frac{1}{h_{\text{gap}}} + (\frac{\Delta r}{2\lambda})_\ell} & \text{for conduction between two solid cells with different materials.} \end{cases} \quad (\text{A.6})$$

Here, λ is the thermal conductivity, h is the convection heat transfer coefficient, and h_{gap} is the gap conductance between the two materials.

Upon substituting Eq. A.3 into A.2 and rearranging, we obtain

$$(a_t + b_t + b_{t+1})T_t = b_t T_{t-1} + b_{t+1} T_{t+1} + d_t, \quad (\text{A.7})$$

where

$$a = \rho c_p V / \delta t, \quad (\text{A.8})$$

$$b = AU = A/R, \quad (\text{A.9})$$

and

$$d = \dot{q}'''' V + a T^n. \quad (\text{A.10})$$

Here, T^n and T are the temperatures at time t and $(t + \delta t)$, respectively.

Note that A_t is related to the heat capacity of the structural element, b_t is related to the heat transfer coefficient and area, and d is related to the heat source.

A.2.3.1 Cell Adjacent to Coolant

For the case of Cell 1 (Fig. A.7), adjacent to the fluid, the finite-difference energy equation is

$$(a_1 + b_1 + b_2)T_1 = b_1 T_{\text{cool}_1} + b_2 T_2 + d_1. \quad (\text{A.11})$$

Here, a_1 , b_1 , and d_1 have the same meaning as a , b , and d in Eqs. A.8–A.10. Note that b_1 includes the convective contribution. Therefore,

$$b_1 = \frac{A_1}{R_1} = \frac{A_1}{\frac{1}{h_{\text{cool}_1}} + \left(\frac{\Delta r}{2\lambda}\right)_1}. \quad (\text{A.12})$$

Similarly, at the other end of the thermal structure, Cell L is in contact with fluid and we have

$$(a_L + b_L + b_{L+1})T_L = b_L T_{L-1} + b_{L+1} T_{\text{cool}_2} + d_L. \quad (\text{A.13})$$

where

$$b_{L+1} = \frac{A_{L+1}}{R_{L+1}} = \frac{A_{L+1}}{\frac{1}{h_{\text{cool}_2}} + \left(\frac{\Delta r}{2\lambda}\right)_L}. \quad (\text{A.14})$$

A.2.3.2 Cell Adjacent to Different Material

For a cell adjacent to a different material cell, as shown in Fig. A.8.

$$(a_t + b_t + b_{t+1})T_t = b_t T_{t-1} + b_{t+1} T_{t+1} + d_t. \quad (\text{A.15})$$

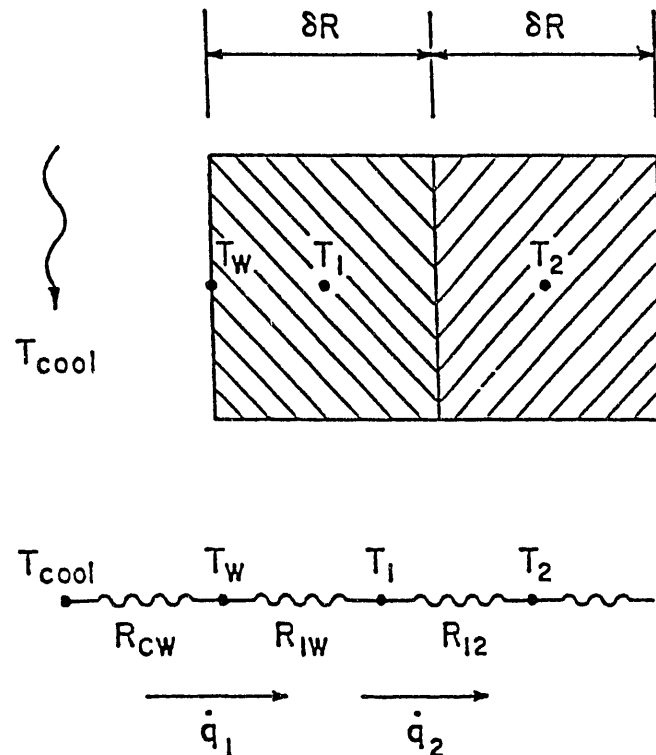


Fig. A.7. Energy balance of Cell 1 adjacent to coolant

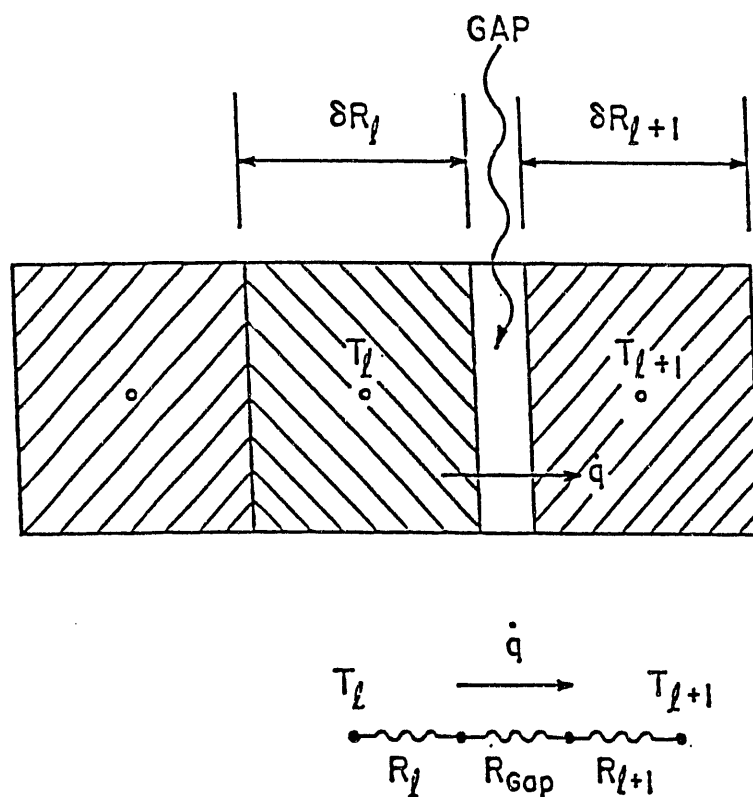


Fig. A.8. Cell surrounded by different materials with air gap between them

Equation A.15 is similar to Eq. A.7. Note that the term $b_{\ell+1}$ includes the gap resistance. Thus,

$$b_{\ell+1} = \frac{A_{\ell+1}}{R_{\ell+1}} = \frac{A_{\ell+1}}{\left(\frac{\Delta r}{2\lambda}\right)_\ell + \frac{1}{h_{gap}} + \left(\frac{\Delta r}{2\lambda}\right)_{\ell+1}}. \quad (\text{A.16})$$

A.2.3.3 End Cell with Adiabatic Boundary Condition

The existence of a symmetry line (or surface) depends not only on geometry, but also on thermal conditions. In solid cylindrical or spherical structures, the other end (symmetry line) has the adiabatic boundary condition. The end cell for this boundary condition is shown in Fig. A.9. There is no heat transfer, so thermal resistance is infinite and the term b_{L+1} goes to zero. The final equation, therefore, is

$$(a_L + b_L)T_L = b_L T_{L-1} + d_L. \quad (\text{A.17})$$

A.2.3.4 Solution of the Discretized Equations

We can see from the formulations of the preceding section that there are L number of equations for L number of unknown temperatures.

- Outside Surface Cell ($\ell = 1$)

$$(a_1 + b_1 + b_2)T_1 = b_2 T_2 + d_1 + b_1 T_{cool_1}. \quad (\text{A.18a})$$

- Intermediate Cells ($\ell = 2, \dots, L-1$)

$$(a_\ell + b_\ell + b_{\ell+1})T_\ell = b_\ell T_{\ell-1} + b_{\ell+1} T_{\ell+1} + d_\ell. \quad (\text{A.18b})$$

- Inside Surface Cell ($\ell = L$)

$$(a_L + b_L + b_{L+1})T_L = b_L T_{L-1} + b_{L+1} T_{cool_2} + d_L \quad (\text{A.18c})$$

if the inside surface is nonadiabatic, and

$$(a_L + b_L)T_L = b_L T_{L-1} + d_L \quad (\text{A.18d})$$

if the inside surface is adiabatic.

Equations A.18 can be rewritten as

$$C'_1 T_1 = b_2 T_2 + A'_1 \quad (\ell = 1) \quad (\text{A.19a})$$

$$C'_\ell T_\ell = b_{\ell+1} T_{\ell+1} + A'_\ell \quad (\ell = 2, \dots, L-1) \quad (\text{A.19b})$$

$$C'_L T_L = b_{L+1} T_{cool_2} + A'_L \quad (\ell = L; \text{nonadiabatic}) \quad (\text{A.19c})$$

$$C'_L T_L = A'_L \quad (\ell = L; \text{adiabatic}). \quad (\text{A.19d})$$

Here,

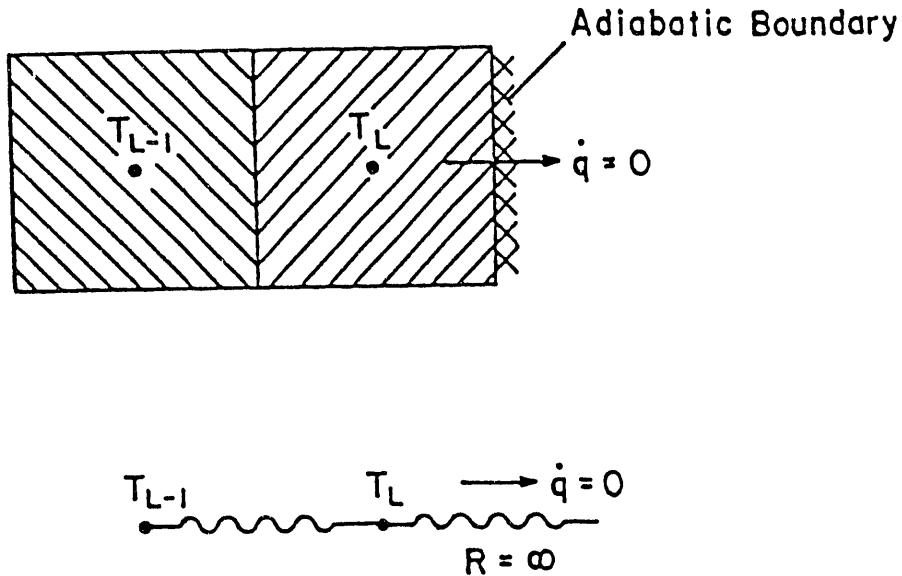


Fig. A.9. Cell with adiabatic boundary

$$A'_\ell = d_\ell + \left(b_\ell A'_{\ell-1} / C'_{\ell-1} \right) \quad (\ell = 2, \dots, L) \quad (A.20a)$$

and

$$C'_\ell = a_\ell + b_\ell + b_{\ell+1} - \left(b_\ell^2 / C'_{\ell-1} \right) \quad (\ell = 2, \dots, L) \quad (A.20b)$$

For $\ell = 1$,

$$A'_1 = d_1 + b_1 T_{cool_1} \quad (A.20c)$$

and

$$C'_1 = a_1 + b_1 + b_2 \quad (A.20d)$$

The inside-surface cell temperature is first calculated from Eq. A.19c or A.19d. Then, the rest of the temperatures are computed with Eqs. A.19a and A.19b.

A.2.3.5 Heat Transfer to Adjacent Fluid

Once the temperature distribution in a structure element is determined, the heat transfer rate to the adjacent fluid can be computed from

$$\begin{aligned} \dot{q} &= \frac{A_1}{R_1} (T_1 - T_f) \\ &= U_1 A_1 (T_1 - T_f) \text{ for the outside surface } (T_f = T_{cool_1}) \end{aligned} \quad (A.21)$$

and

$$\begin{aligned}\dot{q} &= \frac{A_{L+1}}{R_{L+1}} (T_L - T_f) \\ &= U_{L+1} (T_L - T_f) \text{ for the inside surface } (T_f = T_{cool2}).\end{aligned}\quad (A.22)$$

where \dot{q} is the heat transfer rate and U is the overall heat transfer coefficient given by

$$U = \frac{1}{R} = \frac{1}{\frac{1}{h_{cool}} + \left(\frac{\Delta r}{2\lambda}\right)}. \quad (A.23)$$

A is the surface area, T_1 and T_L are the temperatures of the edge partition cells, and T_f is the fluid temperature, either T_{cool1} or T_{cool2} . For the present condenser modeling, the heat transfer rate \dot{q} in Eq. A.21 is used to calculate the steam condensation rate in the shell side and the heat transfer rate \dot{q} in Eq. A.22 is the source term for the tube-side energy equation. Because steam is assumed to always be in the saturated condition, T_{cool1} is known and is determined by the local pressure in the shell side. T_{cool2} is not known a priori and is determined by a consideration of the interaction between the thermal structure and the inside and outside fluid. However, for general engineering applications, the heat transfer rate \dot{q} in Eqs. A.21 and A.22 are specified as distributed heat source \dot{Q} in the energy equation. In this case, we have adopted an implicit treatment of the interaction between the fluid and the thermal structure to increase the speed of convergence in COMMIX-PPC. The integrated (over the main control volume) heat source term can be expressed as

$$\int S_h dx dy dz = V_0 \dot{Q} + \frac{\partial \dot{q}}{\partial h_0} (h_0 - h_0^n). \quad (A.24)$$

where V_0 is the fluid volume, \dot{Q} is the rate of heat generation in the fluid per unit fluid volume, \dot{q} is the heat transfer rate from the thermal structure to the fluid, h_0^n is the enthalpy of the fluid cell adjacent to the thermal structure at old time n , and h_0 is the enthalpy of the fluid cell adjacent to the thermal structure at new time $n+1$. The superscript $n+1$ is omitted for convenience. Equation 5.27 can be written for the energy equation as

$$\int S_h dx dy dz = S_{ch} V_0 + S_{ph} V_0 h_0. \quad (A.25)$$

Comparing Eq. A.24 to Eq. A.25, one has

$$S_{ch} = \dot{Q} - h_0^n \frac{\partial \dot{q}}{\partial h_0} / V_0. \quad (A.26)$$

and

$$S_{ph} = \frac{\partial \dot{q}}{\partial h_0} / V_0. \quad (A.27)$$

In writing Eqs. A.26 and A.27, we have separated the term containing the new time value h_0 from the rest of the terms that are known. When Eq. A.25 is substituted into the energy equation, the term containing h_0 can be combined into the left side of the general discretized finite-volume equation (Eq. 5.35). Thus, the effect of the thermal structure has been accounted for when the energy equation is solved. This is what we mean by the implicit treatment of the interaction between the fluid and the thermal structure.

However, we must derive an expression for $(\partial\dot{q}/\partial h_0)$ so that the two quantities S_{ch} and S_{ph} given by Eqs. A.26 and A.27 can be calculated.

Consider the case where only the outside surface is in contact with the fluid. At old time n , Eq. A.21 can be written as

$$\dot{q}_1^n = U_1 A_1 (T_1^n - T_{cl}^n), \quad (A.28)$$

where T_1 is the temperature for Cell 1 and T_{cl} is the coolant temperature adjacent to Cell 1. At the new time $n+1$,

$$\begin{aligned} \dot{q}_1 &= U_1 A_1 (T_1 - T_{cl}) \\ &= U_1 A_1 [(T_1^n - T_{cl}^n) + (T_1 - T_1^n) - (T_{cl} - T_{cl}^n)] \\ &= \dot{q}_1^n + U_1 A_1 \left(\frac{\partial T_1}{\partial T_{cl}} - 1 \right) (h_0 - h_0^n) / C_{p1}. \end{aligned} \quad (A.29)$$

where $h_0 - h_0^n = C_{p1} (T_a - T_{cl})$, and C_{p1} is the specific heat of the fluid adjacent to the thermal structure. In Eq. A.29, the variables \dot{q}_1 , T_1 , T_{cl} , and h_0 represent the new time value and we have omitted the superscript $n+1$ for these variables. From Eq. A.29, we can obtain the following approximate expression for $(\partial\dot{q}/\partial h_0)$.

$$\frac{\partial\dot{q}_1}{\partial h_0} = \frac{\dot{q}_1 - \dot{q}_1^n}{h_0 - h_0^n} = \frac{U_1 A_1}{C_{p1}} \left(\frac{\partial T_1}{\partial T_{cl}} - 1 \right). \quad (A.30)$$

From Eq. A.19a,

$$\frac{\partial T_1}{\partial T_{cl}} = \frac{1}{C_1} \left(b_2 \frac{\partial T_2}{\partial T_{cl}} + \frac{\partial A_1}{\partial T_{cl}} \right). \quad (A.31)$$

From Eq. A.20c,

$$\frac{\partial A_1}{\partial T_{cl}} = b_1. \quad (A.32)$$

Substituting Eqs. A.31 and A.32 into Eq. A.30,

$$\frac{\partial\dot{q}_1}{\partial h_0} = \frac{U_1 A_1}{C_{p1}} \left[\frac{1}{C_1} \left(\frac{b_2}{C_1} \frac{\partial T_2}{\partial T_{cl}} + \frac{b_1}{C_1} \right) - 1 \right]. \quad (A.33)$$

$(\partial T_2/\partial T_{cl})$ can be calculated in terms of the following two recurrence equations:

$$\frac{\partial T_\ell}{\partial T_{cl}} = \frac{1}{C_\ell} \left(b_{\ell+1} \frac{\partial T_{\ell+1}}{\partial T_{cl}} + \frac{\partial A_\ell}{\partial T_{cl}} \right) \quad (A.34)$$

and

$$\frac{\partial A'_t}{\partial T_{c1}} = \frac{b_t}{C'_{t-1}} \frac{\partial A'_{t-1}}{\partial T_{c1}}. \quad (A.35)$$

which are obtained from Eqs. A.19c and A.20a. From Eq. A.19c, we have

$$\frac{\partial T_L}{\partial T_{c1}} = \frac{1}{C_L} \frac{\partial A'_L}{\partial T_{c1}}. \quad (A.36)$$

for adiabatic and nonadiabatic cases.

In summary, $(\partial \dot{q}_1 / \partial h_0)$ can be calculated analytically by using Eqs. A.32–A.36 when the outside surface of the thermal structure is in contact with the fluid.

If only the inside surface of the thermal structure is in contact with the fluid, an equation similar to Eq. A.30 can be derived:

$$\frac{\partial \dot{q}_L}{\partial h_0} = \frac{\dot{q}_L - \dot{q}_L^n}{h_0 - h_0^n} = \frac{U_L A_L}{C_{PL}} \left(\frac{\partial T_L}{\partial T_{c2}} - 1 \right). \quad (A.37)$$

$(\partial T_L / \partial T_{c2})$ can be calculated by using Eq. A.19c:

$$\frac{\partial T_L}{\partial T_{c2}} = \frac{b_{L+1}}{C_L}. \quad (A.38)$$

where C'_L is given by Eq. A.20b for $t = L$. The recurrence formula, Eq. A.20b, can also be used to evaluate C'_{L-1} :

$$C'_t = a_t + b_t + b_{t+1} - (b_t^2 / C'_{t-1}) \quad (t = 2, \dots, L-1). \quad (A.39b)$$

because C'_1 is known from Eq. A.20d. Thus, if only the inside surface of the thermal structure is in contact with the fluid, $(\partial \dot{q}_L / \partial h_0)$ can be calculated analytically by using Eqs. A.37, A.38, A.20b, and A.20d.

Distribution for ANL-92/2, Vol. IInternal:

T. H. Chien (5)	W. T. Sha (22)	R. W. Weeks
H. M. Domanus	C. E. Till	ANL Patent
C. A. Malefyt (2)	R. A. Valentin	TIS Files

External:

DOE/OSTI (2)

Brian Sheron, NRC, Washington, DC

ANL Libraries

ANL-E

ANL-W

Manager, Chicago Field Office, DOE

Materials and Components Technology Division Review Committee:

H. Birnbaum, University of Illinois at Urbana-Champaign, Urbana

R. Buchanan, University of Cincinnati, Cincinnati, OH

M. S. Dresselhaus, Massachusetts Institute of Technology, Cambridge MA

B. G. Jones, University of Illinois at Urbana-Champaign, Urbana

C.-Y. Li, Cornell University, Ithaca, NY

S. N. Liu, Electric Power Research Institute, Palo Alto, CA

R. E. Smith, Engineering Applied Sciences, Inc., Trafford, PA

E. Lin, Taiwan Power Company, for distribution (20)

END

DATE
FILMED

6/24/93